Angewandte Chemie
Eine Zeitschrift der Gesellschaft Deutscher Chemiker

Supporting Information

Directional Ring Translocation in a pH- and Redox-Driven Tristable [2]Rotaxane

L. Andreoni, J. Groppi, Ö. Seven, M. Baroncini, A. Credi, S. Silvi**

Directional Ring Translocation in a pH- and Redox-Driven Tristable [2]Rotaxane

Leonardo Andreoni,[a,b] Jessica Groppi,*[b,c] Özlem Seven,[b,c] Massimo Baroncini,[b,d] Alberto Credi,[a,b] and Serena Silvi*[b,e]

[a] Dipartimento di Chimica Industriale "Toso Montanari", Università di Bologna, viale del Risorgimento 4, 40136 Bologna, Italy.
[b] CLAN-Center for Light Activated Nanostructures, Institute ISOF-CNR, via Gobetti 101, 40129 Bologna, Italy. Email: serena.silvi@unibo.it, jessica.groppi@isof.cnr.it
[c] Institute for Organic Synthesis and Photoreactivity (ISOF), National Research Council of Italy (CNR), Via P. Gobetti 101, 40129 Bologna, Italy.
[d] Dipartimento di Scienze e Tecnologie Agro-alimentari, Università di Bologna, viale Fanin 44, 40127 Bologna, Italy.
[e] Dipartimento di Chimica "G. Ciamician", Università di Bologna, via Selmi 2, 40126 Bologna, Italy.

SUPPORTING INFORMATION

1. Materials and Methods
2. Synthetic Procedures
3. NMR Spectra
4. Solvent Effect on the Interaction between DB24C8 and the stations Bpy^{2+} and Trz^{+}.
5. ^{1}H NMR Monitoring of DB24C8 Translation to Trz^{+} induced by Chemical Reduction of Bpy^{2+}
6. Electrochemical Measurements
7. Thermodynamic considerations
8. High-Resolution Mass spectra of compounds $\mathbf{1H^{4+}}$, $\mathbf{2^{3+}}$, $\mathbf{3H^{3+}}$, $\mathbf{4H^{2+}}$, $\mathbf{5^{4+}}$ and $\mathbf{6^{3+}}$.

1. Materials and Methods

General. 3,5-Di-tert-butylbenzyl-4-chloromethylbenzylammonium chloride[1] and 3,5-Di-tert-butylbenzylazide[2] were synthesized according to literature procedures. All reagents and chemicals were purchased from Merck, VWR international or Fluorochem and used as received unless otherwise stated. Solvents were dried according to literature procedures. Microwave assisted reactions were performed in a CEM Discover SP-Microwave Synthesizer reactor. Thin layer chromatography was performed on TLC Silica gel 60 F254 coated aluminium plates from Merck. Flash column chromatography was performed using Merck Silica 40 (230-400 mesh size or 40-63 mm) as the stationary phase. Size exclusion chromatography was performed using Biorad Biobeads SX-1 as the stationary phase and dichloromethane as the eluent.

NMR Spectroscopy. NMR spectra were recorded on an Agilent DD2 spectrometer operating at 500 MHz. Chemical shifts are quoted in part per million (ppm) relative to tetramethylsilane using the residual solvent peak as a reference standard and all coupling constants (*J*) are expressed in Hertz (Hz).

Mass Spectrometry. High resolution mass spectrometry (HRMS) measurements were performed on a Waters Xevo G2-XS instrument equipped with an ESI source and a Q-TOF ion analyzer.

Electrochemical Measurements. Cyclic voltammetric (CV) and differential pulse voltammetric (DPV) experiments were carried out in argon-purged CH_2Cl_2 and CH_3CN (Sigma-Aldrich) with an Autolab 30 multipurpose instrument interfaced to a PC. The working electrode was a glassy carbon electrode (Amel, 0.07 cm^2), carefully polished with an alumina-water slurry on a felt surface, immediately before use. The counter electrode was a Pt wire, separated from the solution by a frit, an Ag wire was employed as a quasi-reference electrode and ferrocene was present as an internal standard ($E_{1/2}$= -0.46 V vs SCE in CH_2Cl_2; $E_{1/2}$= -0.395 V vs SCE in CH_3CN). The concentration of the examined compounds was ranging from 0.2 to 0.5 mM. Tetrabutylammonium hexafluorophosphate ($TBAPF_6$) and tetraethylammonium hexafluorophosphate ($TEAPF_6$) were added as supporting electrolyte in CH_2Cl_2 and CH_3CN respectively, in a 100-fold proportion with respect to the sample concentration. Cyclic voltammograms were obtained at scan rates varying from 20 to 3000 mVs^{-1}. Differential pulse voltammetries were performed with a scan rate of 20 mVs^{-1} (pulse height 75 mV). The IR compensation was used and every effort was made throughout the experiments in order to minimize the resistance of the solution. The electrochemical reversibility of the voltammetric wave of ferrocene was taken as an indicator of

the absence of uncompensated resistance effects. For reversible processes, the half-wave potential values ($E_{1/2}$) were obtained from the average of the cathodic and anodic cyclic voltammetric waves. For poorly reversible processes, the peak potential values (E_p) were estimated from the DPV peaks.

2. Synthetic procedures

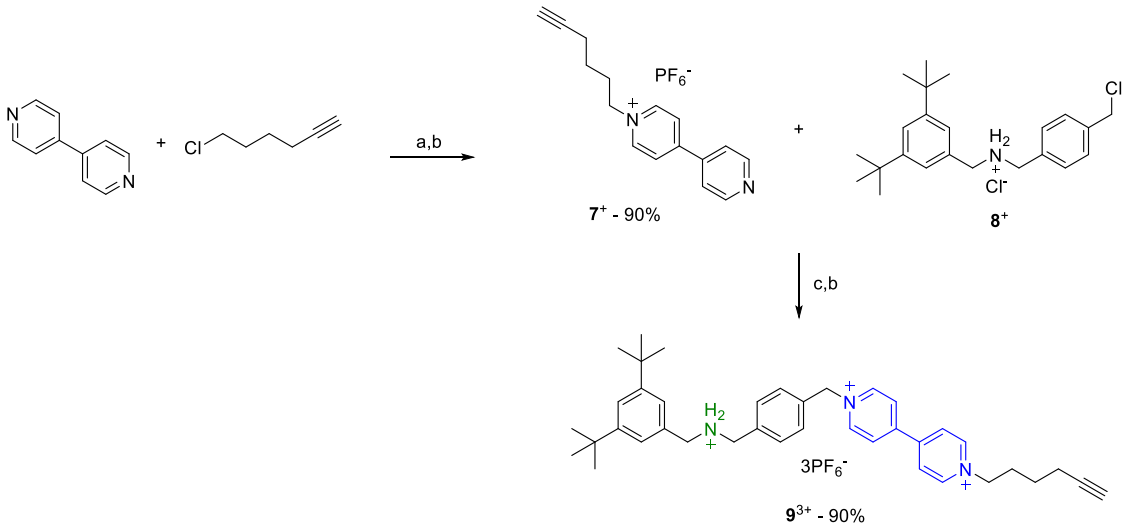

Scheme S1 – Synthetic steps to compound $\mathbf{9}^{3+}$. Conditions: a) DMF, 70°C, 7 days; b) NH_4PF_6, MeOH; c) CH_3CN, μW reactor, 110°C, 2.5 hours.

1-(hex-5-yn-1-yl)-[4,4'-bipyridin]-1-ium hexafluorophosphate (7^+)

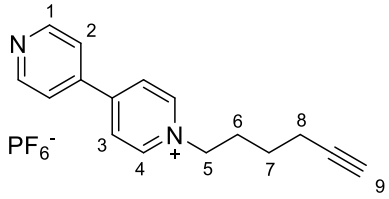

4-4'-dipyridyl (5.6 g, 0.036 mol) was dissolved in DMF (9 ml) and 6-chlorohexyne (4.2 ml, 0.035 mol) was added; the mixture was stirred at 70°C for 7 days. The precipitate formed was filtered and washed with CH_3CN. The solid was then dissolved in water and a saturated solution of NH_4PF_6 (aq) was added to precipitate the product as the hexafluorophosphate salt. The solid was filtered and dried under vacuum, to obtain the product as a white solid in 52% yield (7 g). ^{1}H NMR (500 MHz, DMSO-d_6, 298 K) δ= 9.32 (d, J = 6.8, 2H, H_4), 8.86 (d, J = 6.1, 2H, H_1), 8.67 (d, J = 6.8, 2H, H_3), 8.06 (d, J = 6.1, 2H, H_2), 4.71 (t, J = 7.3, 2H, H_5), 2.83 (t, J = 2.6, 1H, H_9), 2.24 (td,

J_1 = 7.1, J_2 = 2.60, 2H, H_8), 2.02-2.05 (m, 2H, H_6), 1.46-1.52 (m, 2H, H_7). ^{13}C NMR (125 MHz, DMSO-d_6, 298 K) δ= 152.3, 150.9, 145.3, 140.9, 125.5, 121.9, 83.8, 71.8, 59.8, 29.9, 24.5, 17.3.

1-(4-(((3,5-di-tert-butylbenzyl)ammonium)methyl)benzyl)-1'-(hex-5-yn-1-yl)-[4,4'-bipyridine]-1,1'-diium hexafluophosphate (9H^{3+})

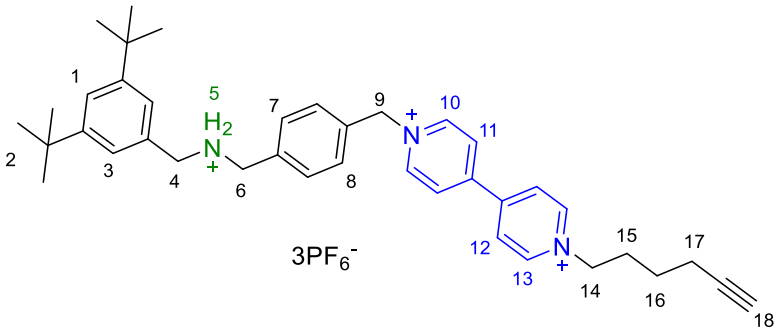

3,5-Di-tert-butylbenzyl-4-chloromethylbenzylammonium chloride (**8**$^+$) (1.15 g, 2.89 mmol) and compound **7**$^+$ (0.37 g, 0.96 mmol) were dissolved in CH_3CN (10 ml). The solution was irradiated in a microwave oven at 100°C for 2.5 hours. The solvent volume was reduced to half *via* rotary evaporation and the solution was added dropwise to diethyl ether (300 ml) to precipitate the product. The solid was recovered by centrifugation and dissolved in MeOH (10 ml). A saturated solution of NH_4PF_6 in MeOH was added to exchange the anion; the solvent volume was reduced and water was added to precipitate the product, which was filtered and dried under vacuum. The product was a white solid obtained in 68% yield (0.65 g). ^{1}H NMR (500 MHz, DMSO-d_6, 298 K) δ = 10.2 (bs, 2H, H_5), 9.75 (d, J = 6.3, 2H, H_{13}), 9.51 (d, J = 6.3, 2H, H_{10}), 8.90 (d, J = 6.3, 2H, H_{12}), 8.87 (d, J = 6.2, 2H, H_{11}), 7.71-7-76 (m, 4H, H_7+H_8), 7.47 (s, 2H, H_3), 7.37 (s, 1H, H_1), 6.10 (s, 2H, H_9), 4.79 (t, J = 7.0, 2H, H_{14}), 4.12 (s, 2H, H_4), 4.05 (s, 2H, H_6), 2.83 (s, 1H, H_{18}), 2.24 (t, J = 6.8, 2H, H_{17}), 2.02-2.08 (m, 2H, H_{15}), 1.46-1.51 (m, 2H, H_{16}), 1.27 (s, 18H, H_2). ^{13}C NMR (125 MHz, DMSO-d_6, 298 K) δ = 150.5, 149.1, 148.6, 145.8, 145.8, 134.7, 133.3, 131.1, 131.0, 129.1, 127.2, 126.8, 124.5, 122.1, 83.8, 71.8, 62.6, 60.2, 50.3, 49.2, 34.6, 31.2, 30.0, 24.4, 17.3.

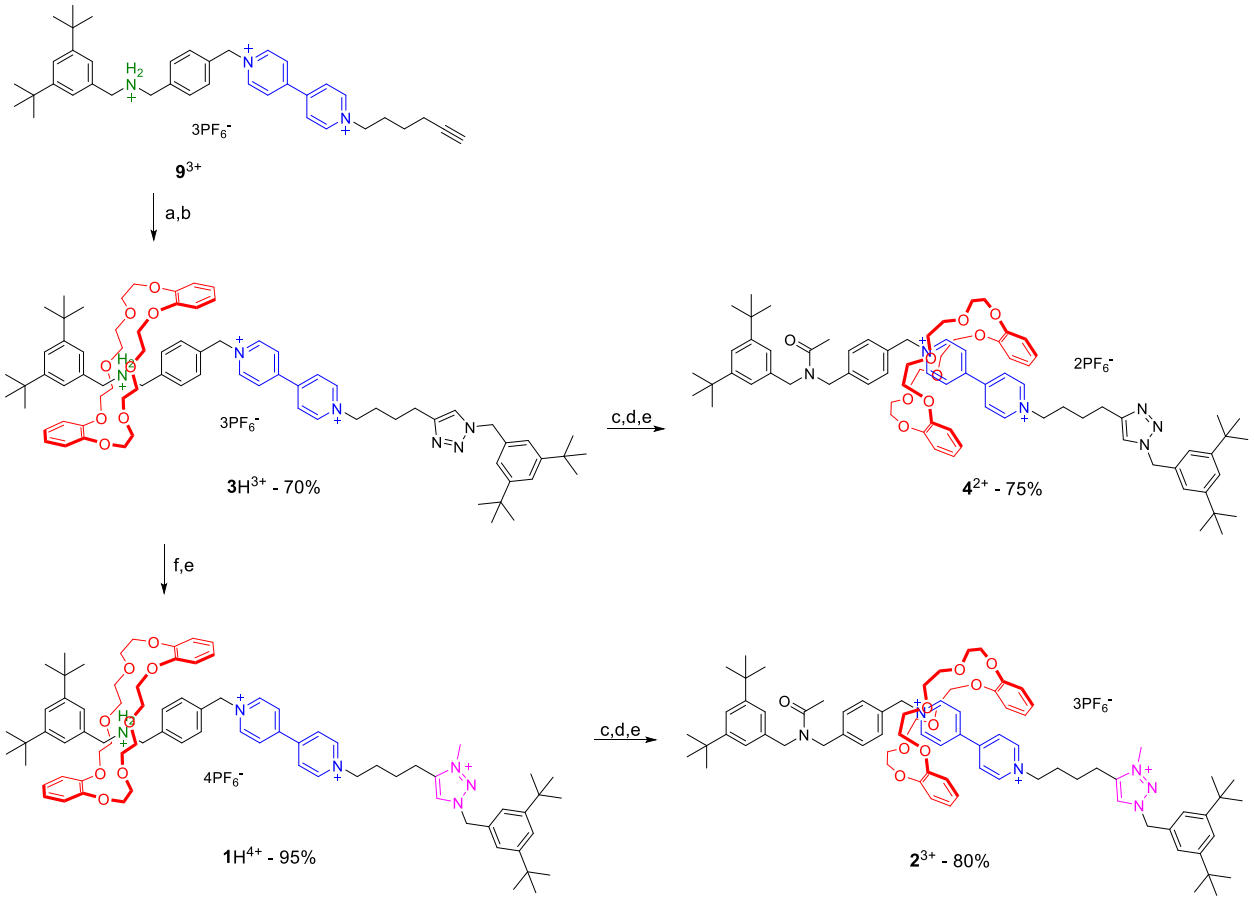

Scheme S2 – Synthetic steps to compounds **1**H^{4+}, **2**$^{3+}$, **3**H^{3+}, **4**$^{2+}$. Conditions: a) DB24C8, CH_2Cl_2, r.t., 1 hour; b) 3,5-di-tert-butylbenzylazide, $Cu(CH_3CN)_4PF_6$, CH_2Cl_2, N_2, r.t., 16 hours; c) $NaHCO_3$ (aq), DCM, r.t., 0.5 hours; d) Acetic anhydride, CH_2Cl_2, r.t., 48 hours; e) NH_4PF_6, MeOH; f) CH_3I, CH_2Cl_2, r.t., 48 hours.

Rotaxane 3H^{3+}

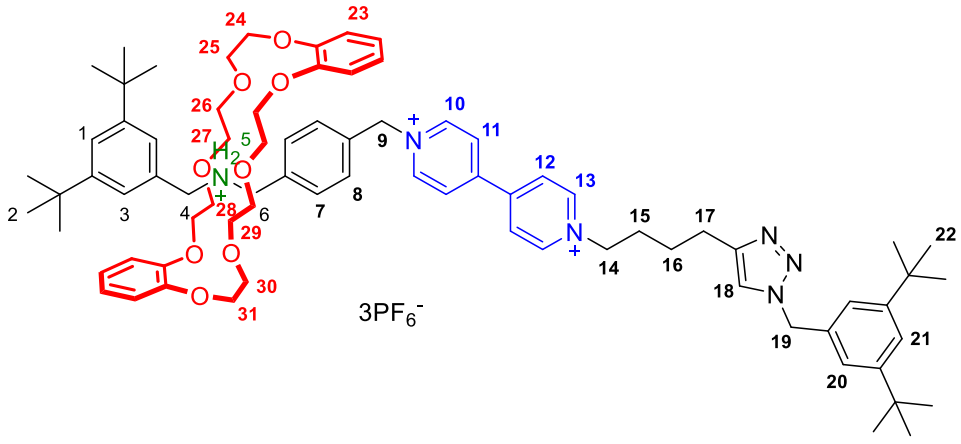

Compound **9**$^{3+}$ (0.50 g, 0.5 mmol) was dissolved in anhydrous DCM (130 ml) and DB24C8 (0.23, 0.5 mmol) was added. The solution was stirred for 2 hours to allow for the formation of the complex. Di-*tert*-butylbenzylazide (0.30 g, 1.2 mmol) was dissolved in anhydrous DCM (10 ml) and added to the stirring solution. The mixture was bubbled with nitrogen for 10 minutes, followed by the addition of $Cu(CH_3CN)_4PF_6$ (0.38 g, 1 mmol). The solution was stirred at room temperature for 16 hours under nitrogen atmosphere. The reaction solvent was removed and the product was purified over silica column (eluent: DCM:MeOH = 9:1). The product was a light yellow solid obtained in 70% yield (0.6 g). ^{1}H NMR (500 MHz, CD_2Cl_2, 298 K) δ= 8.85 (d, *J* = 6.5, 2H, H_{13}), 8.70 (d, *J* = 6.5, 2H, H_{10}), 8.35 (d, *J* = 5.0, 4H, H_{11}+H_{12}), 7.71 (bs, 2H, H_5), 7.42 (s, 2H, H_1+H_{18}) 7.38 (s, 1H, H_{21}), 7.31 (s, 2H, H_3), 7.28 (d, *J* = 8.0, 2H, H_7), 7.11 (s, 2H, H_{20}), 6.97 (d, *J* = 8.0, 2H, H_8), 6.84-6.71 (m, 8H, H_{23}), 5.53 (s, 2H, H_9), 5.41 (s, 2H, H_{19}), 4.72 (t, *J* = 6.2, 2H, H_6), 4.68-4.63 (m, 4H, H_4+H_{14}), 4.11-4.07 (m, 4H, H_{24}), 3.99-3.96 (m, 4H, H_{31}), 3.78-3.71 (m, 8H, H_{26}+H_{27}+H_{28}+H_{29}), 3.66-3.63 (m, 4H, H_{25}), 3.51-3.48 (m, 4H, H_{30}), 2.72 (t, *J* = 7.0, 2H, H_{17}), 2.06-2.12 (m, 2H, H_{15}), 1.74-1.76 (m, 2H, H_{16}), 1.26 (s, 18H, H_{22}), 1.21 (s, 18H, H_2). ^{13}C NMR (125 MHz, CD_2Cl_2, 298 K) δ= 152.1, 152.0, 151.1, 150.5, 145.7, 145.6, 134.7, 133.9, 132.5, 131.4, 130.9, 129.0, 127.9, 127.8, 123.9, 122.9, 122.8, 121.8, 112.7, 70.9, 70.5, 68.0, 64.8, 62.7, 35.2, 35.1, 31.5, 31.4. **HRMS (ESI+):** m/z calc. for $C_{78}H_{105}N_6O_8PF_6^{2+}$ $[M]^{2+}$: 700.3896, found: 700.3896.

Rotaxane 4^{2+}

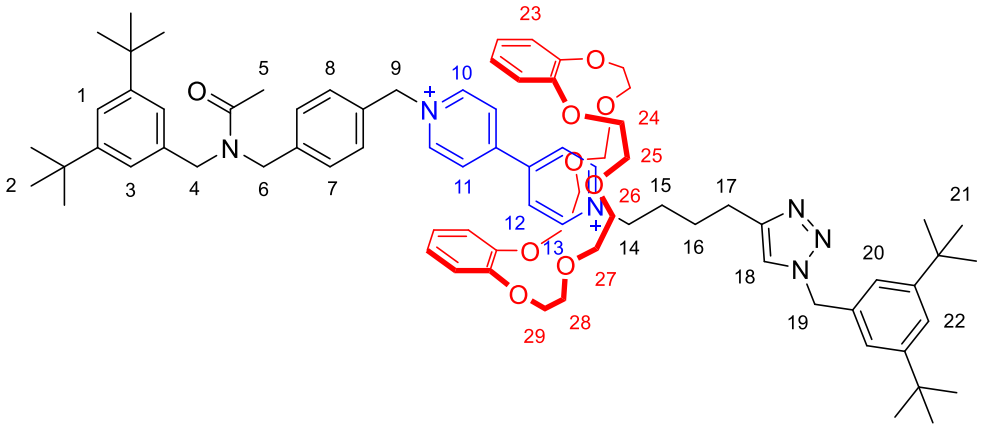

Rotaxane **3**H^{3+} (0.170 g, 0.1 mmol) was dissolved in DCM (15 ml) and a saturated solution of $NaHCO_3$ (aq) (15 ml) was layered onto it. The biphasic mixture was vigorously stirred for 30 minutes to allow for mixing of the two layers and deprotonation of the compound. The mixture was then transferred to a separating funnel and the organic layer recovered. The organic phase was further washed with H_2O (15 ml), dried over Na_2SO_4 and the solvent removed under vacuum to concentrate the solution to half of the volume. Acetic anhydride (5 ml) was added and the

solution was stirred at room temperature for 48 hours. The reaction solvent and excess anhydride were removed under vacuum. The solid obtained was dissolved in MeOH and a saturated solution of NH_4PF_6 in MeOH was added to exchange the anion; the solvent volume was reduced and water was added to precipitate the product, which was filtered and dried under vacuum. The product was purified by size exclusion chromatography. The product was a dark yellow solid obtained in 75% yield (0.12 g). ^{1}H NMR (500 MHz, CD_2Cl_2, 298 K) δ= 9.24 (d, *J* = 5.5, 2H, H_{13}), 8.95 (d, *J* = 5.5, 2H, $H_{10\text{-minor isom.}}$), 8.90 (d, *J* = 6.2, 2H, $H_{10\text{-major isom.}}$), 7.83 (d, *J* = 6.3, 2H, H_{12}), 7.68 (d, *J* = 5.9, 2H, H_{12}), 7.52 (d, *J* = 8.0, 2H, $H_{8\text{-minor isom.}}$), 7.46-7.43 (m, 4H, $H_{8\text{-major isom.}}$+H_{18}+H_{22}), 7.36 (s, 1H, $H_{1\text{-major isom.}}$), 7.33 (s, 1H, $H_{1\text{-minor isom.}}$), 7.31 (d, *J* = 8.0, 2H, $H_{7\text{-major isom.}}$), 7.26 (d, *J* = 7.9, 2H, $H_{7\text{-minor isom.}}$), 7.15 (s, 2H, H_{20}), 7.02 (s, 2H, $H_{3\text{-minor isom.}}$), 6.98 (s, 2H, $H_{3\text{-major isom.}}$), 6.68-6.62 (m, 8H, H_{23}), 5.81 (s, 2H, $H_{9\text{-minor isom.}}$), 5.77 (s, 2H, $H_{9\text{-major isom.}}$), 5.46 (s, 2H, H_{19}), 4.80 (t, *J* = 8.1, 2H, H_{14}), 4.57 (s, 2H, $H_{6\text{-major isom.}}$), 4.55 (s, 2H, $H_{6\text{-minor isom.}}$), 4.48 (s, 2H, $H_{4\text{-major isom.}}$), 4.47 (s, 2H, $H_{4\text{-minor isom.}}$), 4.04-4.01 (m, 4H, H_{29}), 3.92-3.87 (m, 4H, H_{24}), 3.82-3.79 (m, 4H, H_{28}), 3.73-3.70 (m, 4H, H_{25}), 3.58 (s, 8H, H_{26}+H_{27}), 2.76 (t, *J* = 7.4, 2H, H_{17}), 2.29-2.23 (m, 2H, H_{15}), 2.20 (s, 3H, $H_{5\text{-major isom.}}$), 2.15 (s, 3H, $H_{5\text{-minor isom.}}$), 1.80-1.73 (m, 2H, H_{17}), 1.29-1.28 (m, 54H, $H_{2\text{-major isom.}}$+$H_{2\text{-minor isom.}}$+H_{21}). ^{13}C NMR (125 MHz, CD_2Cl_2, 298 K) δ= 171.6, 171.2, 152.2, 152.0, 151.5, 150.8, 148.6, 147.5, 147.2, 145.6, 145.4, 140.8, 139.9, 136.7, 135.8, 134.2, 130.8, 130.4, 129.4, 128.0, 127.0, 126.8, 124.5, 124.4, 123.2, 122.9, 122.6, 122.0, 121.8, 121.6, 121.0, 112.5, 71.2, 70.4, 68.4, 65.1, 65.0, 61.8, 55.4, 52.4, 51.0, 49.1, 48.4, 35.1, 35.0, 31.5, 29.5, 26.7, 25.4, 21.9, 21.8. **HRMS (ESI+):** m/z calc. for $C_{80}H_{106}N_6O_9PF_6^+$ $[M]^+$: 1439.7664, found: 1439.7664.

Rotaxane 1H^{4+}

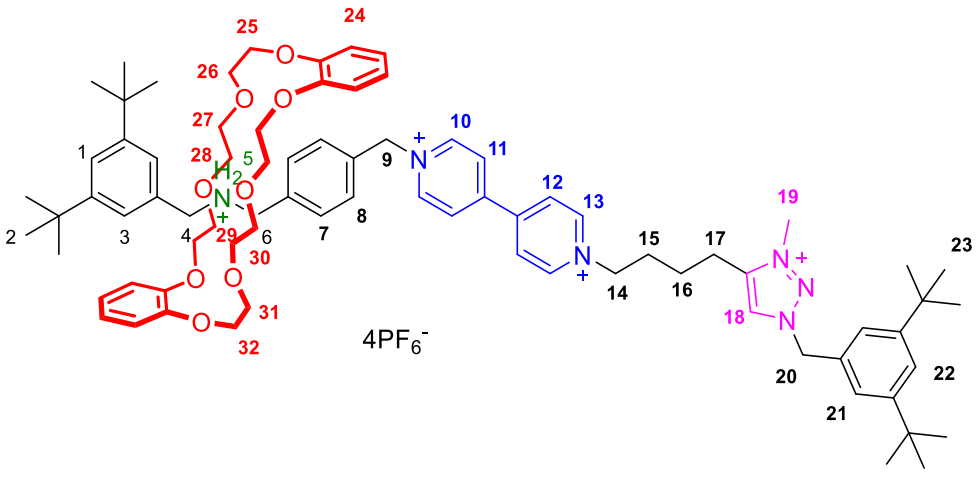

Rotaxane **3**H^{3+} (0.6 g, 0.35 mmol) was dissolved in CH_3I (10 ml) and the solution was left stirring at room temperature for 48 hours. The excess CH_3I was removed under vacuum and the crude

was dissolved in MeOH. A saturated solution of NH_4PF_6 was added to exchange the anion. The solvent volume was reduced and H_2O was added to precipitate the product, which was then filtered and dried under vacuum. The product was purified by size exclusion chromatography to obtain a light yellow solid in 95% yield (0.61 g). ^{1}H NMR (500 MHz, CD_2Cl_2, 298 K) δ= 8.82 (d, *J* = 6.5, 2H, H_{13}), 8.69 (d, *J* = 6.5, 2H, H_{10}), 8.31 (d, *J* = 6.6, 2H, H_{11}), 8.27 (d, *J* = 6.5, 4H, H_{12}), 8.14 (s, 1H, H_{18}), 7.71 (bs, 2H, H_5), 7.47 (s, 1H, H_{21}), 7.42 (s, 1H, H_1), 7.31 (s, 2H, H_3), 7.28-7.27 (m, 4H, H_7+H_{21}), 6.96 (d, *J* = 8.0, 2H, H_8), 6.84-6.71 (m, 8H, H_{24}), 5.53 (bs, 4H, H_9+H_{20}), 4.73 (t, *J* = 6.2, 2H, H_6), 4.68-4.64 (m, 4H, H_4+H_{14}), 4.12 (s, 3H, H_{19}), 4.11-4.07 (m, 4H, H_{25}), 3.99-3.96 (m, 4H, H_{32}), 3.78-3.71 (m, 8H, H_{27}+H_{28}+H_{29}+H_{30}), 3.66-3.63 (m, 4H, H_{26}), 3.51-3.48 (m, 4H, H_{31}), 2.85 (t, *J* = 7.4, 2H, H_{17}), 2.16-2.11 (m, 2H, H_{15}), 1.82-1.76 (m, 2H, H_{16}), 1.28 (s, 18H, H_{23}), 1.21 (s, 18H, H_2). ^{13}C NMR (125 MHz, CD_2Cl_2, 298 K) δ= 152.7, 152.1, 151.6, 150.6, 147.6, 145.7, 145.6, 144.1, 133.9, 132.5, 131.4, 130.9, 130.4, 129.0, 127.9, 127.8, 124.4, 124.0, 123.9, 121.8, 112.7, 70.9, 70.6, 68.0, 64.8, 62.3, 58.4, 52.3, 37.8, 35.2, 35.1, 31.4, 30.3, 23.3, 22.7. **HRMS (ESI+):** m/z calc. for $C_{79}H_{108}N_6O_8P_3F_{18}^+$ $[M]^+$: 1703.7155, found: 1703.7155.

Rotaxane 2^{3+}

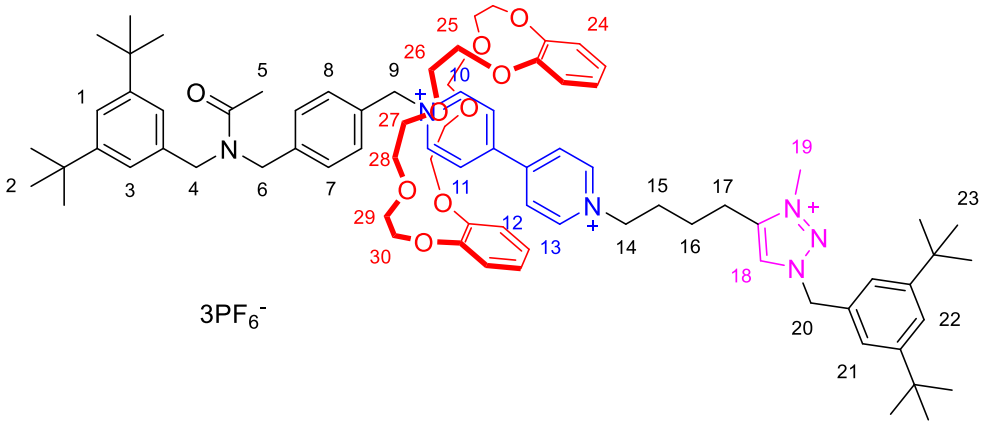

Rotaxane **1**H^{4+} (0.270 g, 0.15 mmol) was dissolved in DCM (20 ml) and a saturated solution of $NaHCO_3$ (aq) (20 ml) was layered onto it. The biphasic mixture was vigorously stirred for 30 minutes to allow for mixing of the two layers and deprotonation of the compound. The mixture was then transferred to a separating funnel and the organic layer recovered. The organic phase was further washed with H_2O (20 ml), dried over Na_2SO_4 and the solvent removed under vacuum to concentrate the solution to half of the volume. Acetic anhydride (5 ml) was added and the solution was stirred at room temperature for 48 hours. The reaction solvent and excess anhydride were removed under vacuum. The solid obtained was dissolved in MeOH and a saturated solution of NH_4PF_6 in MeOH was added to exchange the anion; the solvent volume was reduced and H_2O

was added to precipitate the product, which was filtered and dried under vacuum. The product was purified by size exclusion chromatography. The product was a dark yellow solid obtained in 80% yield (0.2 g). ^{1}H NMR (500 MHz, CD_2Cl_2, 298 K) δ= 9.37 (d, *J* = 5.9, 2H, $H_{10\text{-minor isom.}}$), 9.27 (d, *J* = 6.2, 2H, $H_{10\text{-major isom.}}$), 8.97 (d, *J* = 5.1, 2H, H_{13}), 8.13 (s, 1H, $H_{18\text{-minor isom.}}$), 8.11 (s, 1H, $H_{18\text{-major isom.}}$), 7.99-7.96 (m, 4H, $H_{11\text{-major isom.}}$+ $H_{11\text{-minor isom.}}$), 7.89-7.85 (m, *4*H, $H_{12\text{-major isom.}}$+ $H_{12\text{-minor isom.}}$), 7.58 (d, *J* = 8.0, 2H, $H_{8\text{-minor isom.}}$), 7.51 (s, 1H, H_{22}), 7.50 (d, *J* = 8.0, 2H, $H_{8\text{-major isom.}}$), 7.35 (s, 1H, $H_{1\text{-major isom.}}$), 7.33 (s, 1H, $H_{1\text{-minor isom.}}$), 7.31 (s, 2H, H_{21}), 7.21 (d, *J* = 7.9, 2H, $H_{7\text{-major isom.}}$), 7.15 (d, *J* = 7.8, 2H, $H_{7\text{-minor isom.}}$), 7.00 (s, 2H, $H_{3\text{-minor isom.}}$), 6.96 (s, 2H, $H_{3\text{-major isom.}}$), 6.77-6.68 (m, 8H, H_{24}), 5.94 (s, 2H, $H_{9\text{-minor isom.}}$), 5.88 (s, 2H, $H_{9\text{-major isom.}}$), 5.59 (s, 2H, H_{20}), 4.70-4-66 (m, 4H, $H_{14\text{-minor isom.}}$+ $H_{14\text{-major isom.}}$), 4.51 (s, 2H, $H_{6\text{-minor isom.}}$), 4.49 (s, 2H, $H_{6\text{-major isom.}}$), 4.45 (s, 2H, $H_{4\text{-major isom.}}$), 4.38 (s, 2H, $H_{4\text{-minor isom.}}$), 4.12 (s, 3H, H_{19}), 3.99 (bs, 8H, H_{25}+H_{30}), 3.76-3.68 (m, 8H, H_{26}+H_{29}), 3.43 (s, 8H, H_{27}+H_{28}), 2.80 (m, 2H, H_{17}), 2.19 (bs, 5H, H_{15}+ $H_{5\text{-major isom.}}$), 2.14 (s, 3H, $H_{5\text{-minor isom.}}$), 1.78-1.74 (m, 2H, H_{17}), 1.31 (s, 18H, H_{23}), 1.29 (s, 18H, $H_{2\text{-major isom.}}$), 1.28 (s, 18H, $H_{2\text{-minor isom.}}$). ^{13}C NMR (125 MHz, CD_2Cl_2, 298 K) δ= 171.3, 170.9, 152.8, 151.9, 151.5, 150.7, 150.4, 147.6, 147.2, 146.7, 145.8, 145.7, 144.3, 144.2, 140.3, 139.2, 136.7, 135.9, 131.4, 131.0, 130.8, 130.7, 128.9, 128.2, 128.1, 127.5, 126.7, 126.6, 125.9, 125.6, 124.6, 122.5, 122.0, 121.8, 121.0, 112.5, 112.3, 71.4, 71.3, 70.5, 70.4, 66.0, 64.6, 64.4, 64.3, 61.7, 61.6, 58.7, 52.4, 51.0, 49.0, 48.4, 37.8, 35.2, 35.1, 35.0, 31.5, 31.4, 31.0, 29.8, 23.7, 23.6, 23.0, 22.0, 21.8. **HRMS (ESI+):** m/z calc. for $C_{81}H_{109}N_6O_9P_2F_{12}^+$ $[M]^+$: 1599.7539, found: 1599.7539.

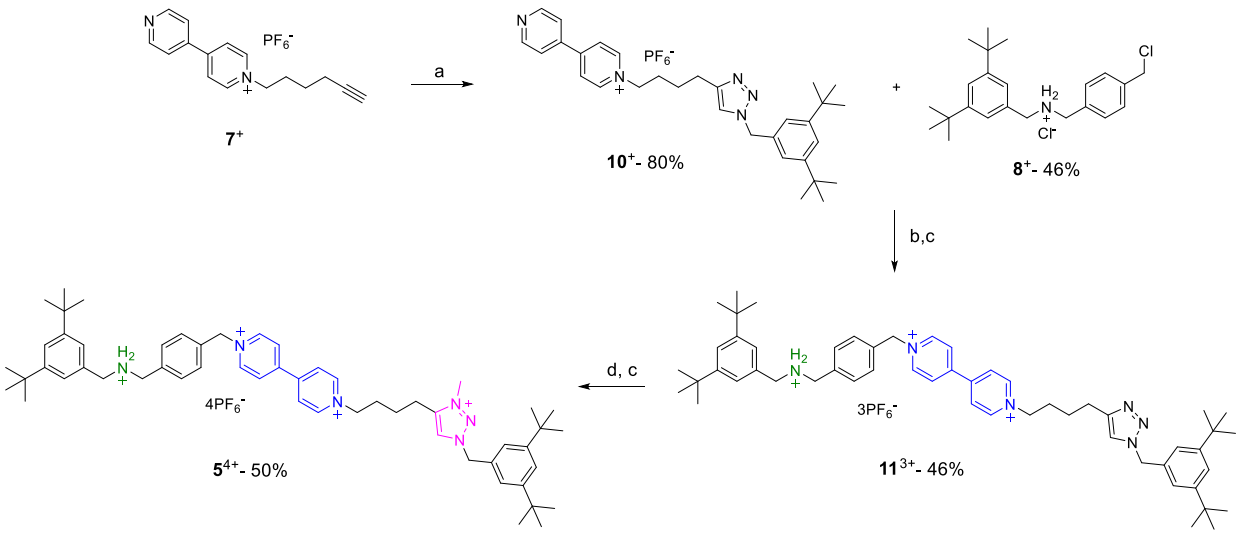

Scheme S3 - Synthetic steps to compound **5**$^{4+}$. Conditions: a) 3,5-di-tert-butylbenzylazide, $Cu(CH_3CN)_4PF_6$, μW reactor, DMF, 100°C, 3 hours; b) μW reactor, CH_3CN, 110°C, 2.5 hours; c) NH_4PF_6, MeOH; d) CH_3I, CH_3CN, r.t., 48 hours.

1-(4-(1-(3,5-di-tert-butylbenzyl)-1H-1,2,3-triazol-4-yl)butyl)-[4,4'-bipyridin]-1-ium hexafluorophosphate (10^+)

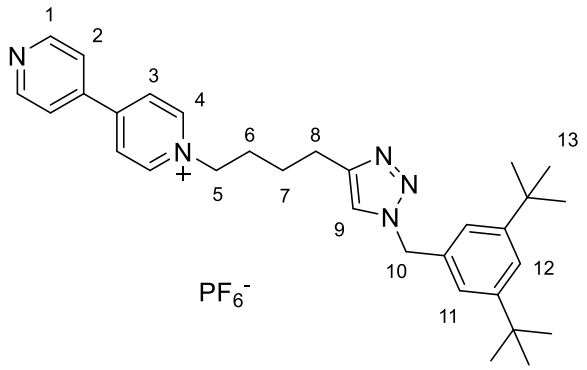

Compound 7^+ (1.0 g, 2.6 mmol) and di-tert-butylbenzylazide (0.740 g, 3 mmol) were dissolved in DMF (15 ml) and the catalyst $Cu(CH_3CN)_4PF_6$ (0.560 g, 1.5 mmol) was added. The reaction mixture was irradiated in the microwave reactor at 100°C for 3 hours. The solution was diluted with EDTA (aq, 25 mM) (100 ml) and the crude product extracted with DCM (2x100 ml). The organic phase was further washed with EDTA (aq, 25 mM) (100 ml) and H_2O (100 ml), dried over Na_2SO_4 and the solvent removed under vacuum. The product was purified over silica column (Eluent: DCM:MeOH = 9:1, then DCM:MeOH = 8:2) to obtain a white solid in 80% yield (1.3 g). ^{1}H NMR (500 MHz, DMSO-d_6, 298 K) δ= 9.22 (d, *J* = 6.8, 2H, H_4), 8.87 (d, *J* = 6.1, 2H, H_1), 8.63 (d, *J* = 6.8, 2H, H_3), 8.03 (d, *J* = 6.1, 2H, H_2), 7.93 (s, 1H, H_9), 7.33 (s, 1H, H_{12}), 7.09 (s, 2H, H_{11}), 5.50 (s, 2H, H_{10}), 4.66 (t, *J* = 7.3, 2H, H_5), 2.68 (t, *J* = 7.5, 2H, H_8), 2.03-1.97 (m, 2H, H_6), 1.66-1.60 (m, 2H, H_7), 1.23 (s, 18H, H_{13}). ^{13}C NMR (125 MHz, DMSO-d_6, 298 K) δ= 152.4, 151.0, 150.7, 146.4, 145.3, 140.9, 135.4, 125.4, 122.1, 121.9, 121.8, 121.6, 60.1, 53.2, 34.5, 30.3, 25.5, 24.3

1-(4-(1-(3,5-di-tert-butylbenzyl)-1H-1,2,3-triazol-4-yl)butyl)-1'-(4-(((3,5-di-tert-butylbenzyl)ammonio)methyl)benzyl)-[4,4'-bipyridine]-1,1'-diium hexafluorophosphate (11^{3+})

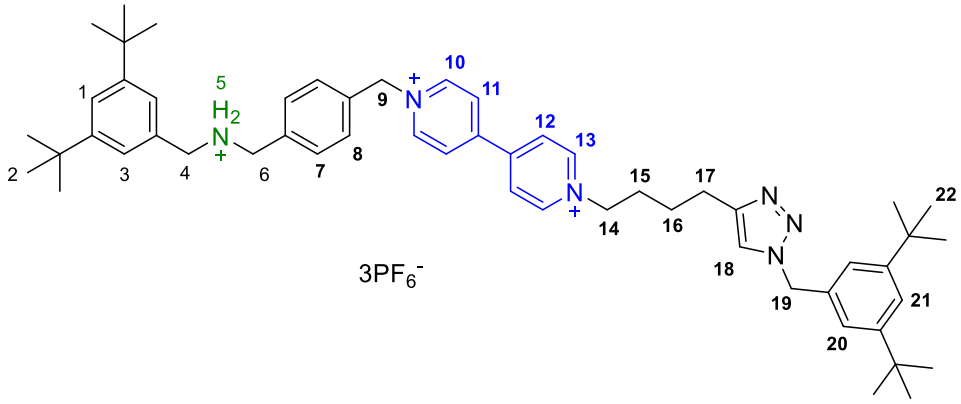

Compound 8^+ (0.84 g, 2.13 mmol) and compound **10**$^+$ (0.27 g, 0.42 mmol) were dissolved in CH_3CN (10 ml). The solution was irradiated in a microwave oven at 100°C for 2.5 hours. The reaction solvent was removed *via* rotary evaporation and the solid was dissolved in MeOH (10 ml). A saturated solution of NH_4PF_6 in MeOH was added to exchange the anion. The solvent was removed and the crude residue suspended in DCM (50 ml). The organic phase was washed with H_2O (2x50 ml), dried over Na_2SO_4 and the solvent removed. The product was purified over silica column (Eluents: DCM:MeOH= 9:1, then NH_4PF_6 in CH_3CN (5 mg/ml)). The solid obtained was washed with H_2O to remove the excess of NH_4PF_6 salt, filtered and dried under vacuum. The product was a white solid obtained in 46% yield (0.24 g). ^{1}H NMR (500 MHz, DMSO-d_6, 298 K) δ = 9.48 (d, *J* = 6.7, 2H, H_{13}), 9.36 (d, *J* = 6.7, 2H, H_{10}), 9.16 (bs, 2H, H_5), 8.76 (d, *J* = 6.8, 2H, H_{12}), 8.72 (d, *J* = 6.7, 2H, H_{11}), 7.93 (s, 1H, H_{18}), 7.67 (d, *J* = 8.1, 2H, H_8), 7.58 (d, *J* = 8.0, 2H, H_7), 7.44 (s, 1H, H_1), 7.33 (s, 1H, H_{21}), 7.29 (s, 2H, H_3), 7.10 (s, 2H, H_{20}), 5.95 (s, 2H, H_9), 5.50 (s, 2H, H_{19}), 4.71 (t, *J* = 7.2, 2H, H_{14}), 4.23 (bs, 2H, H_4), 4.15 (bs, 2H, H_6), 2.68 (t, *J* = 7.5, 2H, H_{17}), 2.05-2.00 (m, 2H, H_{15}), 1.66-1.60 (m, 2H, H_{16}), 1.28 (s, 18H, H_2), 1.23 (s, 18H, H_{22}). ^{13}C NMR (125 MHz, CD_3CN, 298 K) δ = 152.9, 152.5, 151.63, 150.8, 146.7, 146.5, 136.4, 135.0, 133.3, 132.4, 132.1, 130.8, 130.5, 130.2, 128.5, 128.4, 128.3, 125.4, 124.8, 124.4, 123.4, 123.3, 122.6, 65.1, 62.8, 54.8, 53.1, 51.7, 35.5, 31.6, 31.5, 31.4, 26.4, 25.3, 23.7, 23.4.

1-(4-(1-(3,5-di-tert-butylbenzyl)-3-methyl-1H-1,2,3-triazol-3-ium-4-yl)butyl)-1'-(4-(((3,5-di-tert-butylbenzyl)ammonio)methyl)benzyl)-[4,4'-bipyridine]-1,1'-diium hexafluorophosphate (5^{4+})

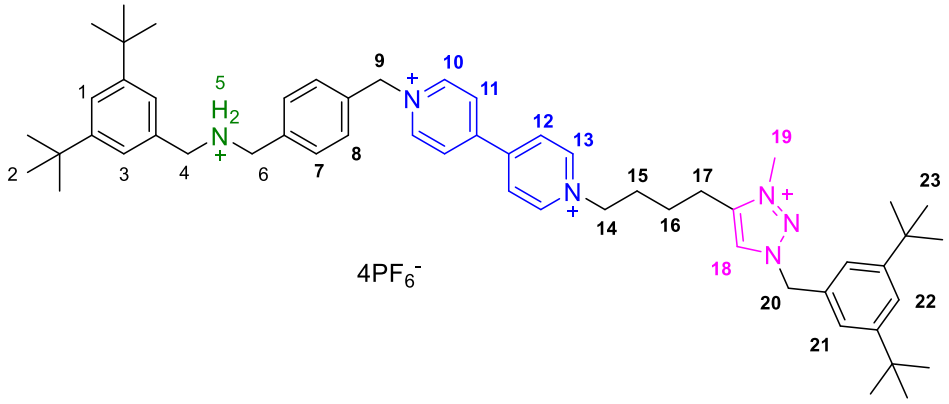

Compound **11**$^{3+}$ (0.1 g, 0.82 mmol) was dissolved in CH_3I (5 ml) and the solution was left stirring at room temperature for 48 hours. The excess CH_3I was removed under vacuum and the crude was dissolved in MeOH. A saturated solution of NH_4PF_6 was added to exchange the anion. The solvent volume was reduced and H_2O was added to precipitate the product, which was then filtered and dried under vacuum. The product was purified by size exclusion chromatography to obtain a white solid in 50% yield (0.07 g). ^{1}H NMR (500 MHz, CD_3CN, 298 K) δ = 8.97 (d, *J* = 6.7, 2H, H_{13}), 8.90 (d, *J* = 6.7, 2H, H_{10}), 8.41-8.39 (m, 4H, H_{11}+H_{12}), 8.18 (s, 1H, H_{18}), 7.69 (bs, 2H, H_5), 7.61 (d, *J* = 8.2, 2H, H_8), 7.56-7.52 (m, 4H, H_7+ H_1+ H_{21}), 7.34 (d, *J* = 1.7, 2H, H_3), 7.31 (d, *J* = 1.7, 2H, H_{20}), 5.85 (s, 2H, H_9), 5.63 (s, 2H, H_{19}), 4.64 (t, *J* = 7.2, 2H, H_{14}), 4.24 (bs, 2H, H_4), 4.19 (bs, 2H, H_6), 4.11 (s, 3H, H_{19}), 2.85 (t, *J* = 7.7, 2H, H_{17}), 2.13-2.07 (m, 2H, H_{15}), 1.81-1.73 (m, 2H, H_{16}), 1.32 (s, 18H, H_2), 1.31 (s, 18H, H_{22}). ^{13}C NMR (125 MHz, CD_3CN, 298 K) δ = 153.1, 152.8, 151.5, 150.9, 146.7, 146.6, 145.1, 134.9, 133.5, 132.4, 132.3, 130.7, 128.7, 128.5, 128.3, 125.5, 125.4, 124.8, 124.6, 124.5, 65.1, 62.3, 58.4, 52.9, 51.5, 38.5, 35.6, 31.6, 31.5, 30.9, 24.0, 23.2. **HRMS (ESI+):** m/z calc. for $C_{55}H_{76}N_6P_2F_{12}^{2+}$ $[M]^{2+}$: 556.2786, found: 556.2786.

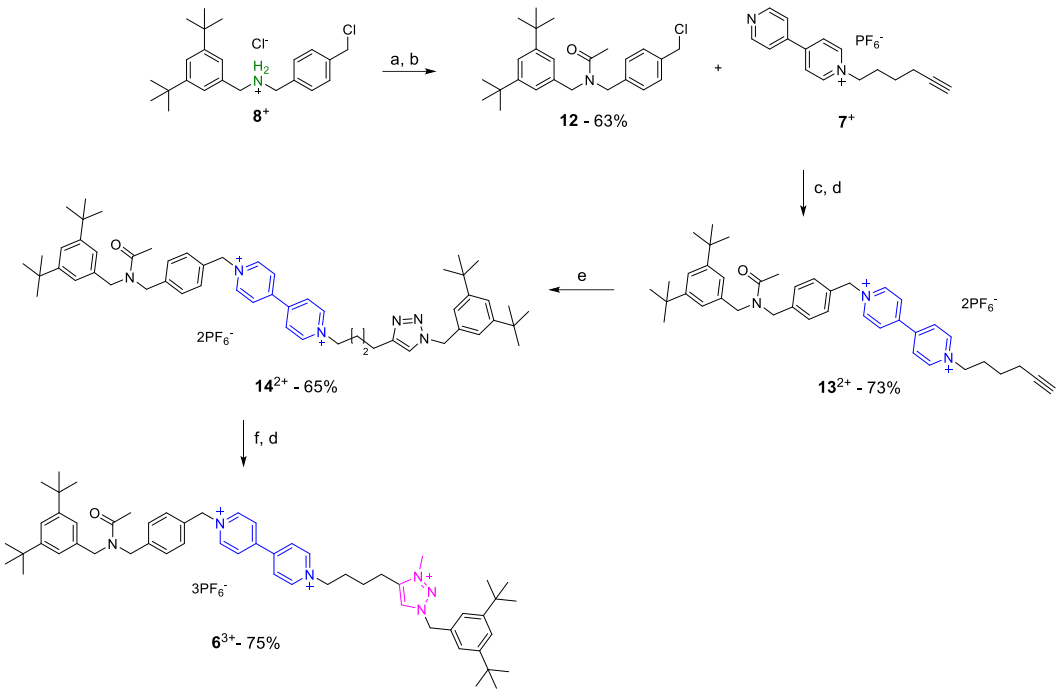

Scheme S4 - Synthetic steps to compound **6**$^{3+}$. Conditions: a) $NaHCO_3$ (aq), DCM, r.t., 0.5 hours; b) Acetic anhydride, CH_2Cl_2, r.t., 48 hours; c) μW reactor, CH_3CN, 110°C, 2.5 hours; d) NH_4PF_6, MeOH; e) 3,5-di-tert-butylbenzylazide, $Cu(CH_3CN)_4PF_6$, CH_2Cl_2, N_2, r.t., 16 hours; f) CH_3I, CH_3CN, r.t., 48 hours.

N-(4-(chloromethyl)benzyl)-N-(3,5-di-tert-butylbenzyl)acetamide (12)

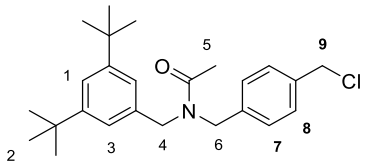

Compound **8**$^{+}$ (0.850 g, 2 mmol) was dissolved in ethyl acetate (100 ml) and the solution was washed with saturated $NaHCO_3$ (aq, 3x100 ml) to deprotonate the amine. The organic phase was dried over Na_2SO_4 and the solvent removed. The oil obtained was dissolved in DCM (20 ml) and acetic anhydride (10 ml) was added. The solution was stirred at room temperature for 24 hours. The solvent was removed and the product was purified over silica column (Eluent DCM:MeOH = 9:1), to obtain a colorless oil in 65% yield (0.51 g). ^{1}H NMR (500 MHz, $CDCl_3$, 298 K) δ = 7.38 (d, *J* = 8.0, 2H, $H_{8\text{-minor isom.}}$), 7.35 (d, *J* = 8.0, 2H, $H_{8\text{-major isom.}}$), 7.33 (s, 1H, $H_{1\text{-major isom.}}$+$H_{1\text{-minor isom.}}$), 7.23 (d, J = 8.0, 2H, $H_{7\text{-major isom.}}$), 7.14 (d, J = 8.0, 2H, $H_{7\text{-minor isom.}}$), 7.03 (s, 2H, $H_{3\text{-minor isom.}}$), 6.95 (s, 2H, $H_{3\text{-major isom.}}$), 4.59 (s, 4H, H_9+$H_{4\text{-minor isom.}}$), 4.44 (s, 2H, $H_{4\text{-minor isom.}}$), 4.44 (bs, 4H, $H_{4\text{-major isom.}}$+ $H_{4\text{-minor isom.}}$), 2.24 (s, 3H, $H_{5\text{-major isom.}}$), 2.20 (s, 3H, $H_{5\text{-minor isom.}}$), 1.31 (s, 18H, $H_{2\text{-major isom.}}$), 1.30 (s, 18H, $H_{2\text{-minor isom.}}$). ^{13}C NMR (125 MHz, $CDCl_3$, 298 K) d = 171.4, 171.1, 151.7, 151.2, 138.0,

137.2, 137.0, 136.7, 136.2, 135.5, 129.3, 129.0, 128.8, 126.9, 121.6, 51.80, 50.6, 48.8, 48.0, 46.1, 45.9, 35.0, 34.9, 31.6, 31.5, 27.1, 21.9, 21.8.

1-(4-((N-(3,5-di-tert-butylbenzyl)acetamido)methyl)benzyl)-1'-(hex-5-yn-1-yl)-[4,4'-bipyridine]-1,1'-diium hexafluorophosphate (13^{2+})

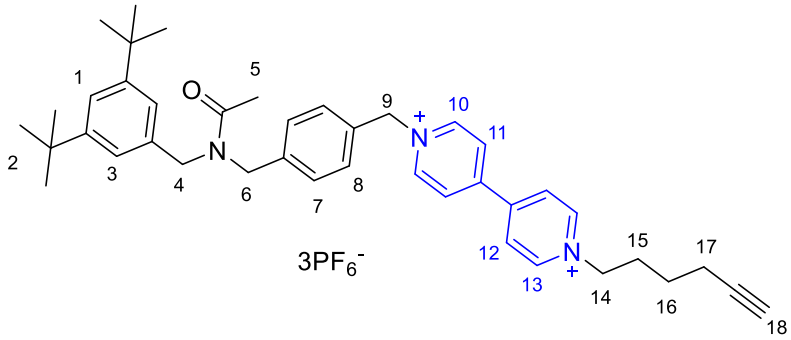

Compound **12** (0.510 g, 1.27 mmol) and compound $\mathbf{7}^{+}$ (0.110 g, 0.29 mmol) were dissolved in CH_3CN (10 ml). The solution was irradiated in a microwave oven at 100°C for 2.5 hours. The solvent volume was reduced to half *via* rotary evaporation and the solution was added dropwise to diethyl ether (300 ml) to precipitate the product. The solid was recovered by centrifugation and dissolved in MeOH (10 ml). A saturated solution of NH_4PF_6 in MeOH was added to exchange the anion and the solvent volume was reduced and water was added to precipitate the product, which was filtered and dried under vacuum. The product was further purified over silica column (Eluent: DCM:MeOH = 8:2, then NH_4PF_6 in CH_3CN (5 mg/ml)). The solid obtained was washed with H_2O to remove the excess of NH_4PF_6 salt, filtered and dried under vacuum. The product was a white solid obtained in 73% yield (0.19 g). ^{1}H NMR (500 MHz, DMSO-d_6, 298 K) δ = 9.47 (d, J = 6.5, 2H, H_{13}), 9.34 (d, J = 6.0, 2H, H_{10}), 8.75-8.70 (m, 4H, H_{11}+H_{12}), 7.59 (d, J = 8.0, 2H, $H_{8\text{-minor isom.}}$),7.55 (d, J = 8.0, 2H, $H_{8\text{-major isom.}}$), 7.30-7.24 (m, 5H, $H_{7\text{-minor isom.}}$+$H_{7\text{-major isom.}}$+$H_{1\text{-minor isom.}}$+$H_{1\text{-major isom.}}$), 7.28 (s, 2H, $H_{3\text{-minor isom.}}$), 6.94 (s, 2H, $H_{3\text{-major isom.}}$), 5.90 (s, 2H, $H_{9\text{-minor isom.}}$) 5.89 (s, 2H, $H_{9\text{-major isom.}}$), 4.70 (t, J = 7.1, 2H, H_{14}), 4.53 (s, 2H, H_4), 4.48 (s, 2H, $H_{6\text{-major isom.}}$), 4.45 (s, 2H, $H_{6\text{-minor isom.}}$), 2.82 (t, J = 2.3, 1H, H_{18}), 2.24 (td, J_1 = 6.95, J_2 = 2.30, 2H, H_{17}), 2.08-2.05 (m, 8H, $H_{5\text{-major isom.}}$+$H_{5\text{-minor isom.}}$+H_{15}), 1.52-1.46 (m, 2H, H_{16}), 1.22 (s, 18H, H_2). ^{13}C NMR (125 MHz, DMSO-d_6, 298 K) d = 170.6, 170.4, 150.7, 150.4, 149.3, 148.8, 145.7, 145.6, 139.8, 139.2, 136.7, 136.3, 132.6, 129.4, 129.1, 128.5, 128.0, 127.4, 127.2, 126.8, 121.9, 120.9, 120.7, 120.6, 109.6, 83.9, 71.9, 63.3, 63.2, 60.6, 52.1, 48.8, 48.3, 34.5, 34.4, 31.3, 31.2, 30.0, 24.5, 21.5, 17.3, 16.3.

1-(4-(1-(3,5-di-tert-butylbenzyl)-1H-1,2,3-triazol-4-yl)butyl)-1'-(4-((N-(3,5-di-tert-butylbenzyl) acetamido)methyl)benzyl)-[4,4'-bipyridine]-1,1'-diium hexafluorophosphate (14^{2+})

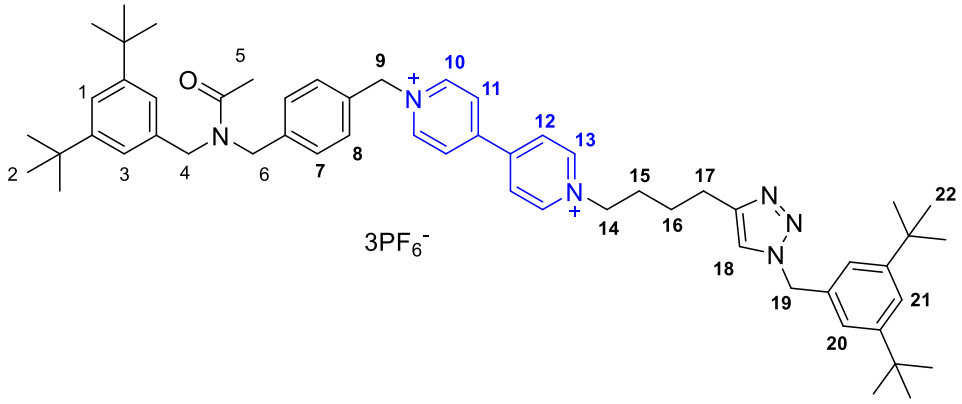

Compound **13**$^{2+}$ (0.187 g, 0.21 mmol) was dissolved in DCM (10 ml) and the solution was bubbled with N_2 for 15 minutes. Di-tert-butylbenzyl azide (0.11 g, 0.45 mmol) and $Cu(CH_3CN)_4PF_6$ (0.17 g, 0.45 mmol) were added and the reaction mixture was left stirring at room temperature for 48 hours under N_2 atmosphere. The product was purified over silica column (Eluent: CH_3CN, then NH_4PF_6 in CH_3CN (5 mg/ml)). The solid obtained was washed with H_2O to remove the excess of NH_4PF_6 salt, filtered and dried under vacuum. The product was a white solid obtained in 65% yield (0.16 g). ^{1}H NMR (500 MHz, DMSO-d_6, 298 K) δ = 9.48 (d, *J* = 6.5, 2H, H_{13}), 9.34 (d, *J* = 6.05, 2H, H_{10}), 8.75-8.70 (m, 4H, H_{11}+H_{12}), 7.92 (s, 1H, H_{18}), 7.58 (d, *J* = 8.0, 2H, $H_{8\text{-minor isom.}}$), 7.54 (d, *J* = 8.0, 2H, $H_{8\text{-major isom.}}$), 7.33-7.25 (m, 6H, $H_{7\text{-minor isom.}}$+$H_{7\text{-major isom.}}$+$H_{1\text{-minor isom.}}$+$H_{1\text{-major isom.}}$+H_{21}), 7.10 (s, 2H, H_{20}), 7.00 (s, 2H, $H_{3\text{-minor isom.}}$), 6.95 (s, 2H, $H_{3\text{-major isom.}}$), 5.90 (s, 2H, $H_{9\text{-minor isom.}}$), 5.89 (s, 2H, $H_{9\text{-major isom.}}$), 5.50 (s, 2H, H_{19}), 4.71 (t, *J* = 7.15, 2H, H_{14}), 4.53 (s, 2H, H_4), 4.48 (s, 2H, $H_{6\text{-major isom.}}$), 4.46 (s, 2H, $H_{6\text{-minor isom.}}$), 2.69 (t, J_1 = 6.95, 2H, H_{17}), 2.09-2.01 (m, 8H, $H_{5\text{-major isom.}}$+$H_{5\text{-minor isom.}}$+H_{15}), 1.66-1.60 (m, 2H, H_{16}), 1.23 (s, 36H, H_2+H_{22}). ^{13}C NMR (125 MHz, DMSO-d_6, 298 K) δ = 170.6, 170.3, 150.8, 150.7, 150.3, 149.3, 148.7, 146.4, 145.7, 145.6, 139.8, 136.6, 136.3, 135.4, 132.6, 129.3, 129.0, 128.4, 127.4, 127.1, 126.8, 122.1, 121.9, 121.7, 120.8, 120.6, 63.3, 60.7, 53.2, 52.0, 50.6, 48.8, 48.2, 34.5, 34.4, 34.3, 31.2, 30.3, 25.5, 24.3, 21.4.

1-(4-(1-(3,5-di-tert-butylbenzyl)-3-methyl-1H-1,2,3-triazol-3-ium-4-yl)butyl)-1'-(4-((N-(3,5-di-tert-butylbenzyl)acetamido)methyl)benzyl)-[4,4'-bipyridine]-1,1'-diium hexafluorophosphate (6^{3+})

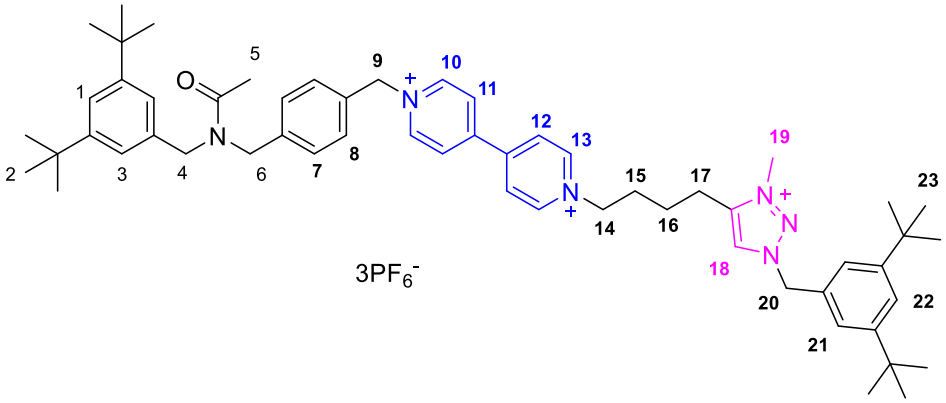

Compound **13**$^{2+}$ (0.16 g, 0.14 mmol) was dissolved in CH_3CN (0.5 ml) and CH_3I (5 ml) was added. The mixture was stirred at room temperature for 48 hours. The solvent and excess CH_3I were removed *via* rotary evaporation and the crude residue was dissolved in MeOH. A saturated solution of NH_4PF_6 in MeOH was added to exchange the anion; the solvent was removed. H_2O was added to the solid obtained to remove the excess of NH_4PF_6. The product was filtered and dried under vacuum, to obtain a white solid in 75 % yield (0.14 g). ^{1}H NMR (500 MHz, DMSO-d_6, 298 K) δ = 9.51 (d, *J* = 6.5, 2H, H_{13}), 9.33 (d, *J* = 6.0, 2H, H_{10}), 8.85 (s, 1H, H_{18}), 8.76-8.74 (m, 4H H_{11}+H_{12}), 7.60 (d, *J* = 8.0, 2H, $H_{8\text{-minor isom.}}$),7.56 (d, *J* = 8.0, 2H, $H_{8\text{-major isom.}}$), 7.44 (s, 1H, H_{22}), 7.33-7.26 (m, 7H, $H_{7\text{-minor isom.}}$+$H_{7\text{-major isom.}}$+$H_{1\text{-minor isom.}}$+$H_{1\text{-major isom.}}$+H_{21}), 7.00 (s, 2H, $H_{3\text{-minor isom.}}$), 6.95 (s, 2H, $H_{3\text{-major isom.}}$), 5.92 (s, 2H, $H_{9\text{-minor isom.}}$), 5.90 (s, 2H, $H_{9\text{-major isom.}}$), 5.78 (s, 2H, H_{20}), 4.71 (t, *J* = 7.0, 2H, H_{14}), 4.54 (s, 2H, H_4), 4.49 (s, 2H, $H_{6\text{-major isom.}}$), 4.46 (s, 2H, $H_{6\text{-minor isom.}}$), 4.20 (s, 3H, H_{19}), 2.90 (t, *J* = 7.5, 2H, H_{17}), 2.09-2.06 (m, 8H, $H_{5\text{-major isom.}}$+$H_{5\text{-minor isom.}}$+H_{15}), 1.76-1.70 (m, 2H, H_{16}), 1.27 (s, 18H, H_{23}), 1.24 (s, 18H, H_2). ^{13}C NMR (125 MHz, DMSO-d_6, 298 K) δ = 170.5, 170.2, 151.3, 150.6, 150.3, 149.0, 148.7, 145.7, 145.6, 143.8, 139.7, 139.2, 136.6, 136.3, 132.8, 132.6, 132.1, 129.3, 129.0, 128.4, 128.1, 127.3, 127.1, 126.6, 123.1, 122.9, 121.8, 120.8, 120.5, 63.3, 60.2, 56.6, 51.9, 50.5, 48.7, 48.2, 37.5, 34.6, 34.4, 34.3, 31.1, 29.7, 22.8, 21.8, 21.4. **HRMS (ESI+):** m/z calc. for $C_{57}H_{77}N_6OP_2F_{12}^+$ $[M]^+$: 1151.5442, found: 1151.5442.

3. NMR Spectra

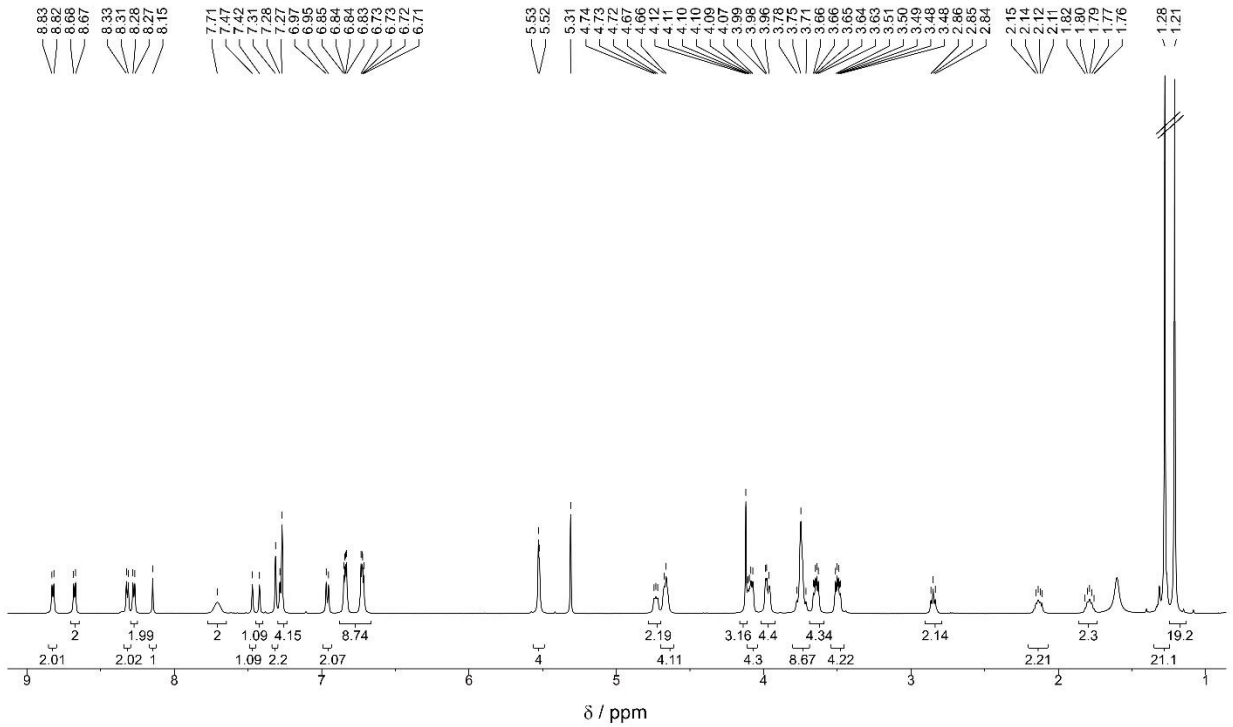

Figure S1 – ^{1}H NMR spectrum of compound **1**H^{4+} (500 MHz, CD_2Cl_2, 298 K).

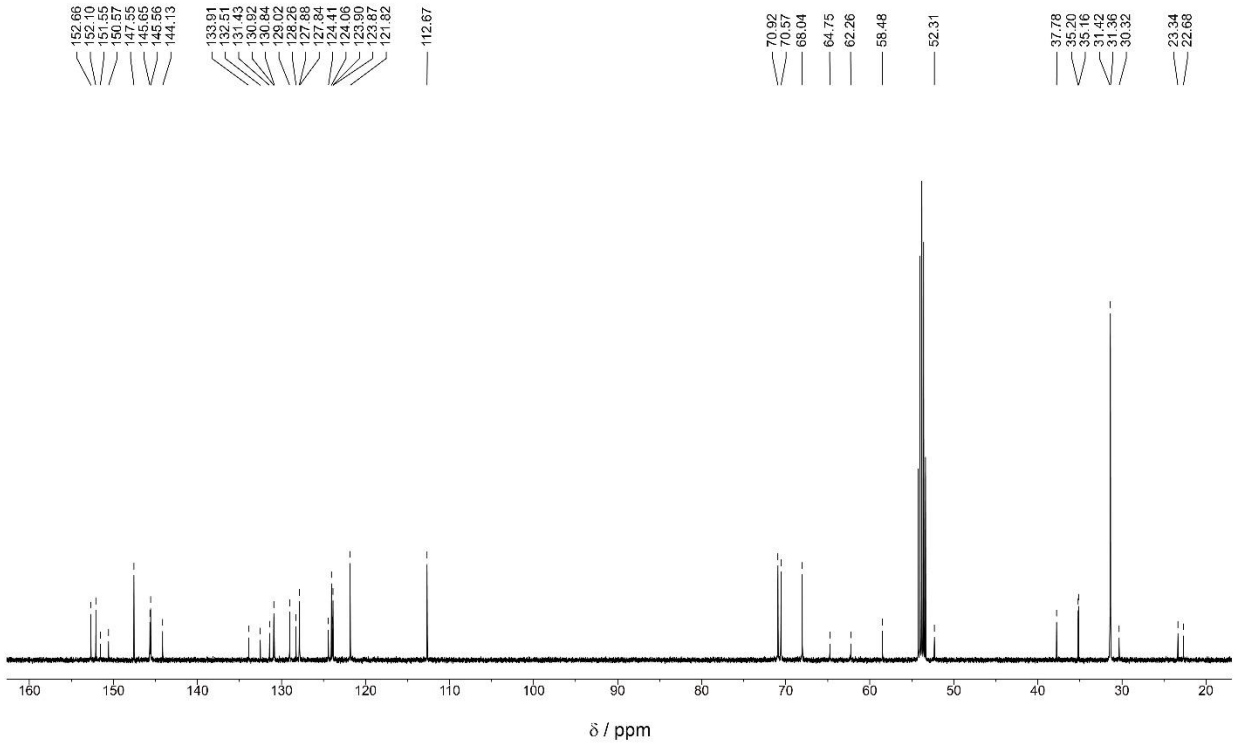

Figure S2 – ^{13}C NMR spectrum of compound **1**H^{4+} (125 MHz, CD_2Cl_2, 298 K).

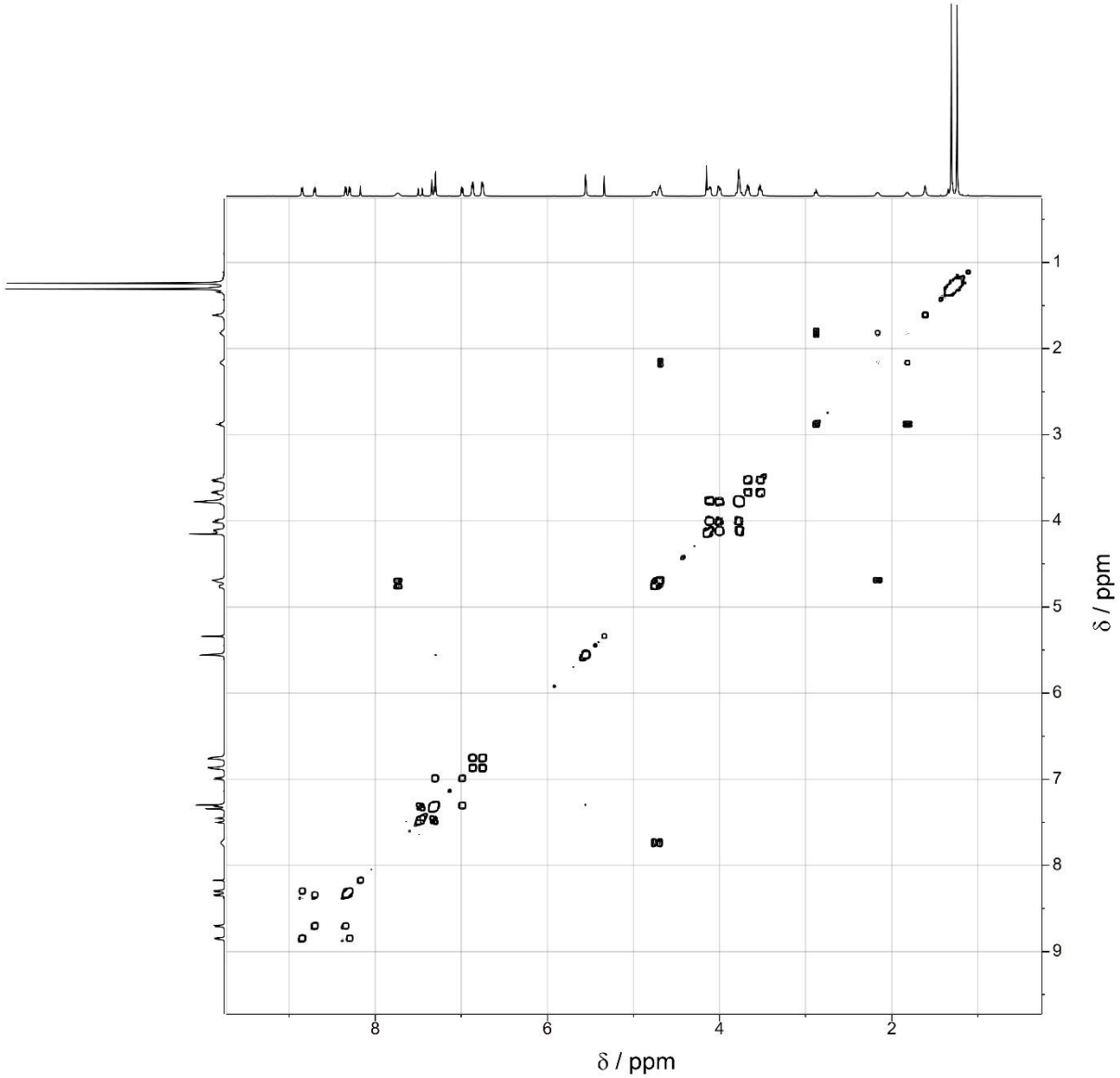

Figure S3 – ^{1}H-^{1}H COSY spectrum **1**H^{4+} (500 MHz, CD_2Cl_2, 298 K).

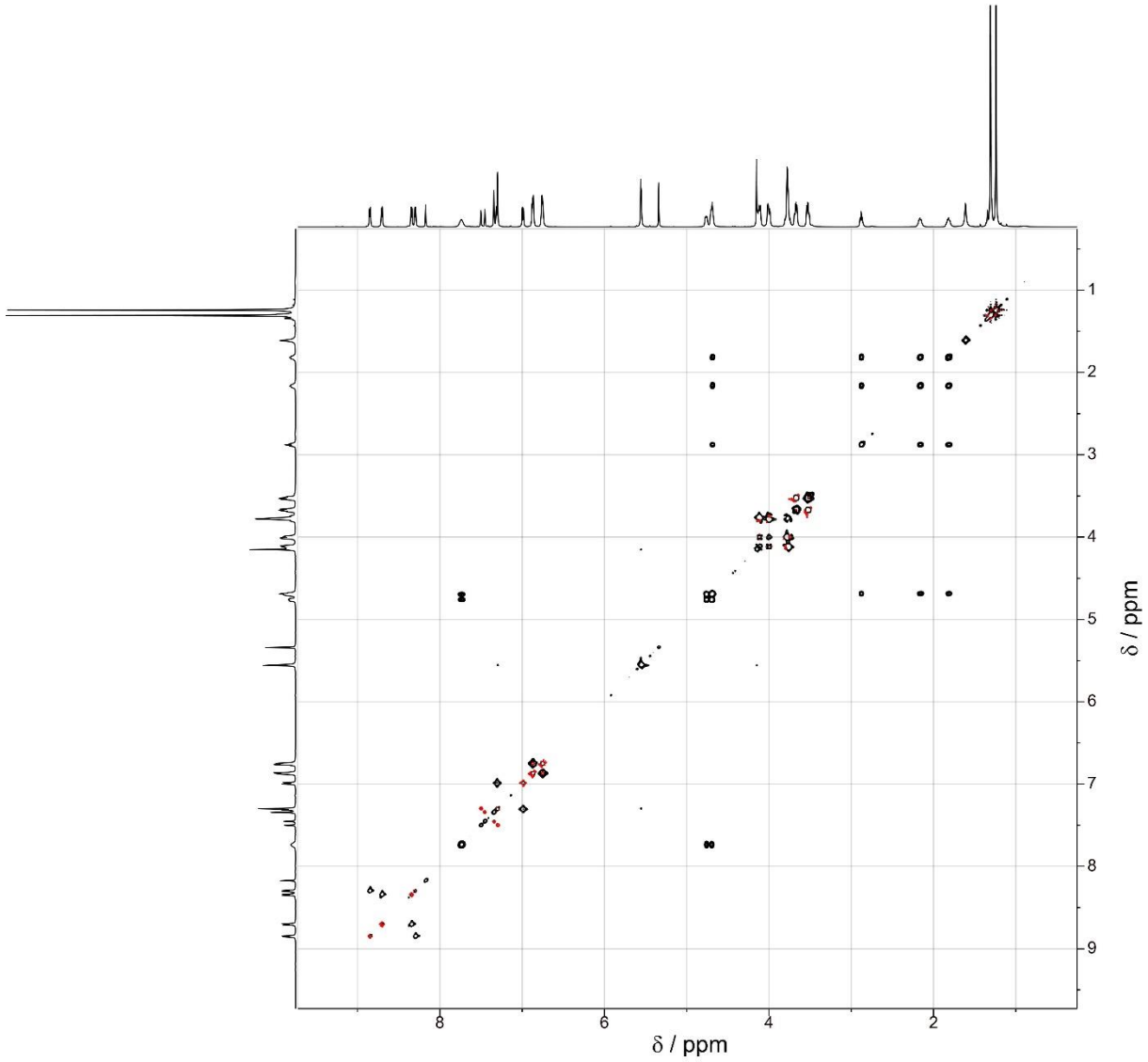

Figure S4 - ^{1}H-^{1}H TOCSY spectrum **1**H^{4+} (500 MHz, CD_2Cl_2, 298 K).

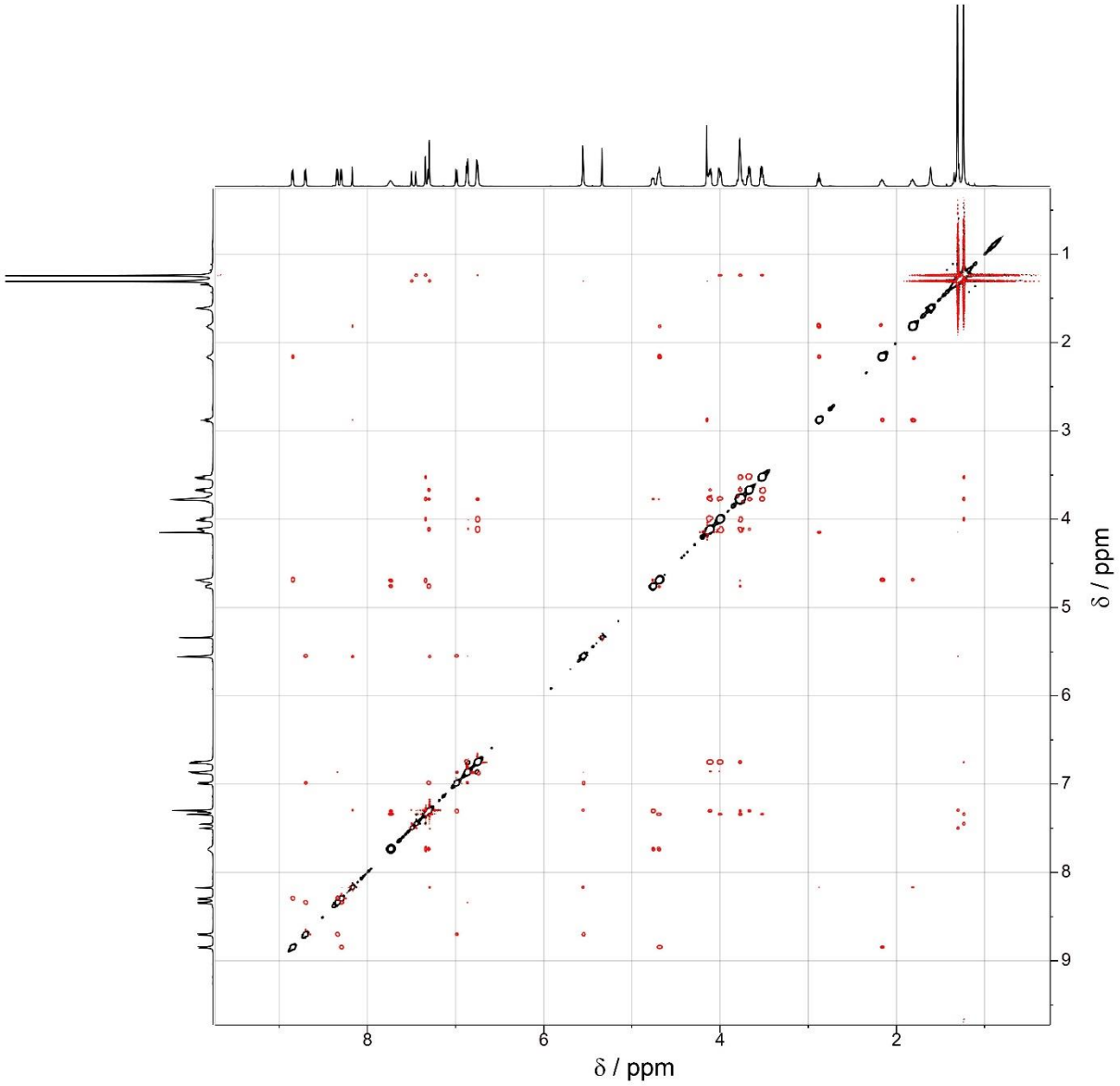

Figure S5 - ^{1}H-^{1}H ROESY spectrum **1**H^{4+} (500 MHz, CD_2Cl_2, 298 K).

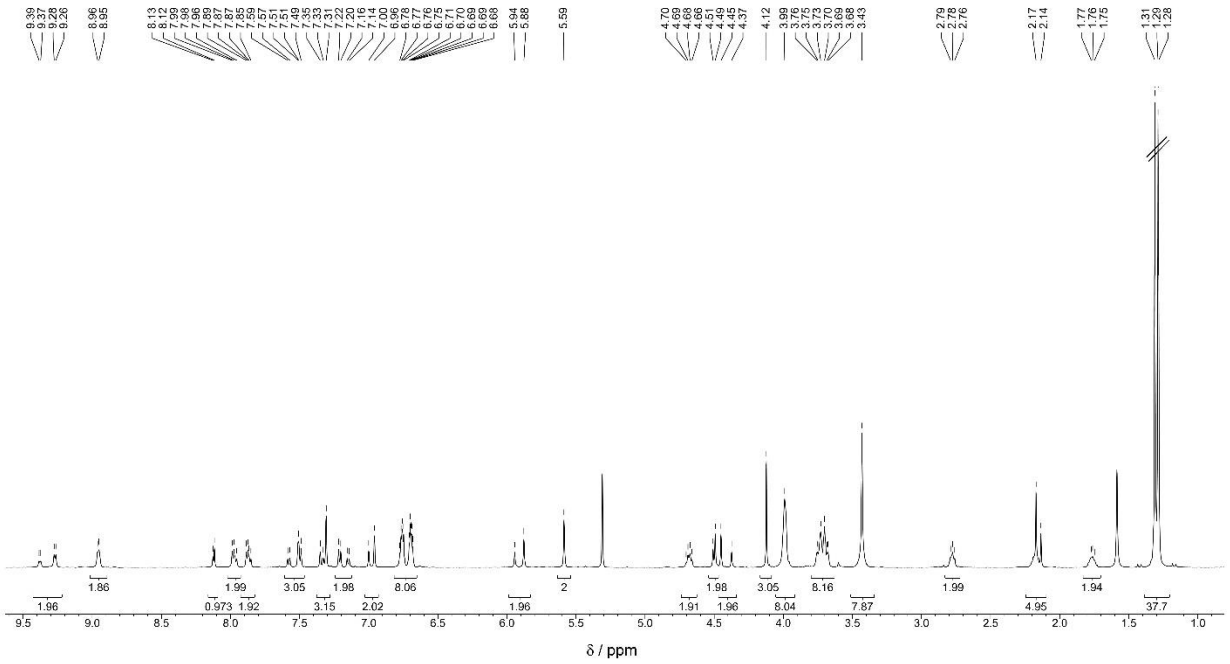

Figure S6 - ^{1}H NMR spectrum of compound **2**$^{3+}$ (500 MHz, CD_2Cl_2, 298 K).

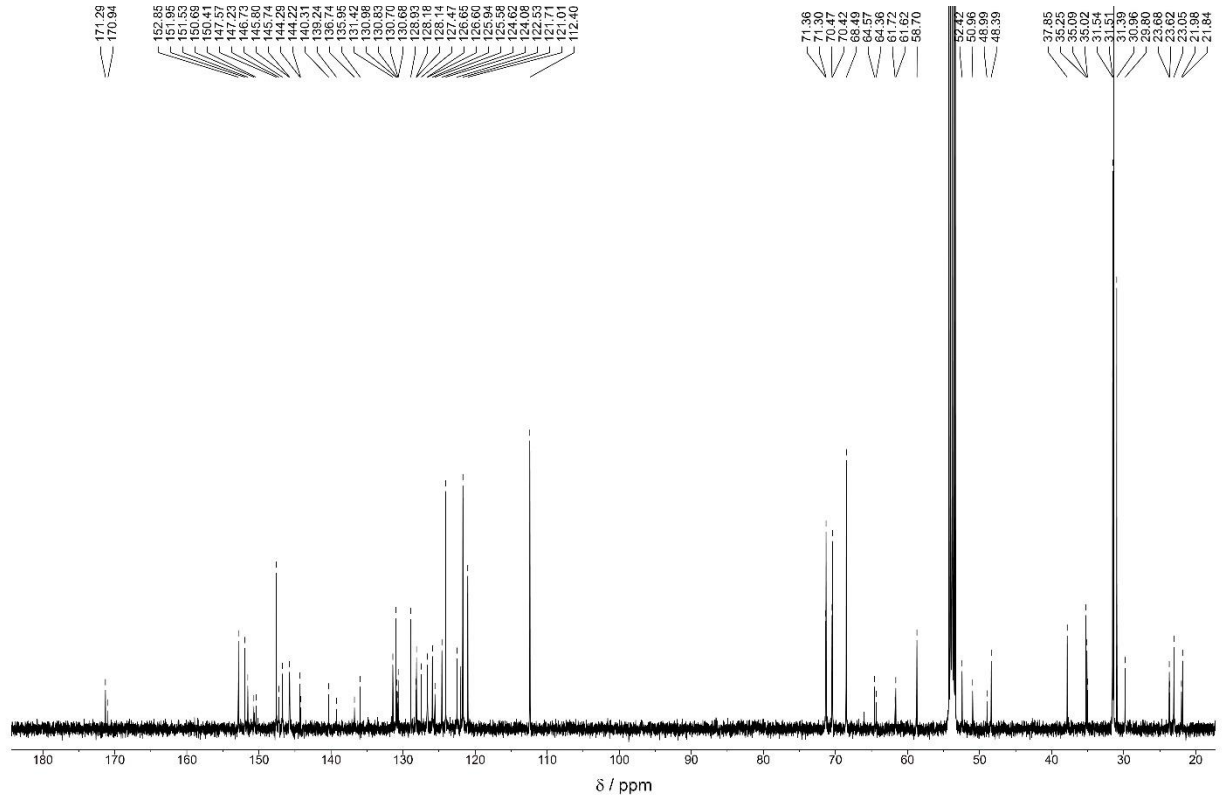

Figure S7 – ^{13}C NMR spectrum of compound **2**$^{3+}$ (125 MHz, CD_2Cl_2, 298 K).

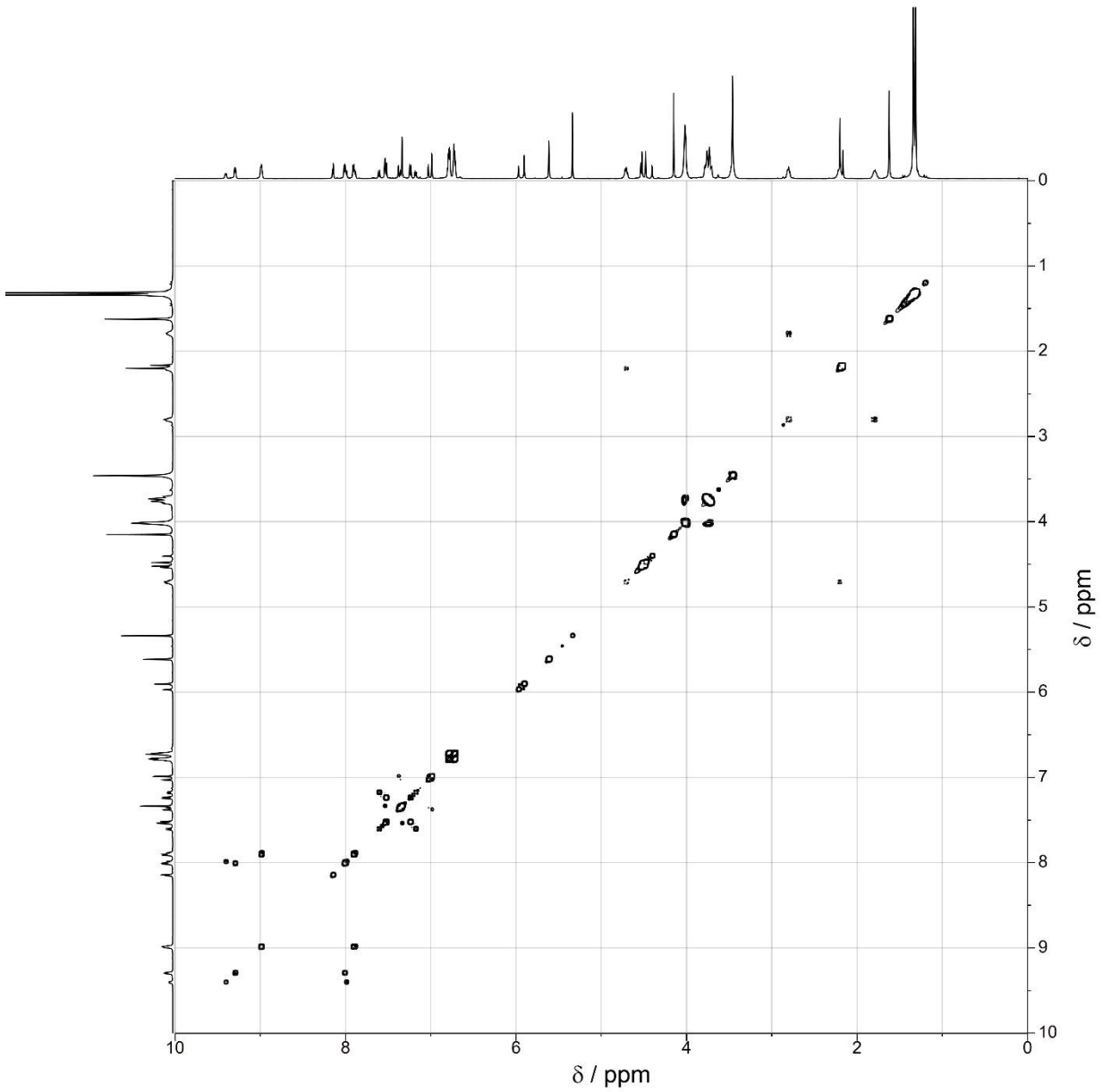

Figure S8 - ^{1}H-^{1}H COSY spectrum **2**$^{3+}$ (500 MHz, CD_2Cl_2, 298 K).

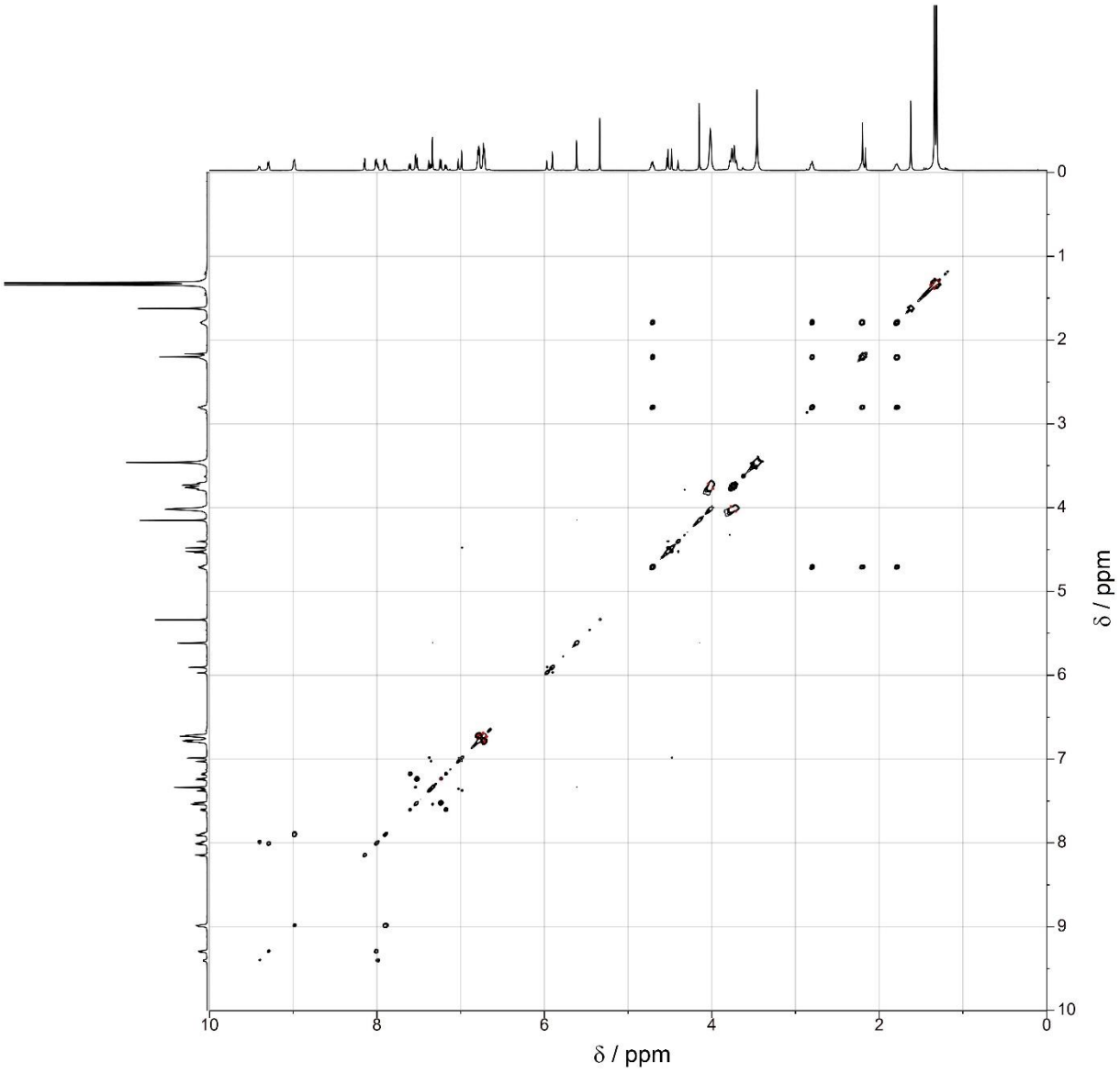

Figure S9 - ^{1}H-^{1}H TOCSY spectrum **2**$^{3+}$ (500 MHz, CD_2Cl_2, 298 K).

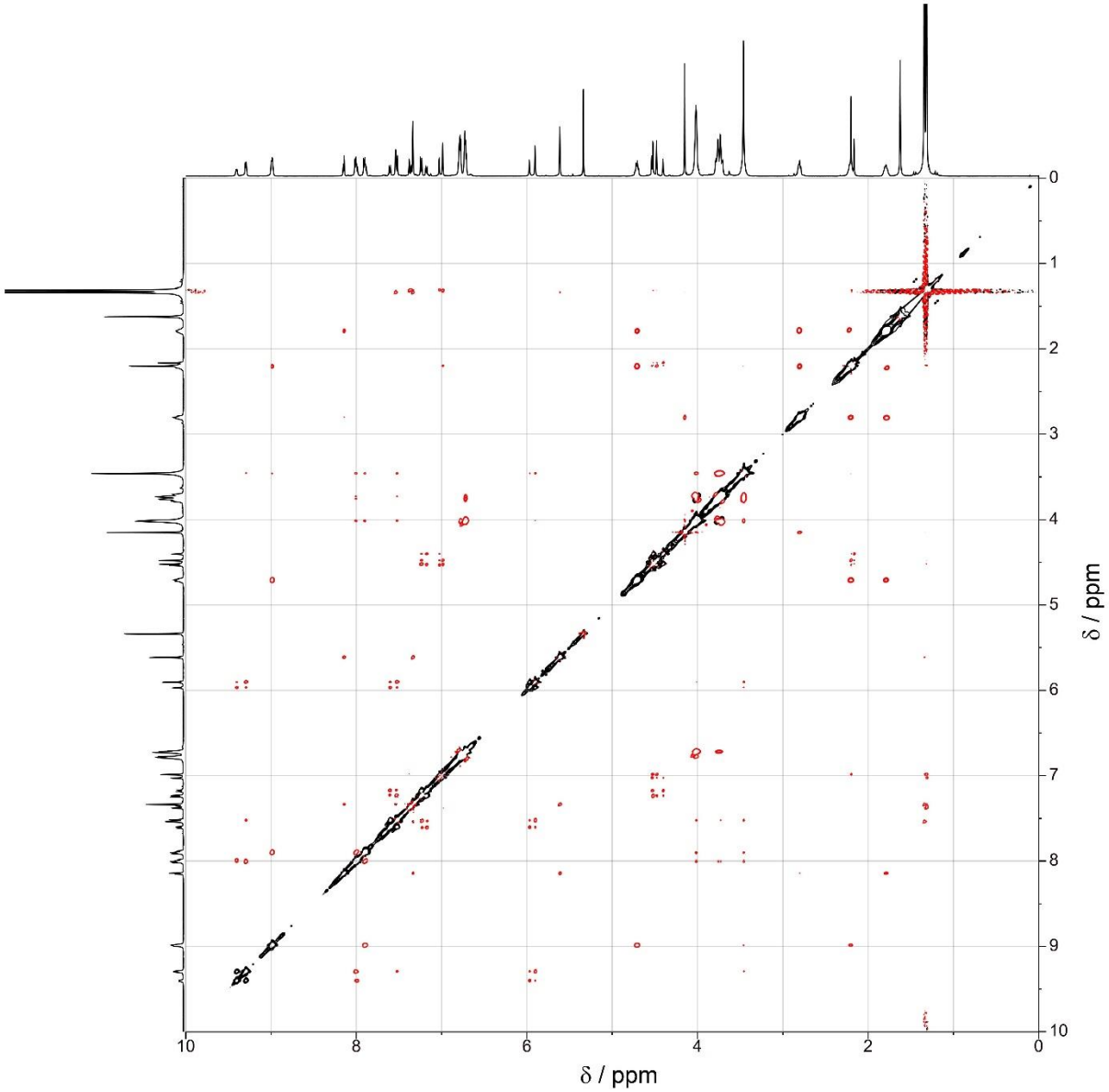

Figure S10 - ^{1}H-^{1}H ROESY spectrum **2**$^{3+}$ (500 MHz, CD_2Cl_2, 298 K).

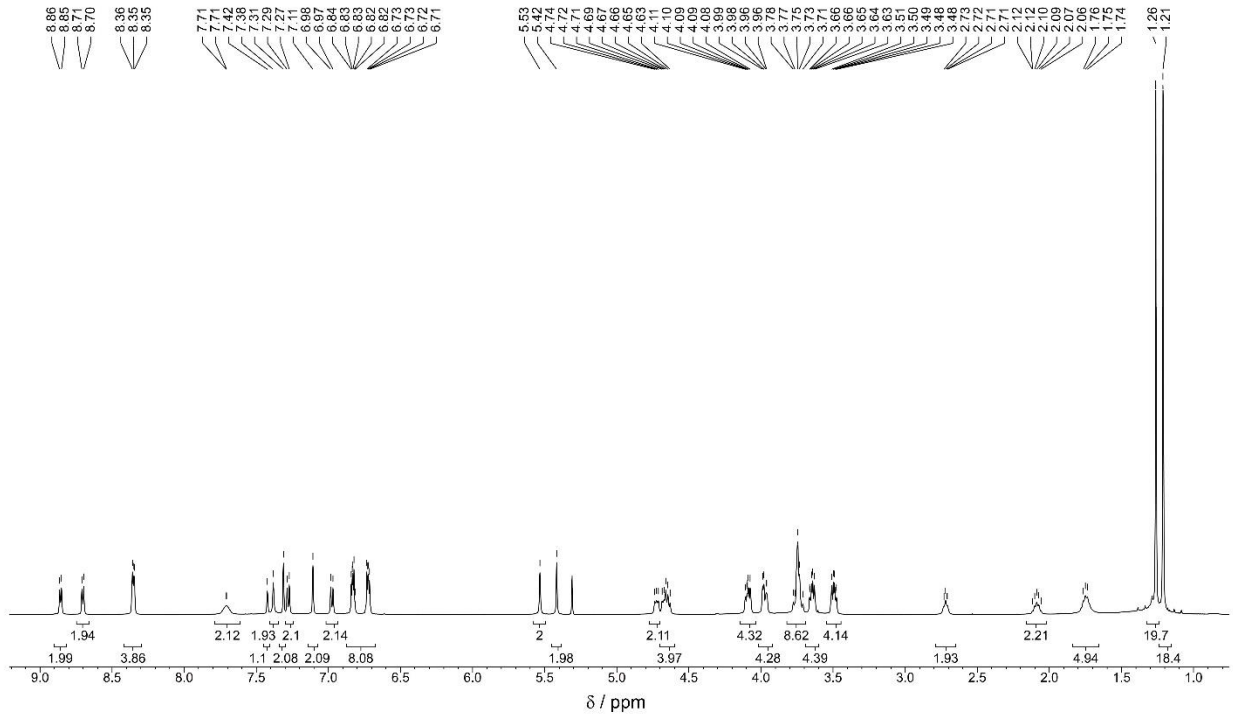

Figure S11 - ^{1}H NMR spectrum of compound **3**H^{3+} (500 MHz, CD_2Cl_2, 298 K).

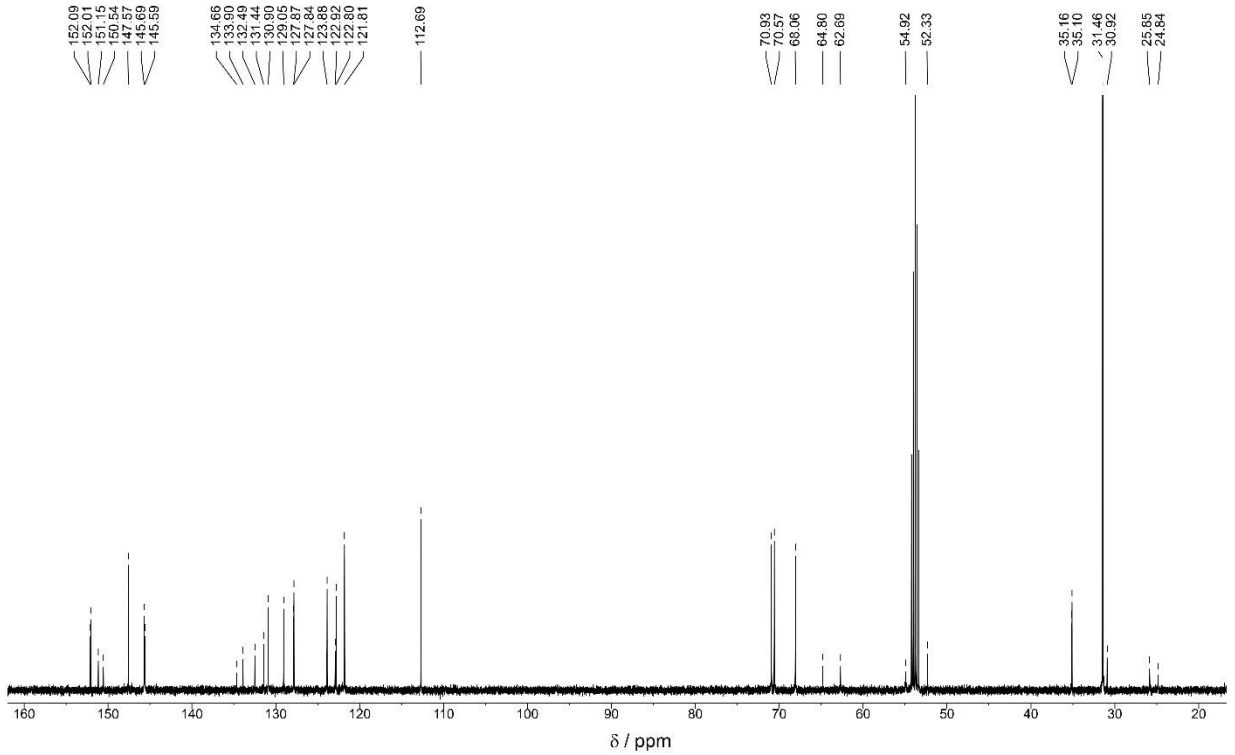

Figure S12 – ^{13}C NMR spectrum of compound **3**H^{3+} (125 MHz, CD_2Cl_2, 298 K).

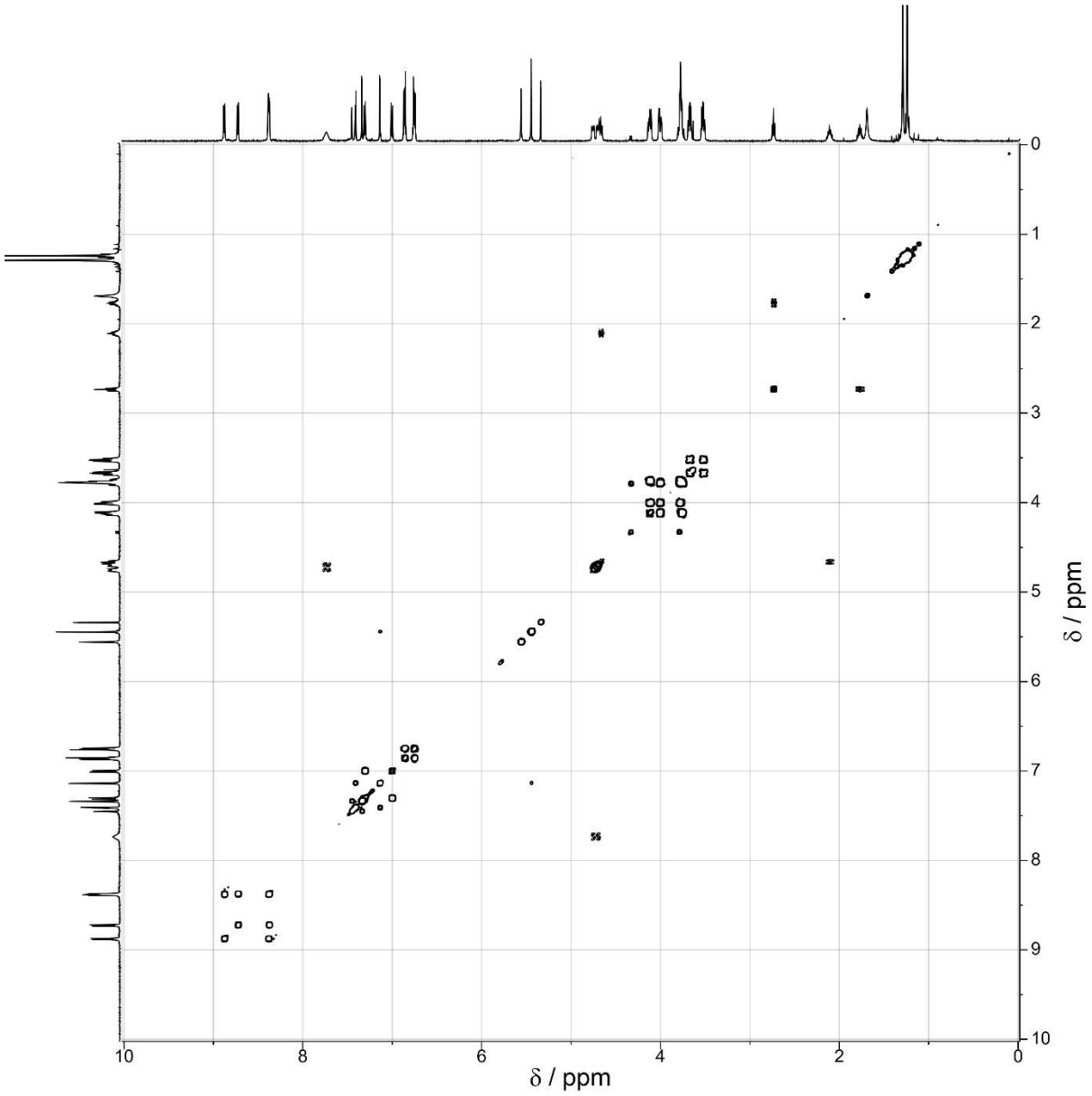

Figure S13 - ^{1}H-^{1}H COSY spectrum **3**H^{3+} (500 MHz, CD_2Cl_2, 298 K).

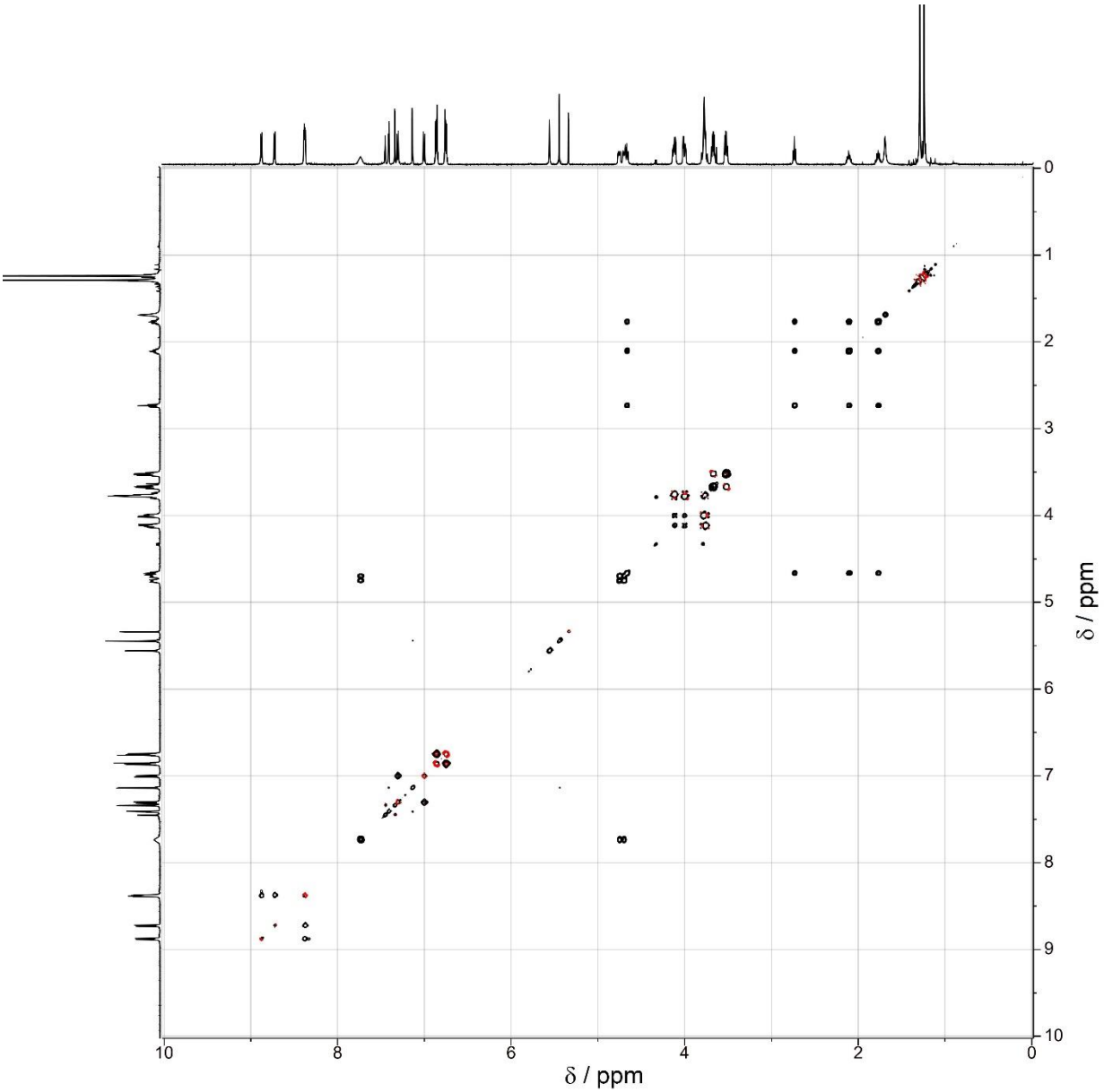

Figure S14 - ^{1}H-^{1}H TOCSY spectrum **3**H^{3+} (500 MHz, CD_2Cl_2, 298 K).

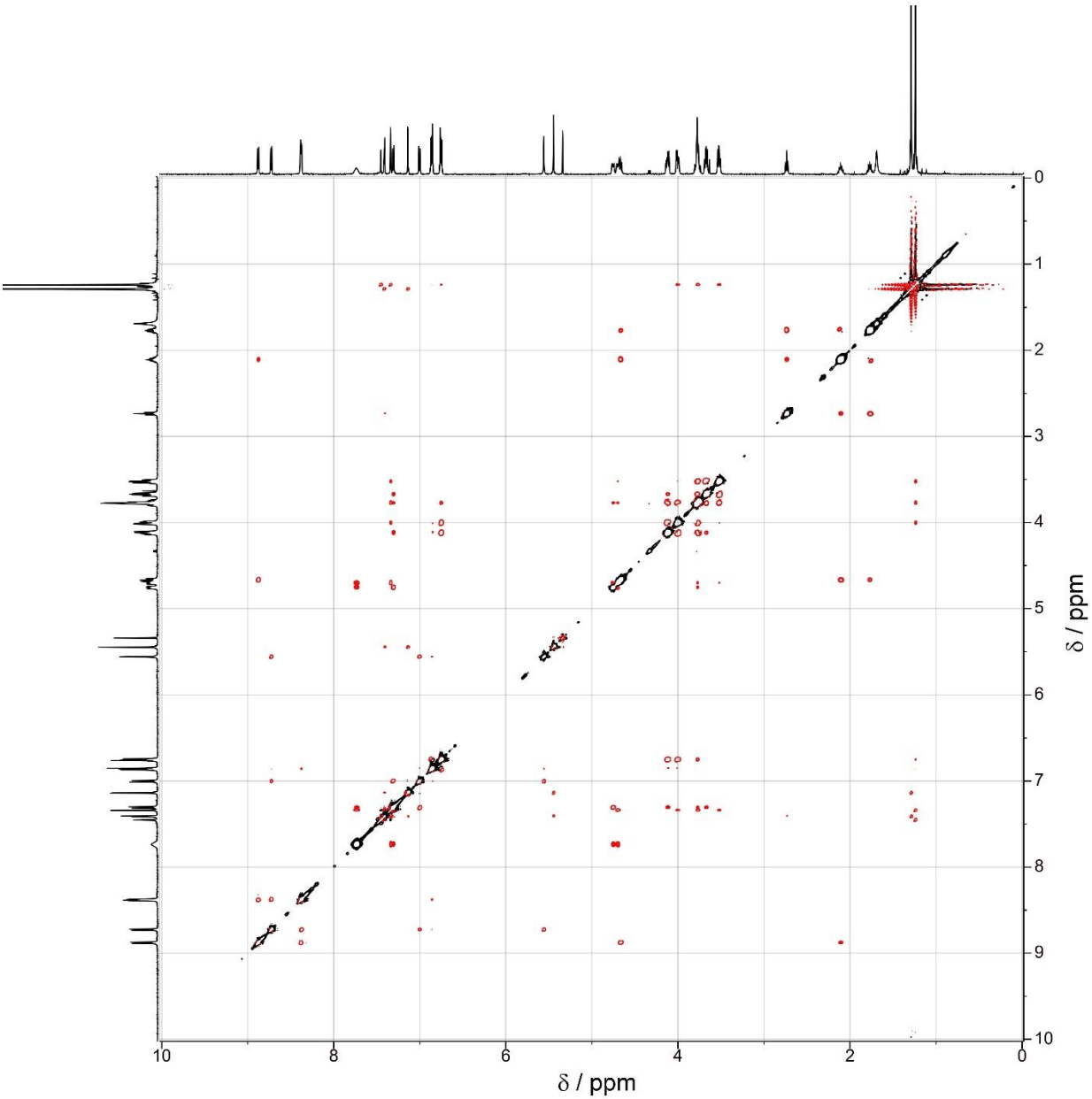

Figure S15 - ^{1}H-^{1}H ROESY spectrum **3**H^{3+} (500 MHz, CD_2Cl_2, 298 K).

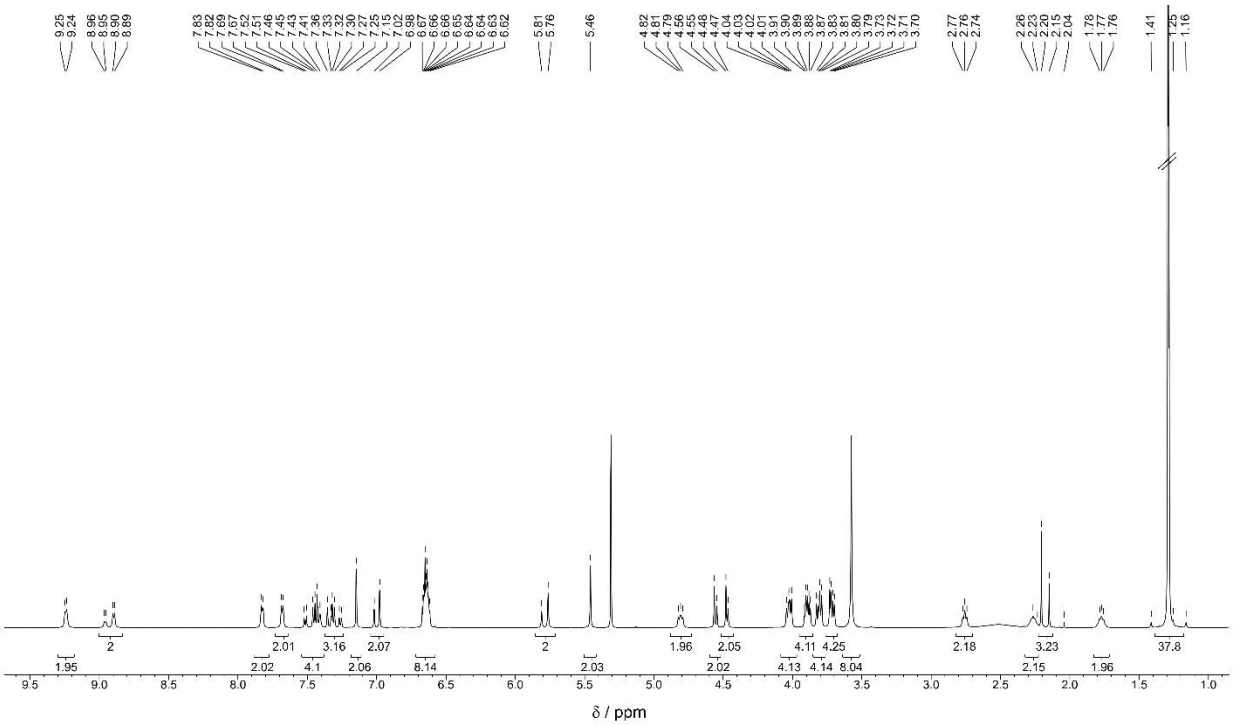

Figure S16 - ^{1}H NMR spectrum of compound **4**$^{2+}$ (500 MHz, CD_2Cl_2, 298 K).

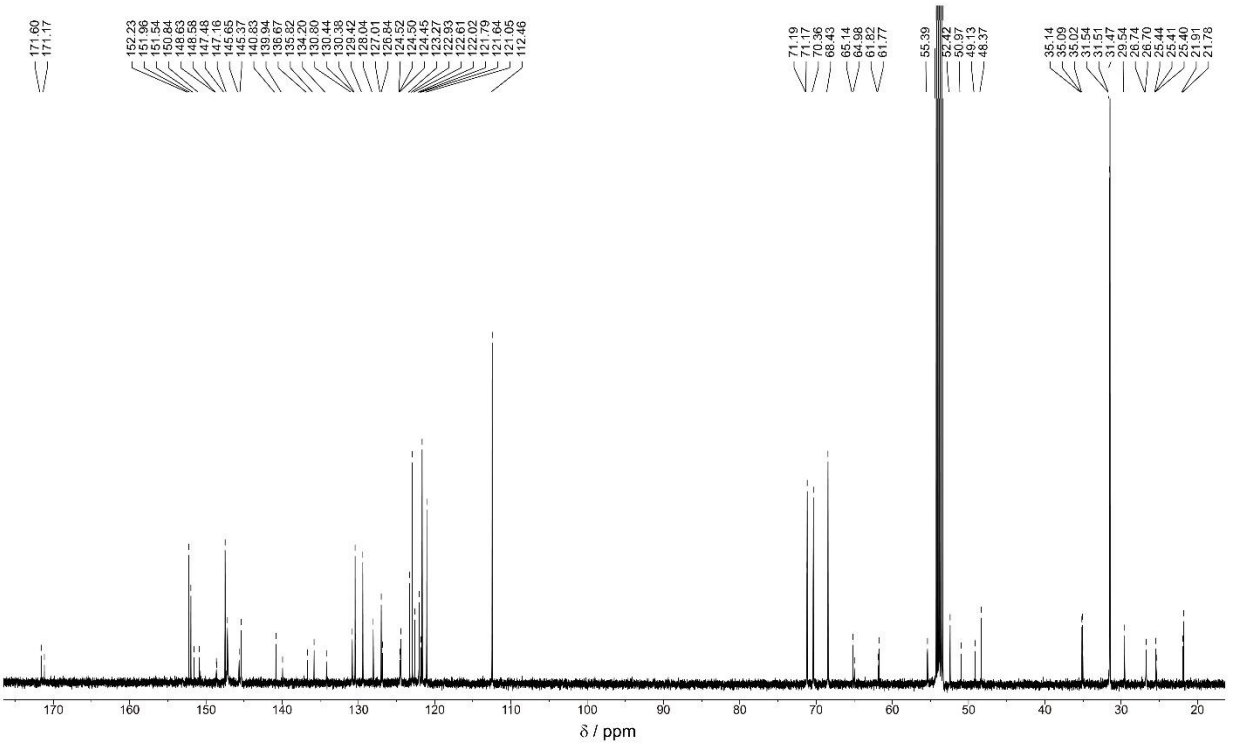

Figure S17 - ^{13}C NMR spectrum of compound **4**$^{2+}$ (125 MHz, CD_2Cl_2, 298 K).

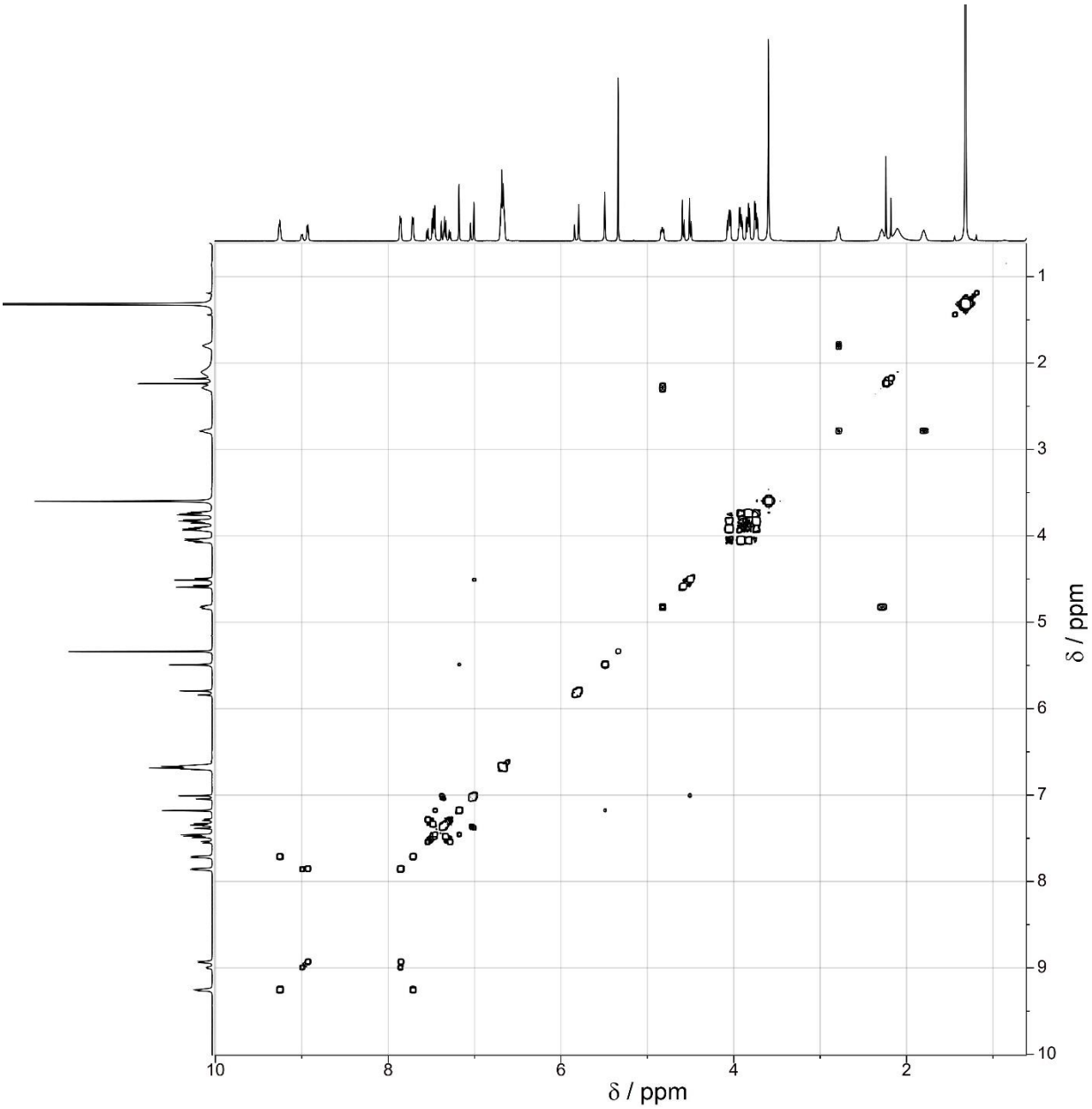

Figure S18 - ^{1}H-^{1}H COSY spectrum **4**$^{2+}$ (500 MHz, CD_2Cl_2, 298 K).

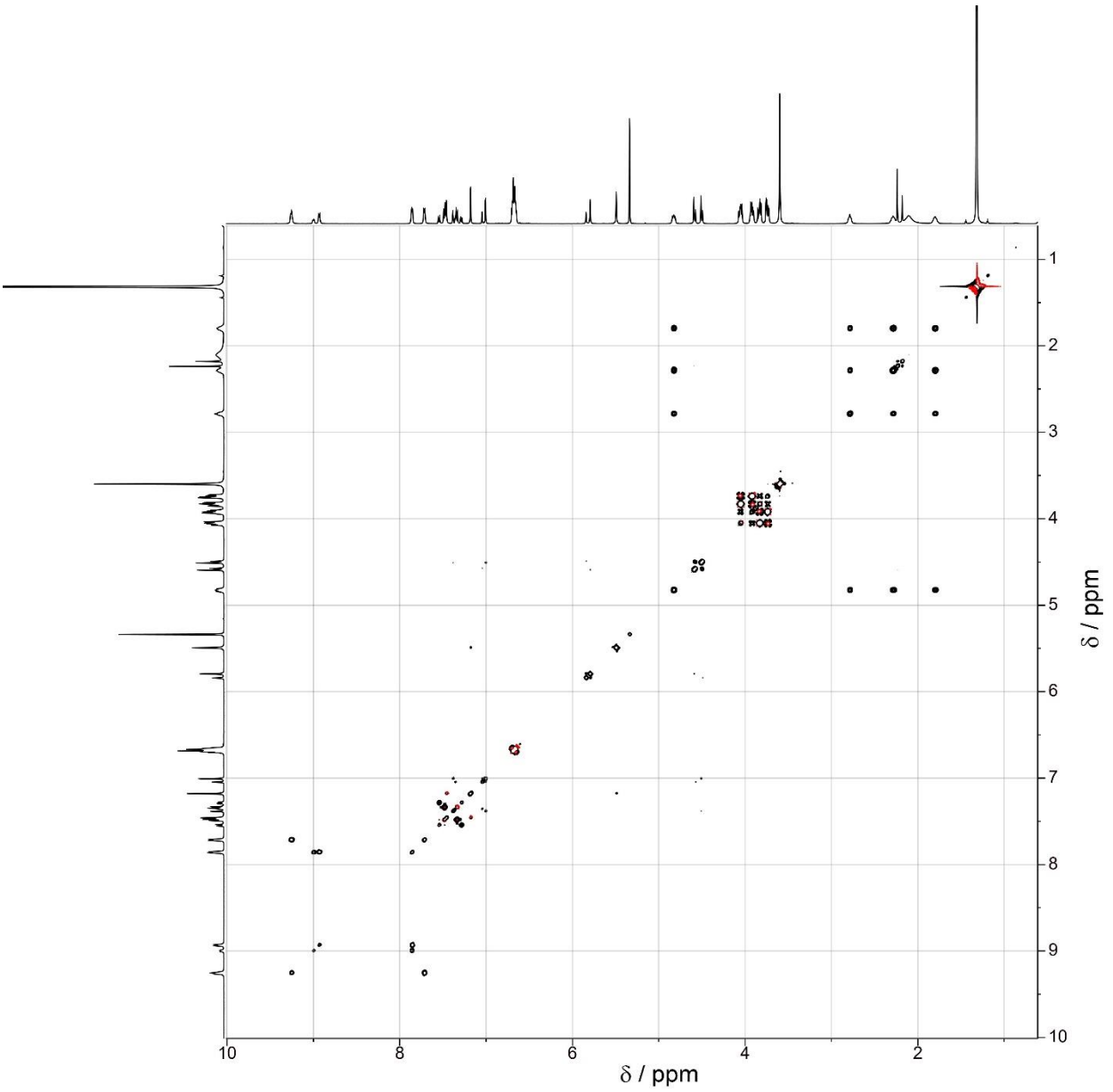

Figure S19 - ^{1}H-^{1}H TOCSY spectrum **4**$^{2+}$ (500 MHz, CD_2Cl_2, 298 K).

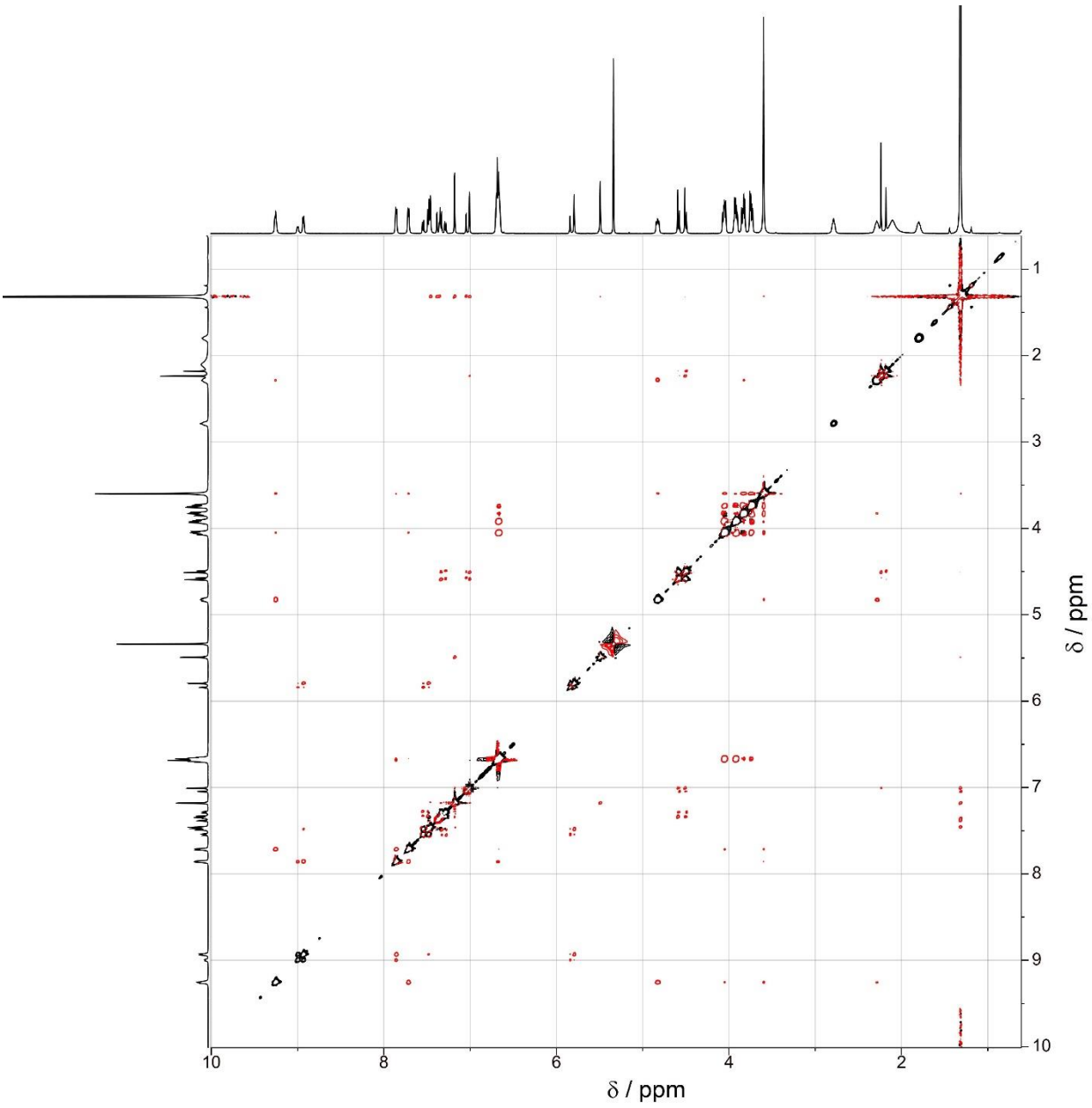

Figure S20 - ^{1}H-^{1}H ROESY spectrum **4**$^{2+}$ (500 MHz, CD_2Cl_2, 298 K).

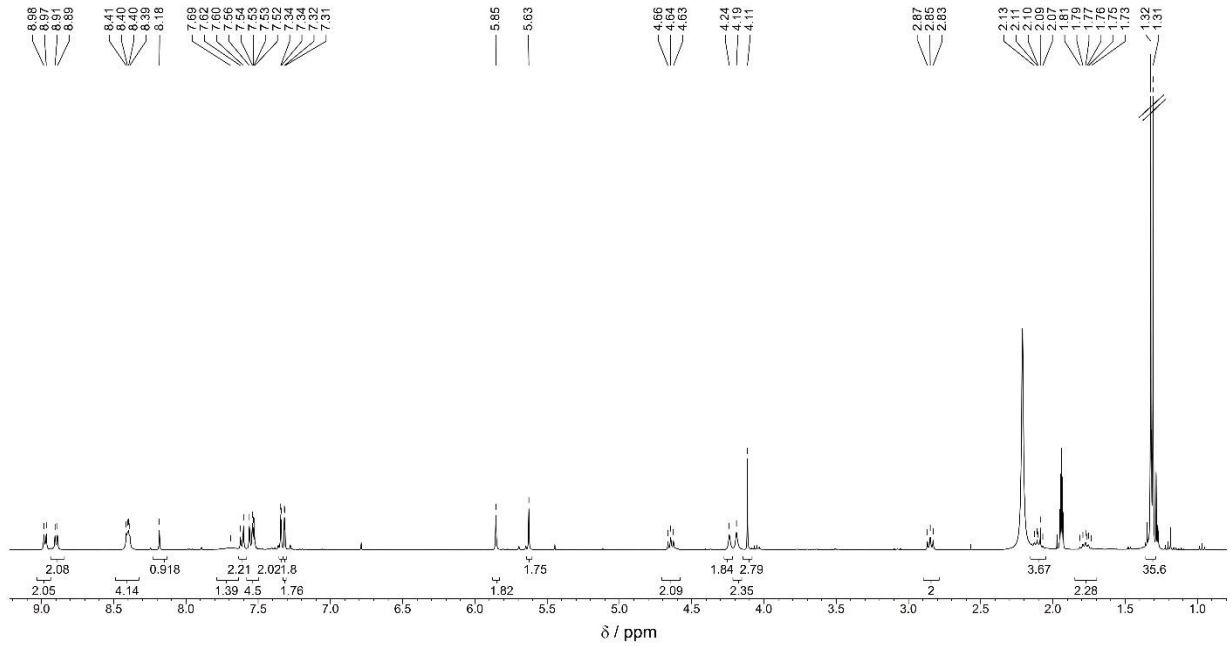

Figure S21 - ^{1}H NMR spectrum of compound **5**H^{4+} (500 MHz, CD_3CN, 298 K).

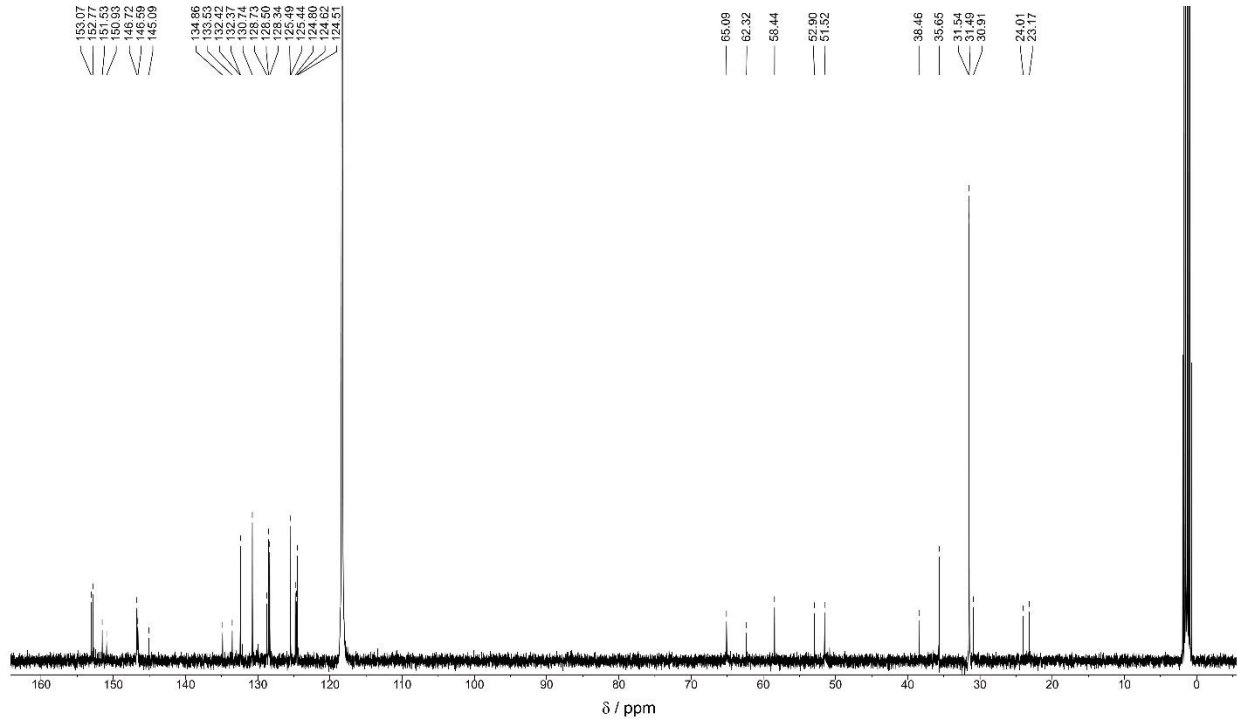

Figure S22 - ^{13}C NMR spectrum of compound **5**H^{4+} (125 MHz, CD_3CN, 298 K).

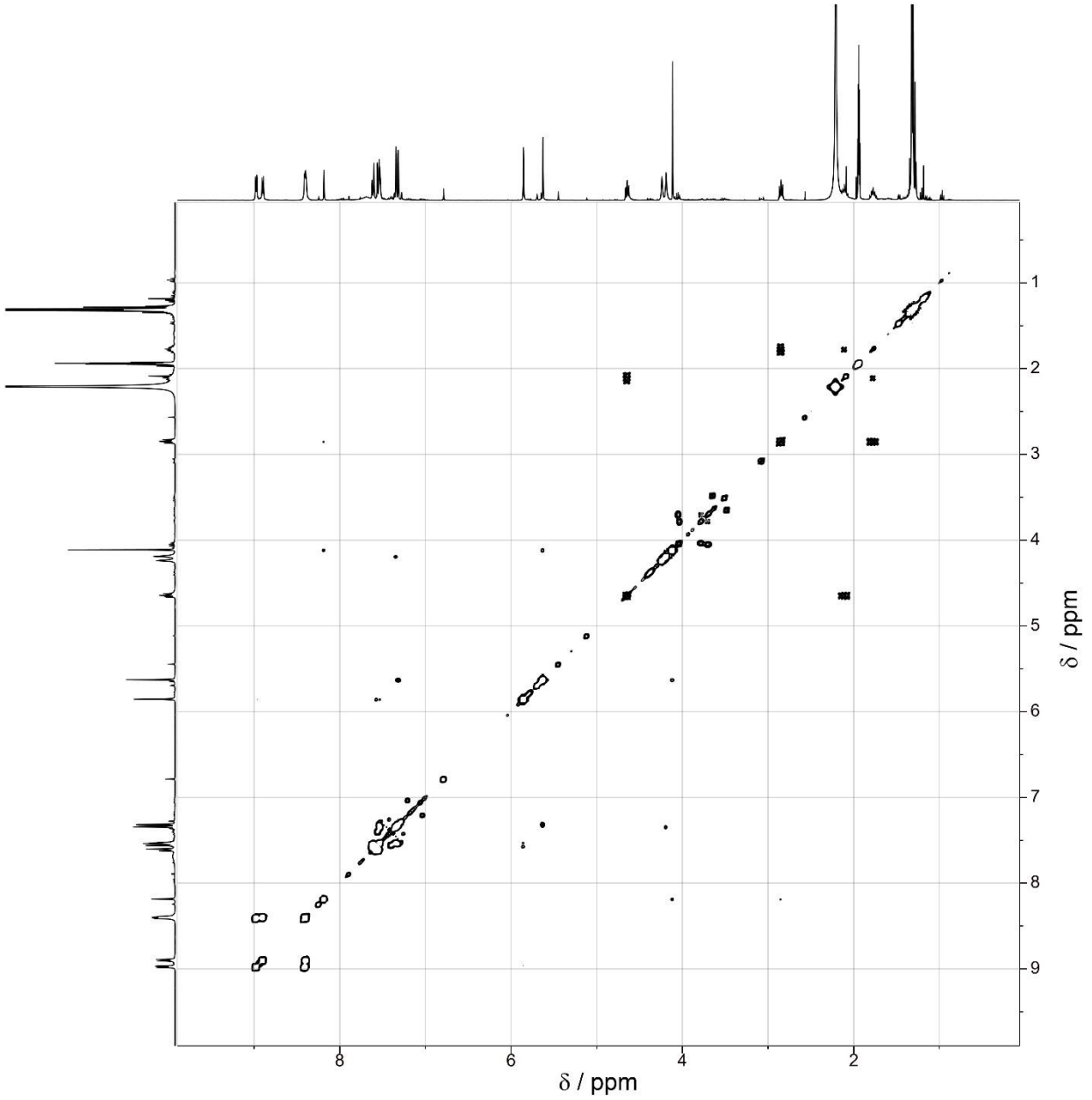

Figure S23 - ^{1}H-^{1}H COSY spectrum **5**H^{4+} (500 MHz, CD_3CN, 298 K).

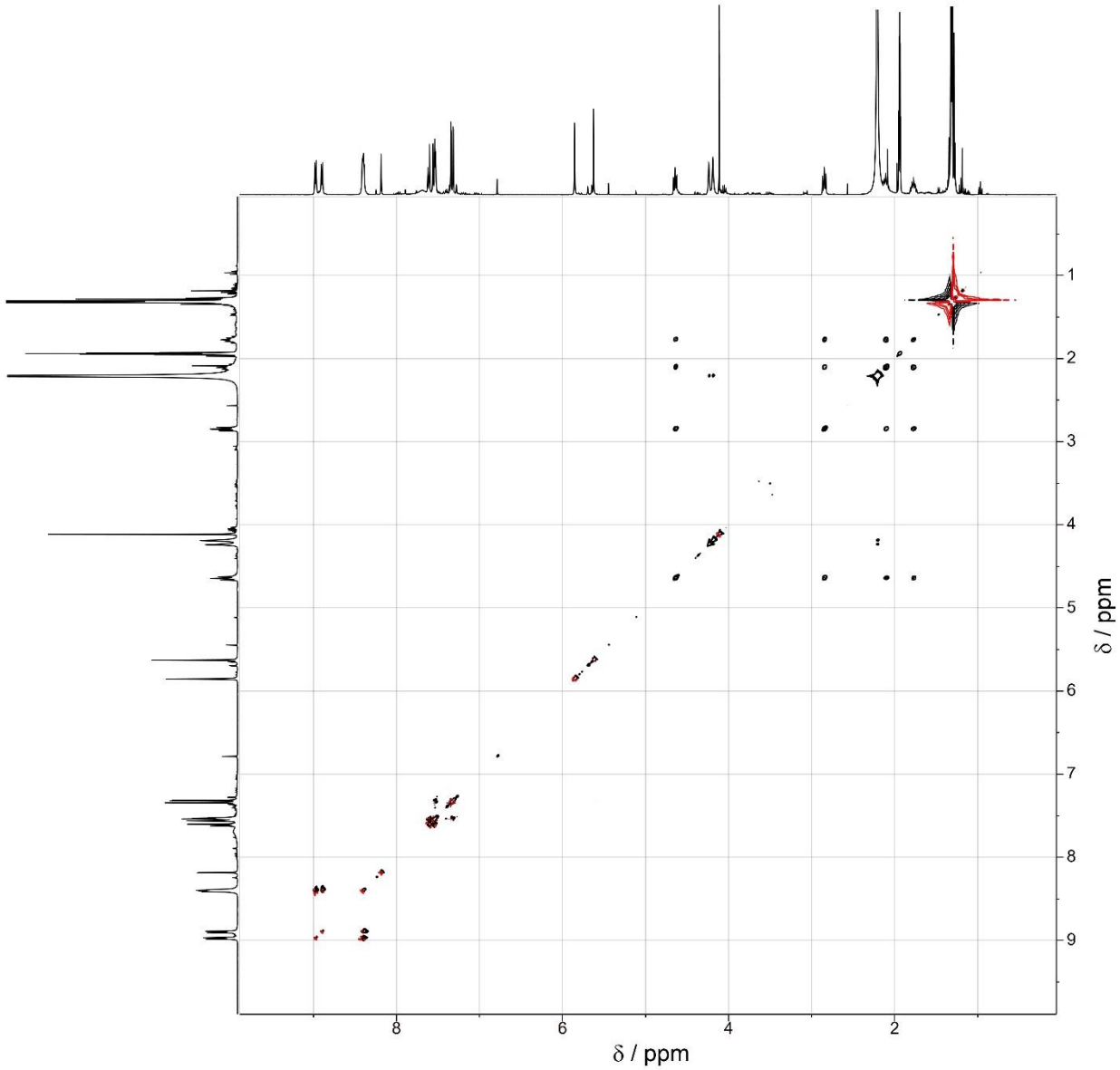

Figure S24 - ^{1}H-^{1}H TOCSY spectrum **5**H^{4+} (500 MHz, CD_3CN, 298 K).

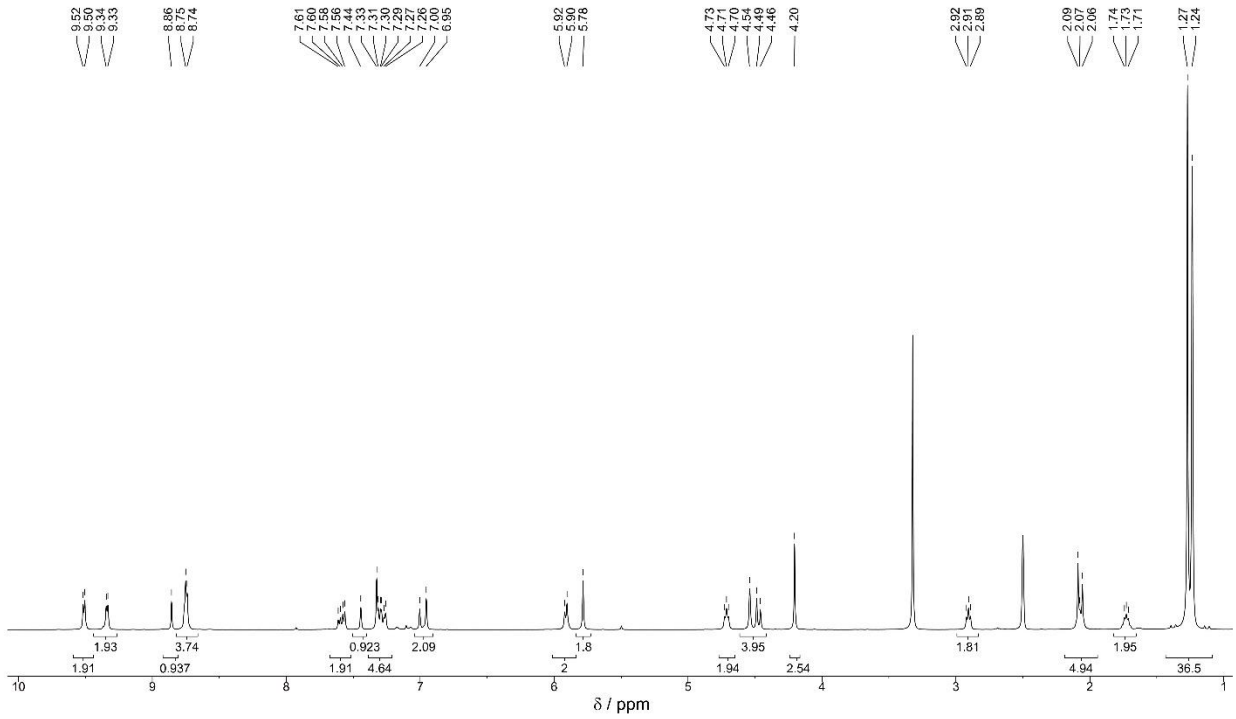

Figure S25 - ^{1}H NMR spectrum of compound **6**$^{3+}$ (500 MHz, DMSO-d$_6$, 298 K).

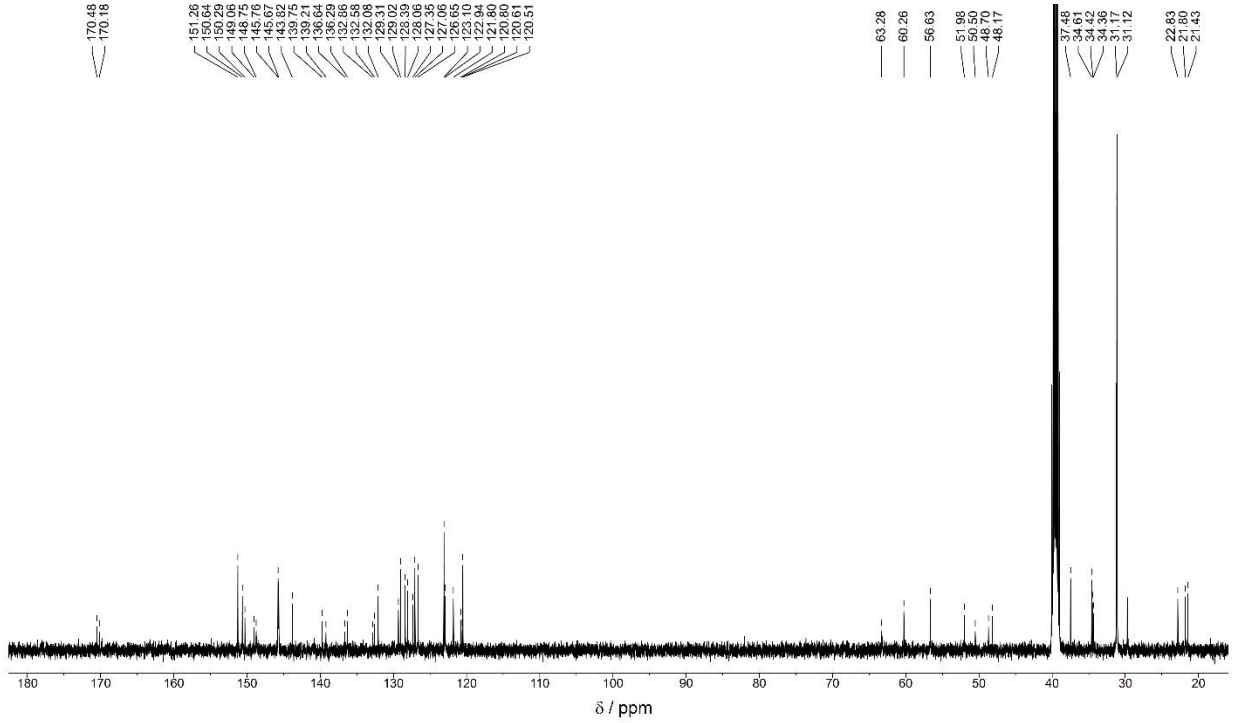

Figure S26 - ^{13}C NMR spectrum of compound **6**$^{3+}$ (125 MHz, DMSO-d$_6$, 298 K).

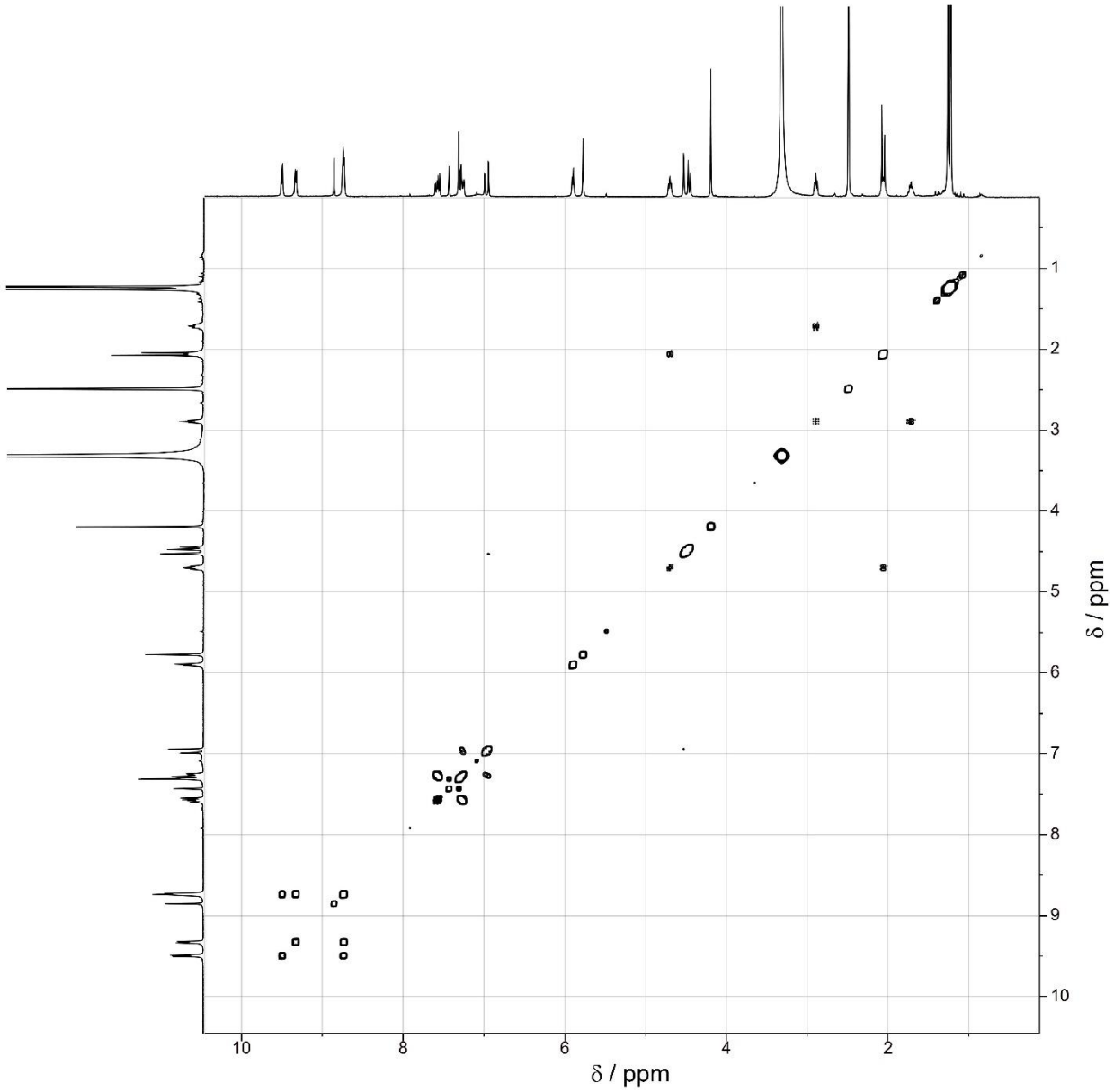

Figure S27 - ^{1}H-^{1}H COSY spectrum **6**$^{3+}$ (500 MHz, DMSO-d$_6$, 298 K).

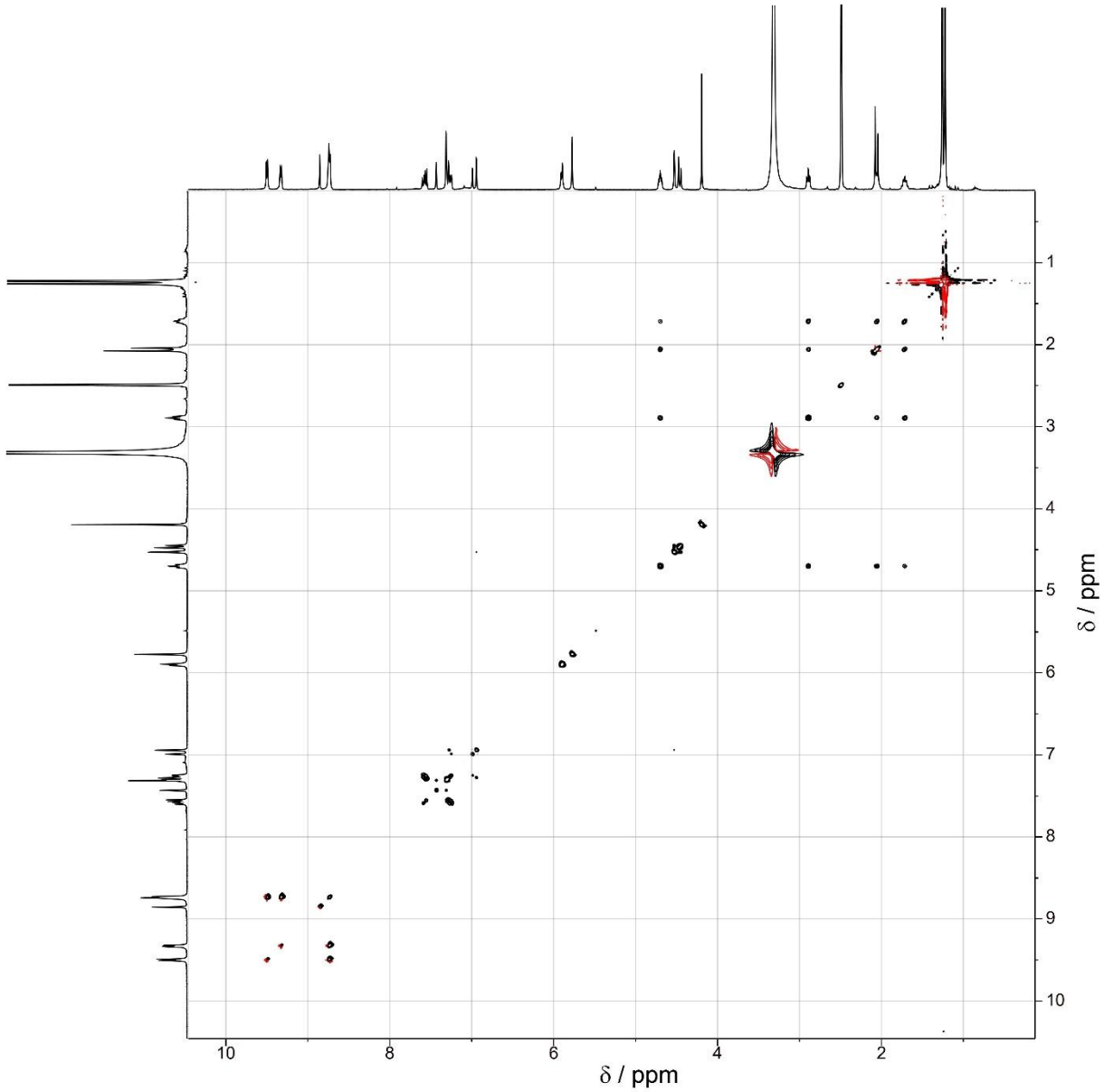

Figure S28 - ^{1}H-^{1}H TOCSY spectrum **6**$^{3+}$ (500 MHz, DMSO-d_6, 298 K).

4. Solvent Effect on the Interaction between DB24C8 and the stations Bpy^{2+} and Trz^{+}.

Figures S29-S34 demonstrate the effect of the solvent on the interaction between the macrocycle and the stations Bpy^{2+} and Trz^{+} upon deactivation of AmH^{+} in either CD_2Cl_2 or CD_3CN. Figure S29 shows the comparison of the ^1H NMR spectra in the two solvents for compounds **1**H^{4+}, before (Fig. S29a,b) and after the addition of base (Fig. S29c,d), and **2**$^{3+}$ (Fig. S29e,f). When DB24C8 is located on AmH^{+}, the signals associated with Trz^{+} present the same chemical shift in both solvents (Fig. S29a,b). Upon deactivation of AmH^{+}, either by deprotonation or acetylation, the macrocycle moves to Bpy^{2+}, and the signals of the Trz^{+} protons shift to higher field in CD_3CN compared to CD_2Cl_2, suggesting that they might undergo shielding due to the proximity of the aromatic groups of DB24C8.

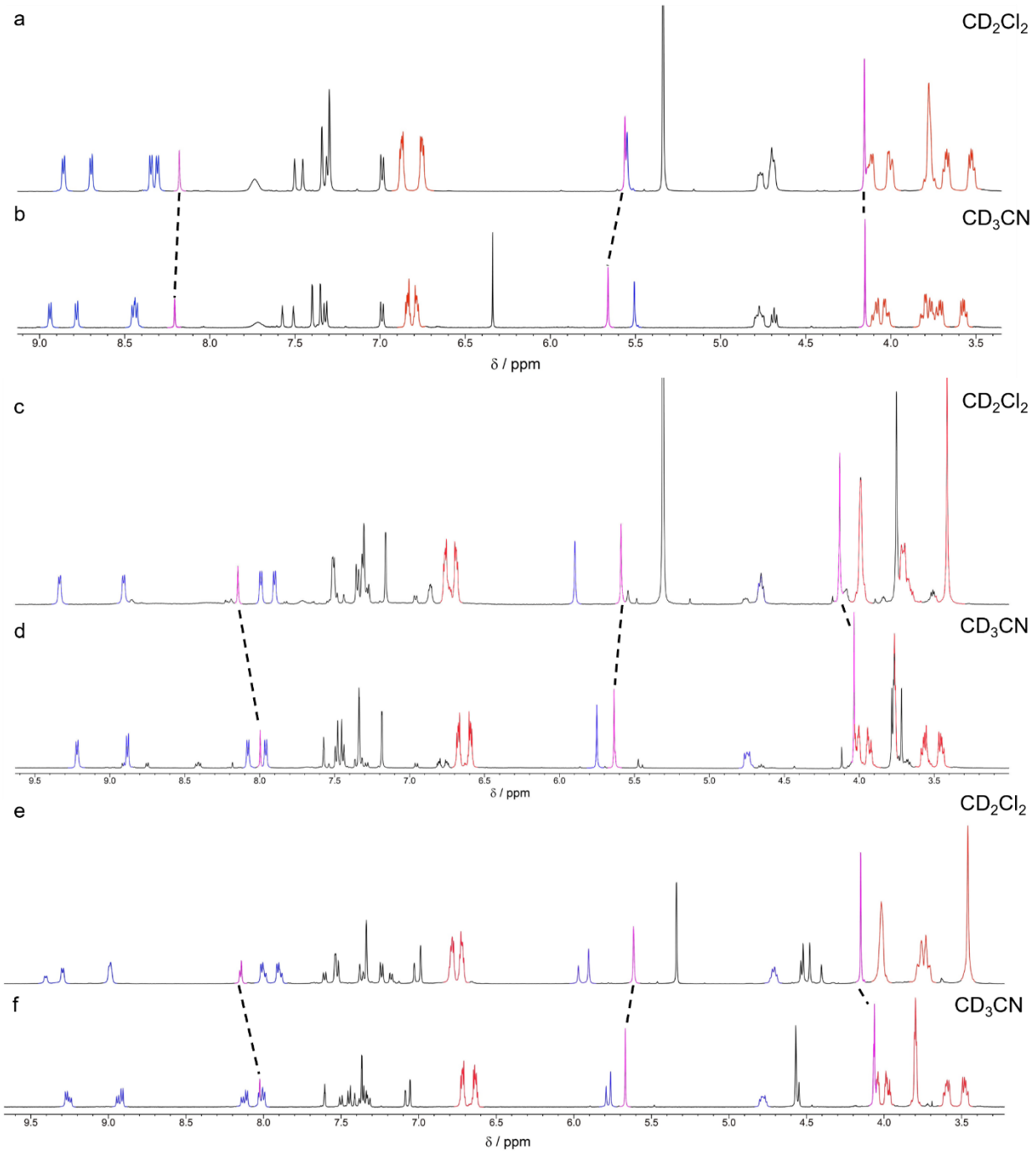

Figure S29 – Comparison of partial ^{1}H NMR spectra (500 MHz, 298 K) of a) **1**H^{4+} in CD_2Cl_2; b) **1**H^{4+} in CD_3CN; c) **1**H^{4+} after the addition of ~1 eq of TBA in CD_2Cl_2; d) **1**H^{4+} after the addition of ~1 eq of TBA in CD_3CN; e) **2**$^{3+}$ in CD_2Cl_2; f) **2**$^{3+}$ in CD_3CN.

The variable temperature experiment (Fig. S30) performed on **2**$^{3+}$, in which the amine is acetylated, shows that decreasing the temperature from 293K to 233K in CD3CN, all the signals associated with the DB24C8 protons broaden, due to the slowing of the dynamics of the system

and alongside it also the signals of both Bpy^{2+} and Trz^{+} are affected suggesting that both recognition sites are affected by the macrocycle.

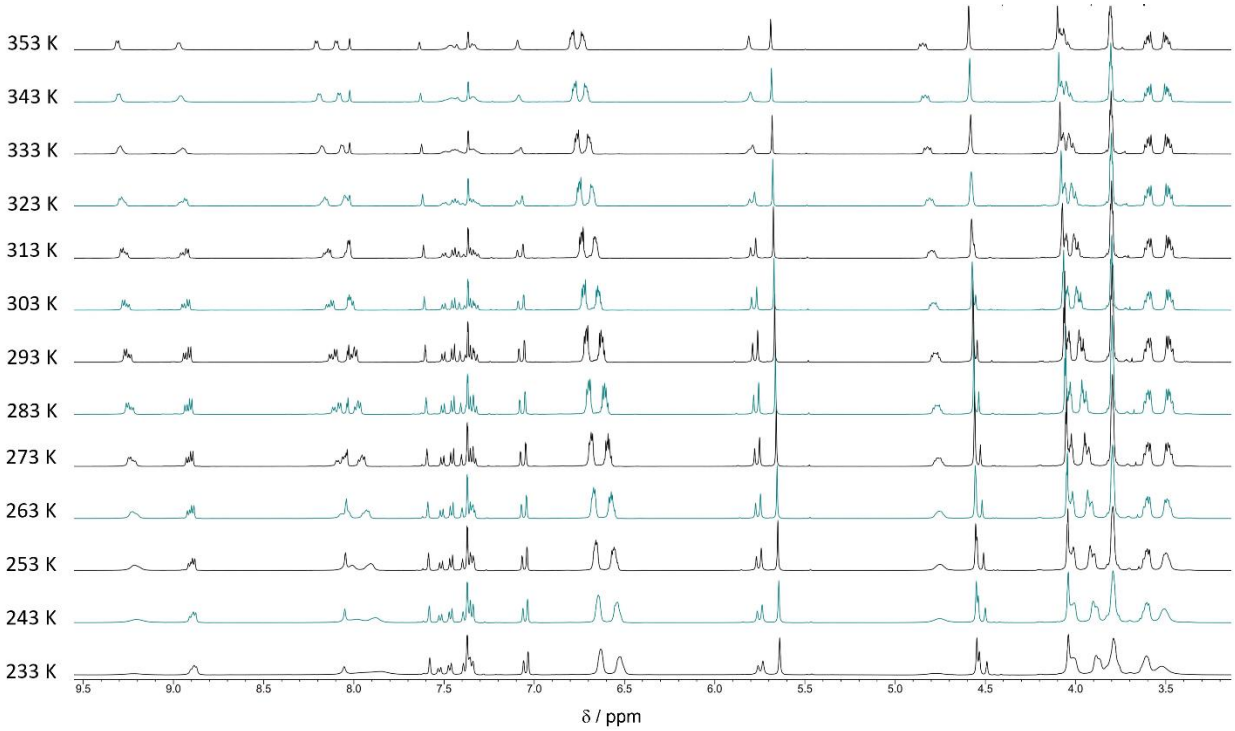

Figure S30 - Comparison of partial ^{1}H NMR spectra of compound $\mathbf{2}^{3+}$ recorded within a variable temperature interval ranging from 233 K to 353 K (CD_3CN, 500 MHz).

The ROESY spectra recorded in CD_2Cl_2 (Fig. S31 and Fig. S32) present a clear set of cross peaks suggesting that DB24C8 is strongly interacting with Bpy^{2+}, orienting its glycol chains toward the acetylated amine side of the molecule. The ROESY spectra recorded in CD_3CN (Fis. S33 and Fig. S34) show a lower number of cross peaks between the signals of the macrocycle and the axle: this might suggest that in this solvent the system is more dynamic. Cross peaks indicate that the macrocycle is orienting its glycol chains toward the triazolium side of the molecule, but no interaction between the macrocycle and the triazolium was detected.

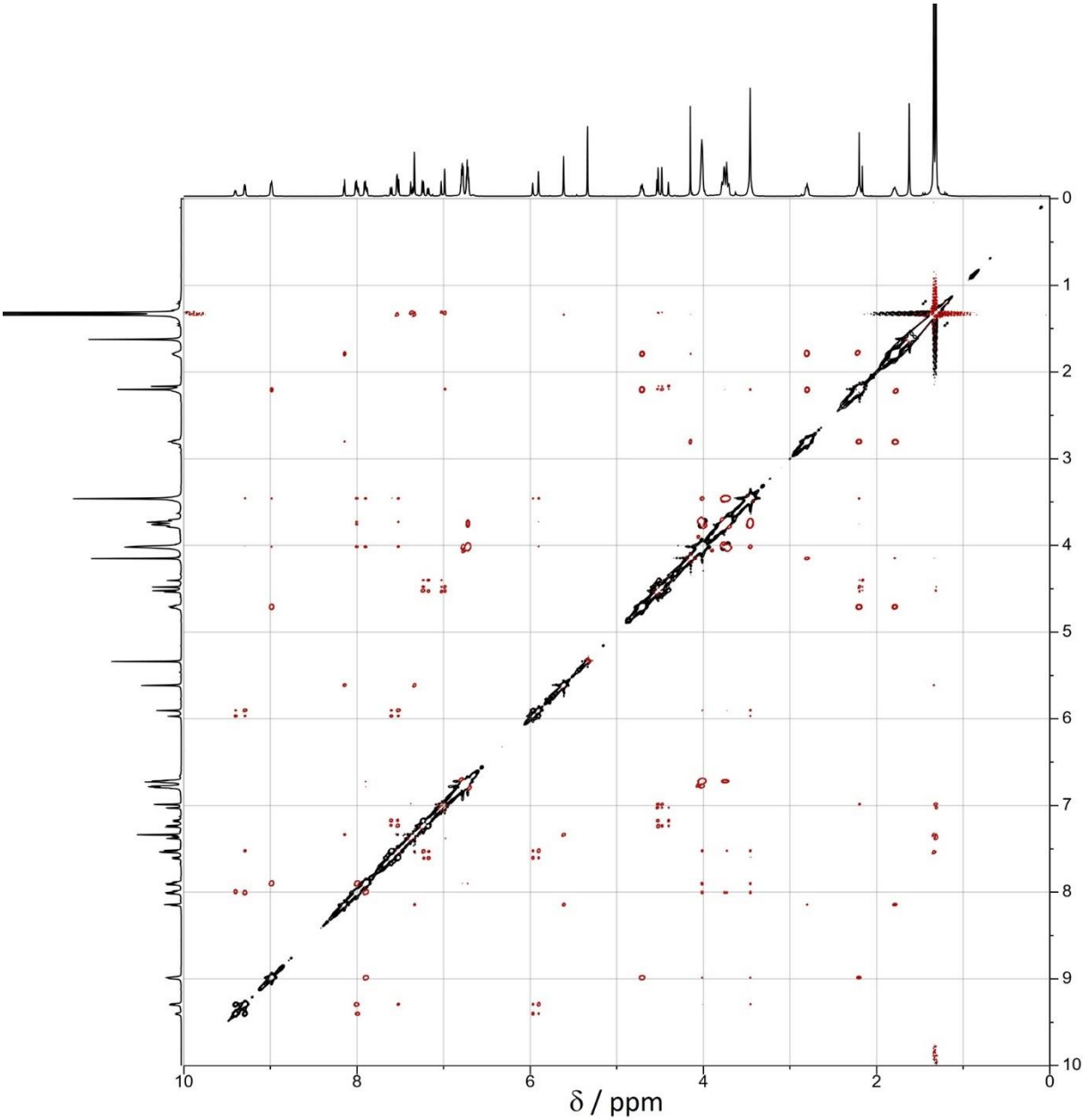

Figure S31 - ^{1}H-^{1}H ROESY spectrum of **2**$^{3+}$ (500 MHz, CD_2Cl_2, 298 K).

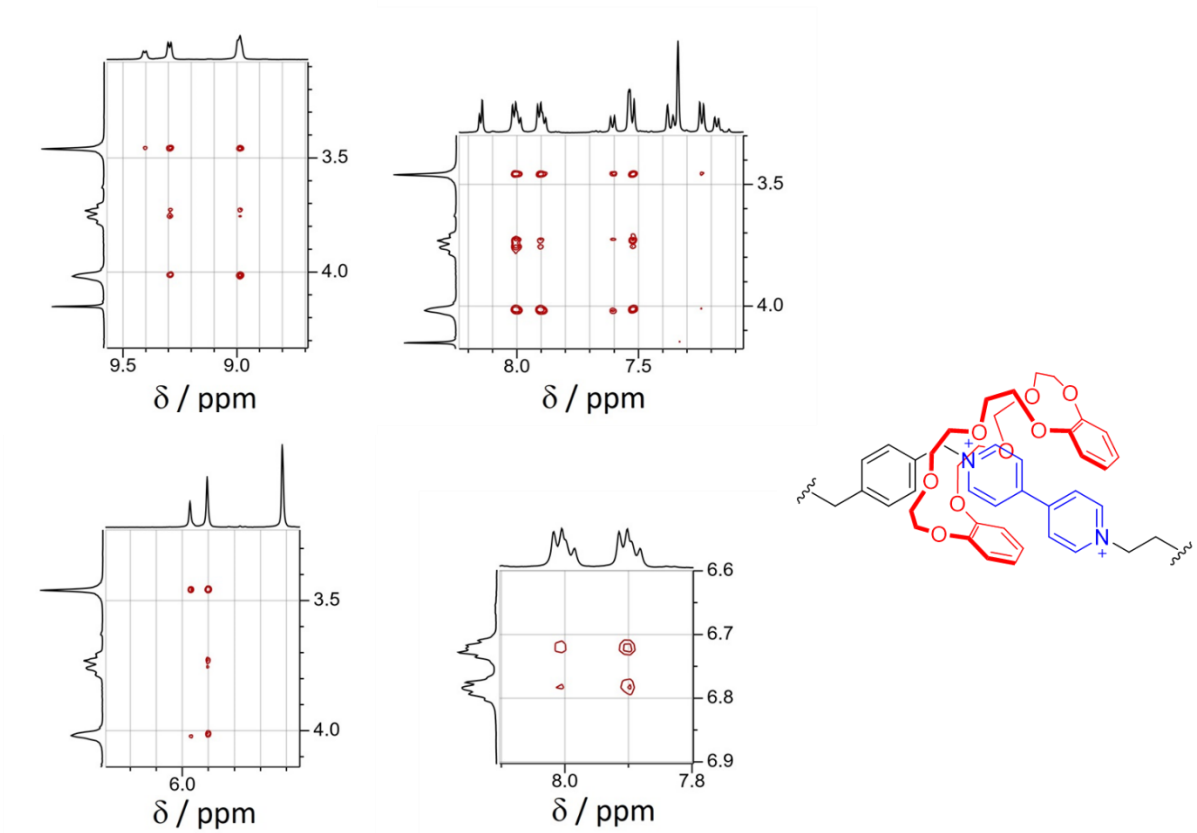

Figure S32 – Sections of the ^{1}H-^{1}H ROESY spectrum of **2**$^{3+}$ (500 MHz, CD_2Cl_2, 298 K), highlighting the cross peaks related to thread/DB24C8 interactions and partial structure hypothesized.

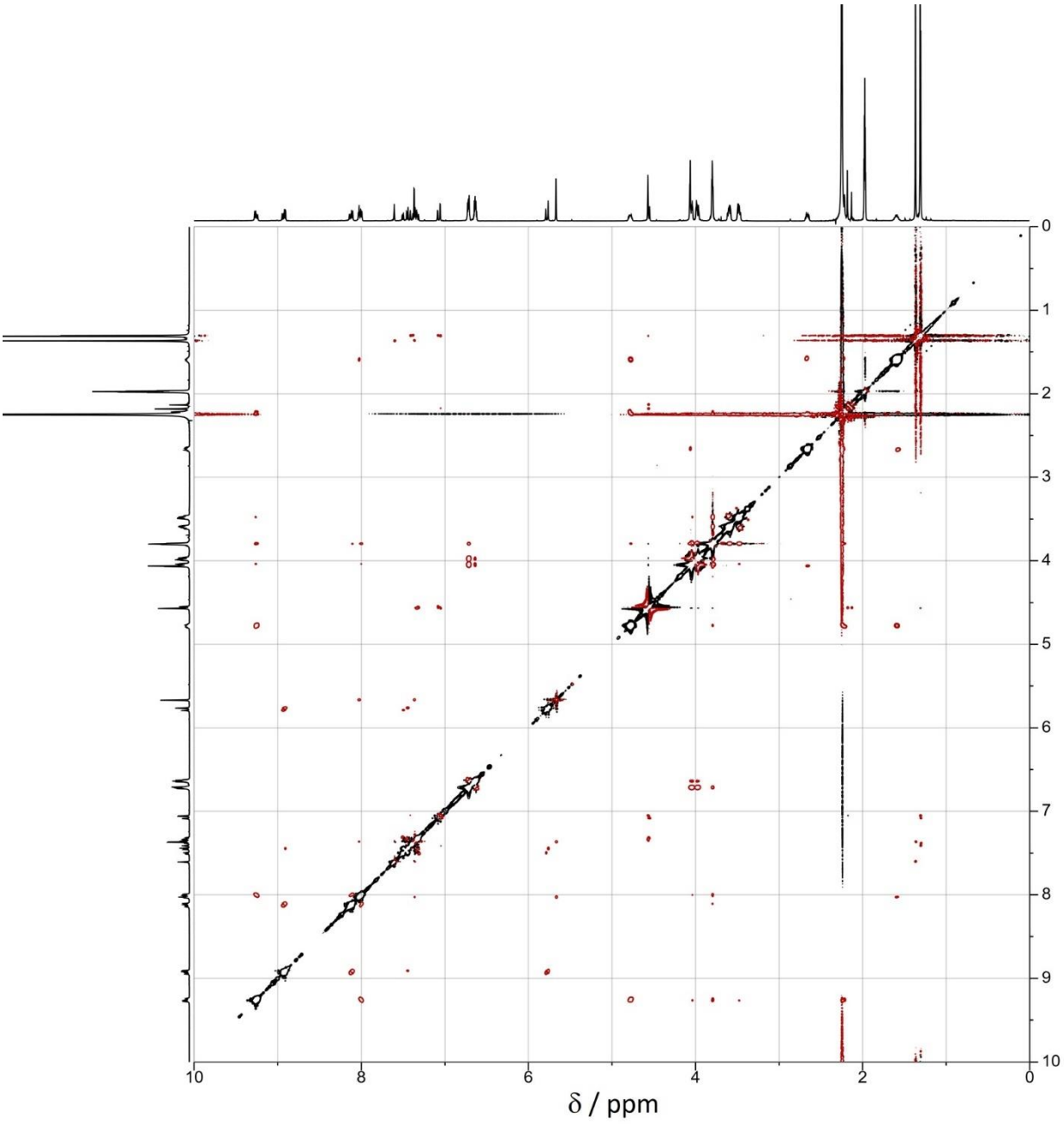

Figure S33 - ^{1}H-^{1}H ROESY spectrum of **2**$^{3+}$ (500 MHz, CD_3CN, 298 K).

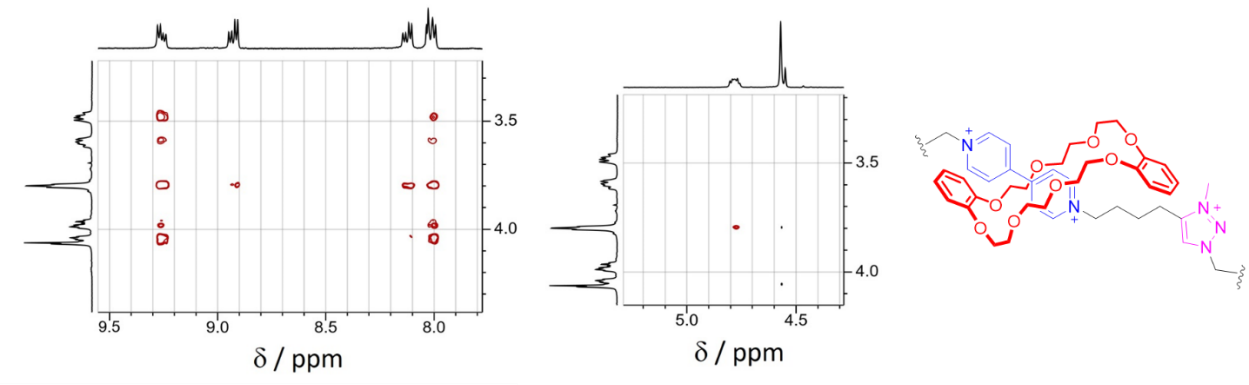

Figure S34 - Sections of the ^{1}H-^{1}H ROESY spectrum of **2**$^{3+}$ (500 MHz, CD_3CN, 298 K), highlighting the cross peaks related to thread/DB24C8 interactions and partial structure hypothesized.

Considering the orientation of the DB24C8 cavity according to the ROESY spectra, alongside the clear shielding of the triazolium protons in the ^{1}H NMR and the set of peaks undergoing broadening at low temperatures, we can hypothesize that in CD_3CN the macrocycle assumes a chair conformation, albeit maintaining a high degree of mobility.

5. ^{1}H NMR Monitoring of DB24C8 Translation to Trz^+ induced by Chemical Reduction of Bpy^{2+}.

The chemical reduction of Bpy^{2+} to $Bpy^{(0)}$ in compound $\mathbf{2}^{3+}$ was achieved using cobaltocene ($CoCp_2$, $E_{1/2}$ = -0.94 V vs. SCE).[3] Sample preparation was performed in a glove box under nitrogen atmosphere; to a 1 mM solution of $\mathbf{2}^{3+}$ in CD_3CN in a Wilmad low pressure/vacuum NMR tube, were added 10 eq of cobaltocene at room temperature. NMR spectra were recorded within 30 minutes after sample preparation. The generated species, if stored in the sealed tube, proved to be stable in time.

Although $Bpy^{(0)}$ is diamagnetic and should present a characteristic set of signals in the range 5 – 6 ppm, the ^{1}H NMR spectrum in Figure S35 do not show any peak either for the $Bpy^{(0)}$ unit or for the protons on neighbouring groups. These observations suggest the presence of a paramagnetic species even after the addition of 10 equivalents of $CoCp_2$, which should reduce the majority of the Bpy^{2+} to the neutral form ($E_{1/2}(Bpy^{2+}/Bpy^{+\cdot})$= -0.50 V vs. SCE, $E_{1/2}$ ($Bpy^{+\cdot}/Bpy^{0}$)= -0.83 V vs. SCE, see Table 1 below). The absence of the $Bpy^{(0)}$ signals is ascribed to an electron self-exchange between the $Bpy^{(0)}$ and traces of $Bpy^{(\cdot+)}$, present even with an excess of reducing agent, as observed in previous works for oxoammonium salts and nitroxide radicals.[4]

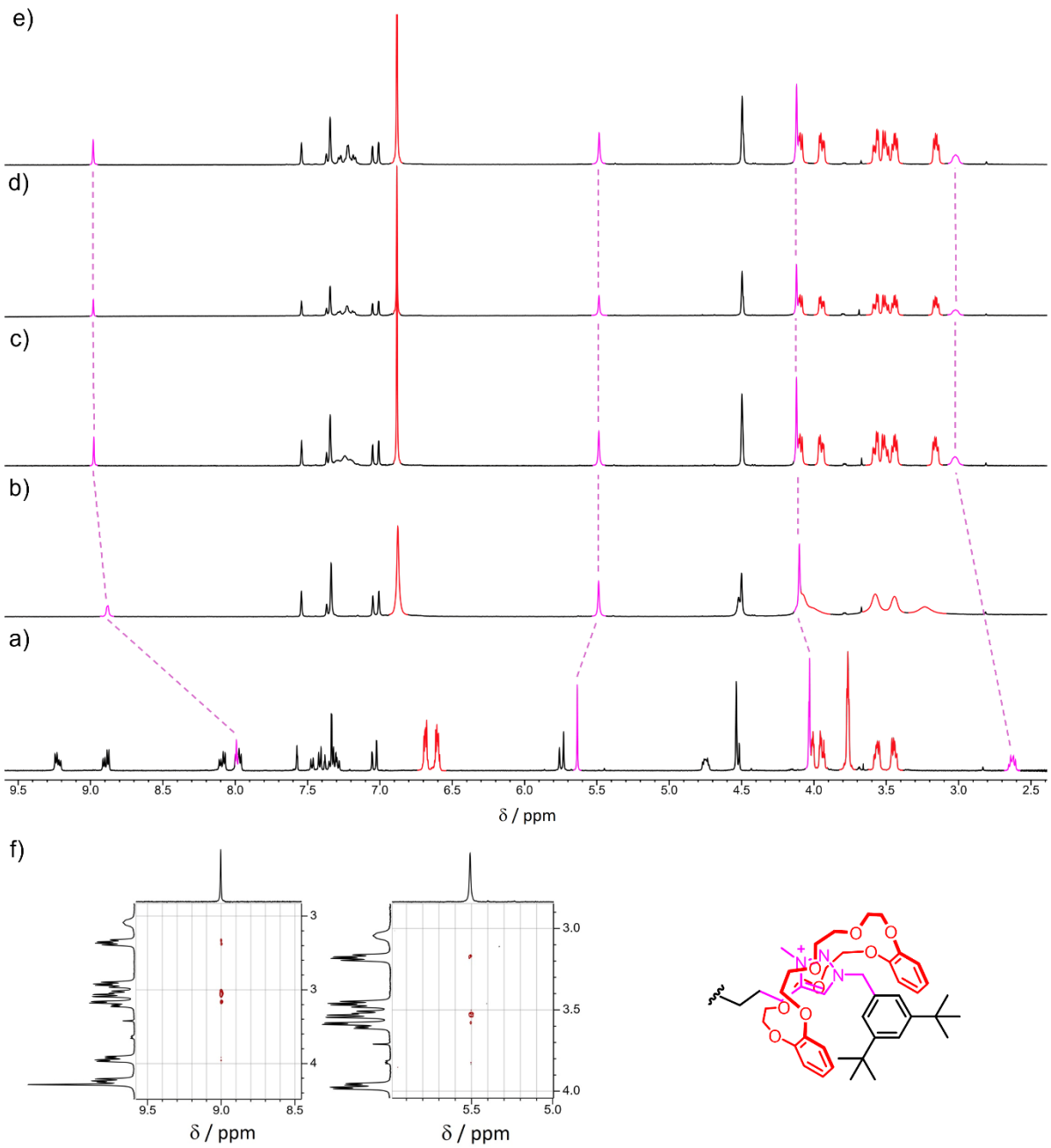

Figure S35 - Partial ^{1}H NMR spectra (500 MHz, CD_3CN, 298 K) of a) compound $\mathbf{2}^{3+}$ (5 mM); b) compound $\mathbf{2}^{3+}$ (1 mM) after the addition of 2 eq. of $CoCp_2$; c) compound $\mathbf{2}^{3+}$ (1 mM) after the addition of 4 eq. of $CoCp_2$; d) compound $\mathbf{2}^{3+}$ (1 mM) after the addition of 6 eq. of $CoCp_2$; e) compound $\mathbf{2}^{3+}$ (1 mM) after the addition of 10 eq. of $CoCp_2$;. Dashed lines highlight the variation of chemical shift of relevant signals assigned to Trz^+ in pink, DB24C8 signals are highlighted in red. f) Partial ROESY spectra (500 MHz, CD_3CN 298 K) recorded for sample (e): the cross peaks show that the triazolium is located within the cavity of DB24C8.

6. Electrochemical Measurements

Table 1- Electrochemical potentials of the investigated species in CH_3CN and CH_2Cl_2. All potential values are expressed as V vs SCE. [a]Half-wave potential of the reversible processes, taken from cyclic voltammetries; [b]peak potential of the poorly reversible process, taken from differential pulse voltammetries.

Compound	CH_3CN			CH_2Cl_2		
	$E_{1/2}$ $(Bpy^{2+}/Bpy^{+\cdot})^a$	$E_{1/2}$ $(Bpy^{+\cdot}/Bpy^{0})^a$	E_p $(Trz^{+}/Trz^{\cdot})^b$	$E_{1/2}$ $(Bpy^{2+}/Bpy^{+\cdot})^a$	$E_{1/2}$ $(Bpy^{+\cdot}/Bpy^{0})^a$	E_p $(Trz^{+}/Trz^{\cdot})^b$
1H^{4+}	-0.35	-0.77	-1.70/-1.92	-0.27	-0.77	-1.70
+ P_1 base (1 eq.)	-0.51	-0.83	-1.92	-0.46	-0.80	\
+ Triflic acid (1 eq.)	-0.36	-0.78	-1.70/-1.92	-0.27	-0.77	-1.69
2^{3+}	-0.50	-0.83	-1.91	-0.45	-0.79	\
3H^{3+}	-0.36	-0.79	/	-0.26	-0.77	\
+ P_1 base (1.5 eq.)	-0.56	-1.00	/	-0.49	-1.01	\
4^{2+}	-0.55	-1.01	/	-0.49	-1.01	\
5H^{4+}	-0.36	-0.78	-1.71	-0.25	-0.78	-1.70
+ P_1 base (1 eq.)	-0.36	-0.79	-1.72	-0.26	-0.78	-1.71
6^{3+}	-0.35	-0.79	-1.73	-0.25	-0.78	-1.73

6.1 Cyclic Voltammetries and Differential Pulse Voltammetries

During the cyclic voltammetric experiment, sweeping the potential up to the reduction of the triazolium unit can cause the appearance of extra waves in the anodic scan, due to the poor reversibility of the triazolium reduction process. In such cases two voltammetries are reported, the first stopping before the triazolium reduction and the second one reaching it. The voltammetric wave of ferrocene is marked with Fc.

Compound $1H^{4+}$ in CH_2Cl_2 and CH_3CN

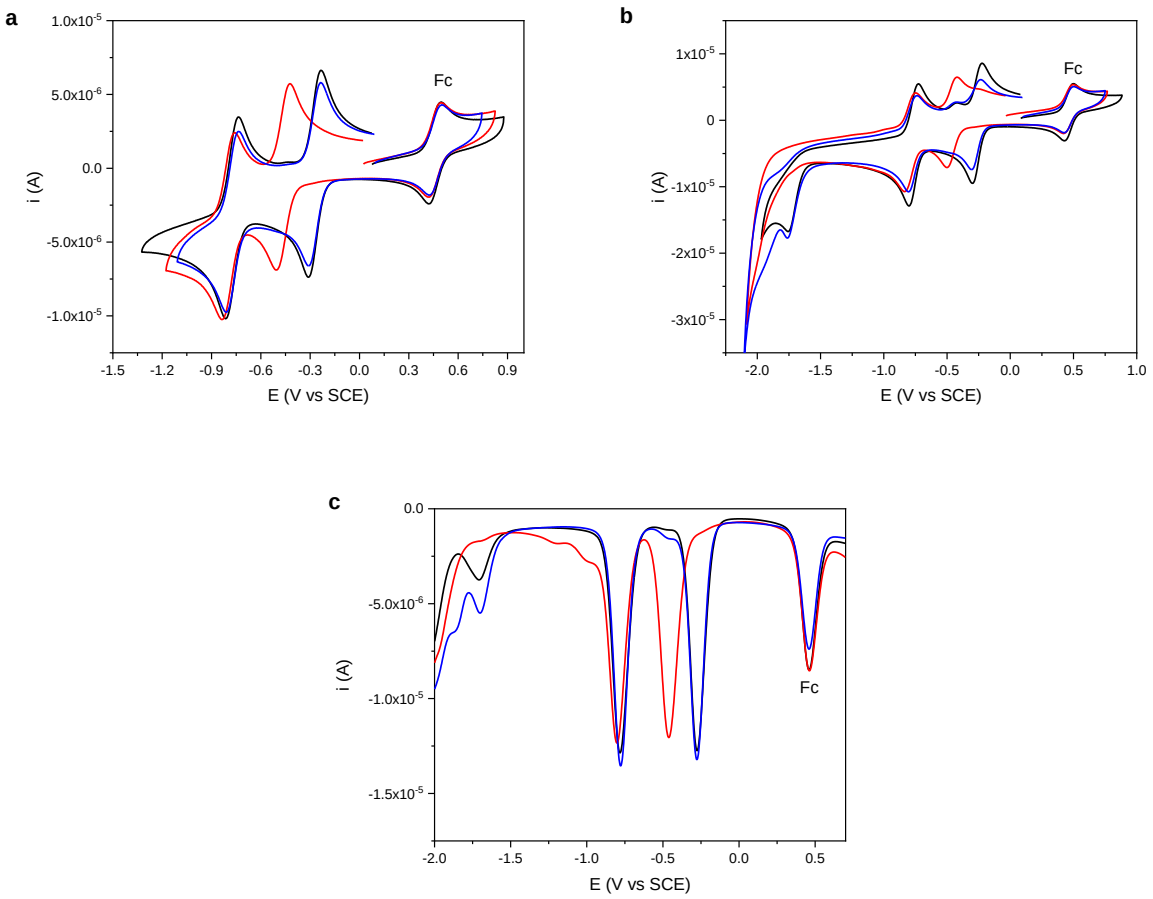

Figure S36 - CV (**a**-**b**, scan rate: 200 mV s^{-1}) and DPV (**c**, scan rate: 20 mV s^{-1}) of a 4.1 × 10^{-4} M solution of **1**H^{4+} (black line) and upon sequential addition of P1 base (1 equivalent, red line) and triflic acid (1 equivalent, blue line). Experimental conditions: argon-purged CH_2Cl_2, room temperature, 100 equivalents of $TBAPF_6$.

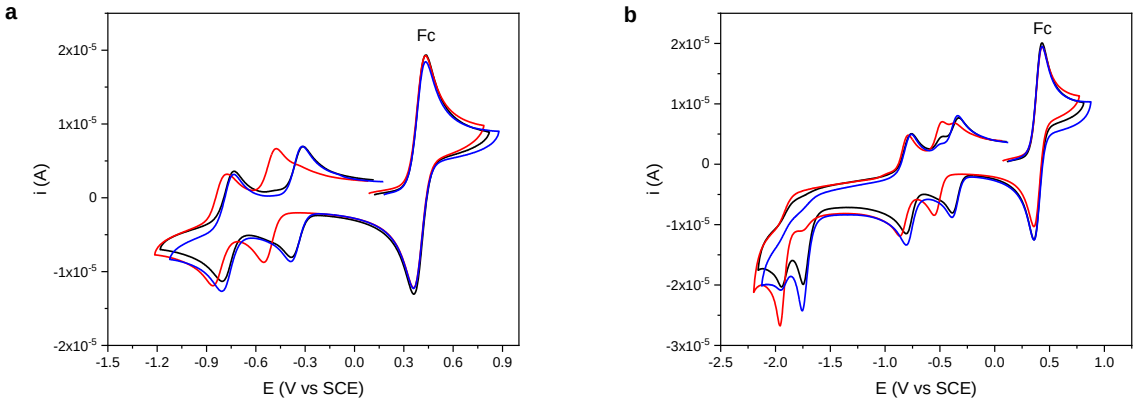

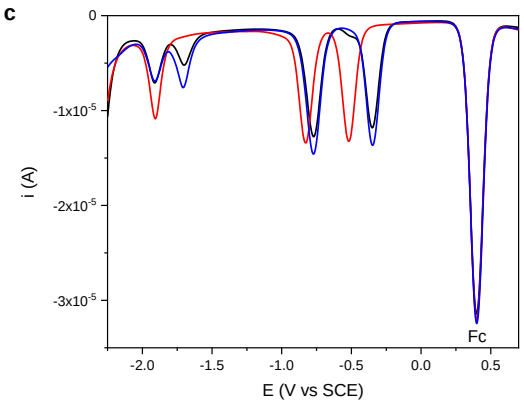

Figure S37- CV (**a**-**b**, scan rate: 200 mV s^{-1}) and DPV (**c**, scan rate: 20 mV s^{-1}) of a 4.0 × 10^{-4} M solution of **1**H^{4+} (black line) and upon sequential addition of P1 base (1 equivalent, red line) and triflic acid (1 equivalent, blue line). Experimental conditions: argon-purged CH_3CN, room temperature, 100 equivalents of $TEAPF_6$.

We hypothesized that the presence of the process at -1.92 V vs SCE in *Figure S36* could be related to the presence of a basic species, formed upon the reduction of the triazolium, capable to deprotonate the ammonium site of the rotaxane. If this deprotonation process would take place intermolecularly, i.e. the ammonium site of another rotaxane is deprotonated, it could cause the shuttling of the macrocycle on the triazolium (as the bipyridinium unit is already bireduced), shifting its reduction towards negative potentials and, overall, leading to the presence of two reduction peaks related to this station. This consideration is supported by the fact that the anodic portion of the curve is affected by the reduction of the triazolium unit (*Figure S36b*): indeed, a new weak peak emerges around -0.5 V vs SCE, a potential value compatible with the monoreduced bipyridinium site encircled by the crown ether, sign of the presence of the deprotonated rotaxane. The hypothesis was tested repeating the electrochemical measurement of **1**H^{4+} in presence of 1 equivalent of triflic acid (*Figure S37*). The addition of triflic acid causes the disappearance of the process at -1.92 V vs SCE. Therefore, it can be concluded that the presence of this process is related to a proton transfer triggered by the reduction of the triazolium, which cause the deprotonation of the rotaxane.

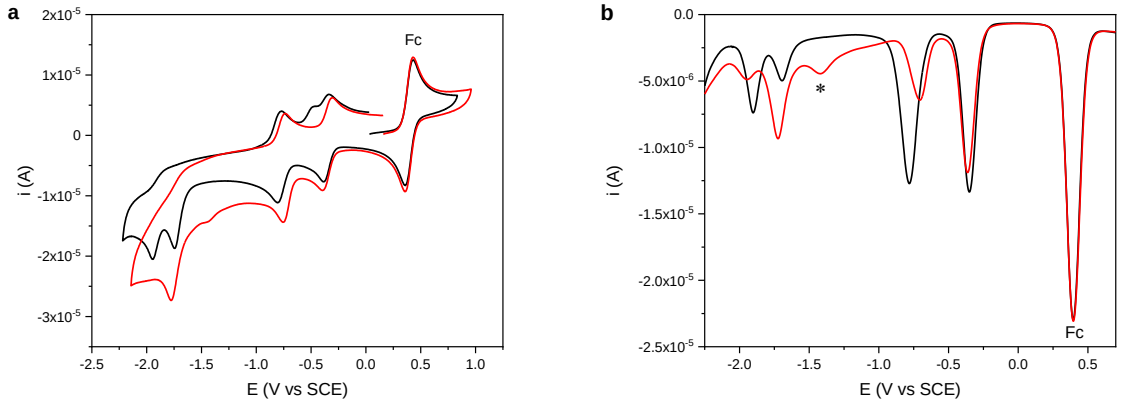

Figure S38 - CV (**a**, scan rate: 200 mV s^{-1}) and DPV (**b**, scan rate: 20 mV s^{-1}) of a 4.0 × 10^{-4} M solution of **1**H^{4+} (black line) and upon addition of triflic acid (1 equivalent, red line). Experimental conditions: argon-purged CH_3CN, room

temperature, 100 equivalents of $TEAPF_6$. The peak marked with an asterisk is assigned to a reduction process related to the triflic acid.

Compound 2^{3+} in CH_2Cl_2 and CH_3CN

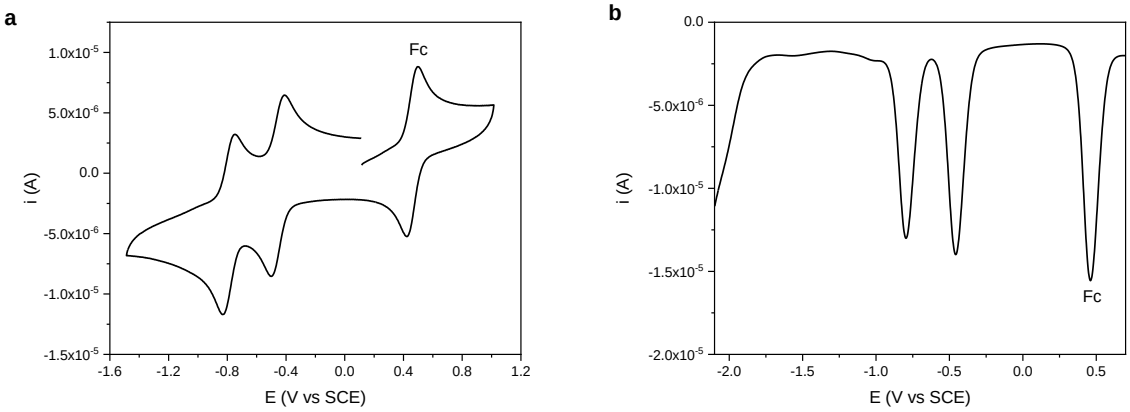

Figure S39 - CV (**a**, scan rate: 200 mV s^{-1}) and DPV (**b**, scan rate: 20 mV s^{-1}) of a 3.5 × 10^{-4} M solution of $\mathbf{2}^{3+}$. Experimental conditions: argon-purged CH_2Cl_2, room temperature, 100 equivalents of $TBAPF_6$.

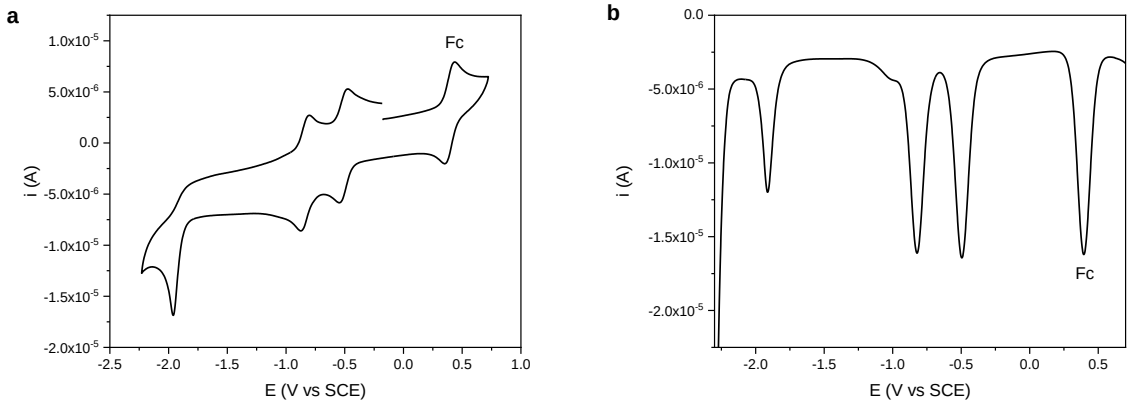

Figure S40 - CV (**a**, scan rate: 50 mV s^{-1}) and DPV (**b**, scan rate: 20 mV s^{-1}) of a 3.3 × 10^{-4} M solution of $\mathbf{2}^{3+}$. Experimental conditions: argon-purged CH_3CN, room temperature, 100 equivalents of $TEAPF_6$.

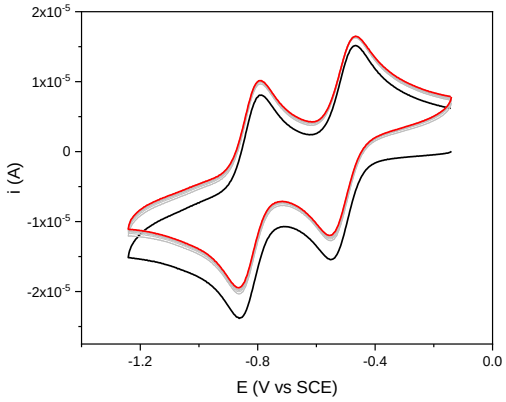

Figure S41 - Stacked plot of 10 CVs (scan rate: 500 mV s^{-1}) of a 3.3 × 10^{-4} M solution of **2**$^{3+}$ (scan 1: black line, scans 2-9: gray lines, scan 10: red line), recorded without renewing the diffusion layer. The only difference observed in the CVs is related to a decrease of the background current after the first scan. Experimental conditions: argon-purged CH_3CN, room temperature, 100 equivalents of $TEAPF_6$.

Compound 3H^{3+} in CH_2Cl_2 and CH_3CN

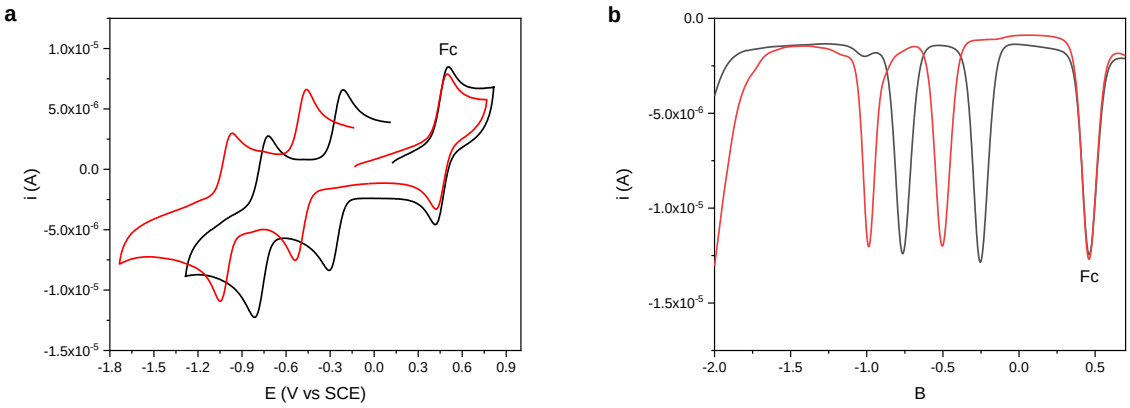

Figure S42 - CV (**a**, scan rate: 200 mV s^{-1}) and DPV (**b**, scan rate: 20 mV s^{-1}) of a 3.7 × 10^{-4} M solution of **3**H^{3+} (black line) and upon addition of P1 base (1.5 equivalents, red line). Experimental conditions: argon-purged CH_2Cl_2, room temperature, 100 equivalents of $TBAPF_6$.

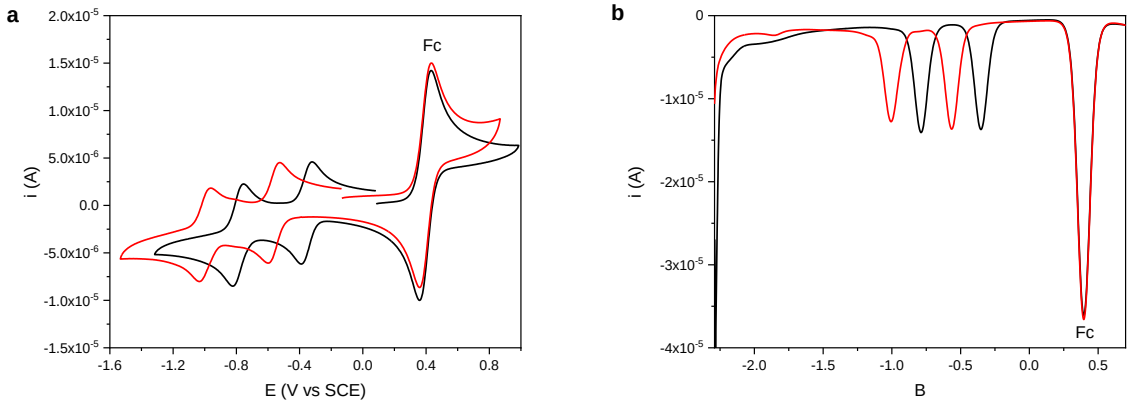

Figure S43 - CV (**a**, scan rate: 100 mV s^{-1}) and DPV (**b**, scan rate: 20 mV s^{-1}) of a 4.1 × 10^{-4} M solution of **3**H^{3+} (black line) and upon addition of P1 base (1.5 equivalents, red line). Experimental conditions: argon-purged CH_3CN, room temperature, 100 equivalents of $TEAPF_6$.

Compound 4^{2+} in CH_2Cl_2 and CH_3CN

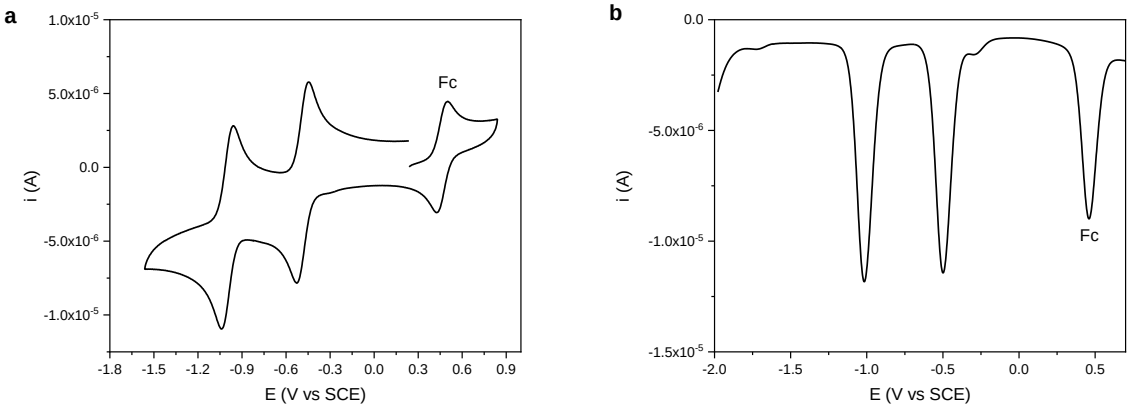

Figure S44 - CV (**a**, scan rate: 200 mV s^{-1}) and DPV (**b**, scan rate: 20 mV s^{-1}) of a 3.6 × 10^{-4} M solution of **4**$^{2+}$. Experimental conditions: argon-purged CH_2Cl_2, room temperature, 100 equivalents of $TBAPF_6$.

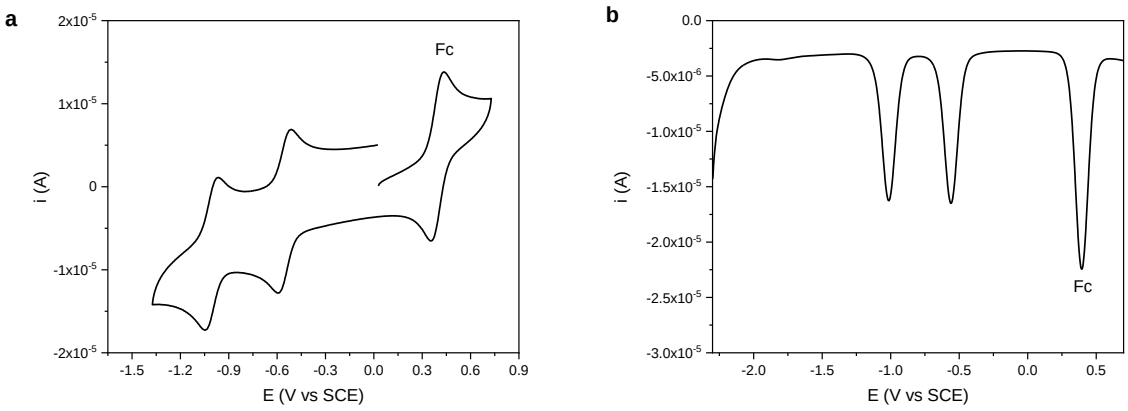

Figure S45 - CV (**a**, scan rate: 200 mV s^{-1}) and DPV (**b**, scan rate: 20 mV s^{-1}) of a 3.4 × 10^{-4} M solution of $\mathbf{4}^{2+}$. Experimental conditions: argon-purged CH_3CN, room temperature, 100 equivalents of $TEAPF_6$.

Compound $5H^{4+}$ in CH_2Cl_2 and CH_3CN

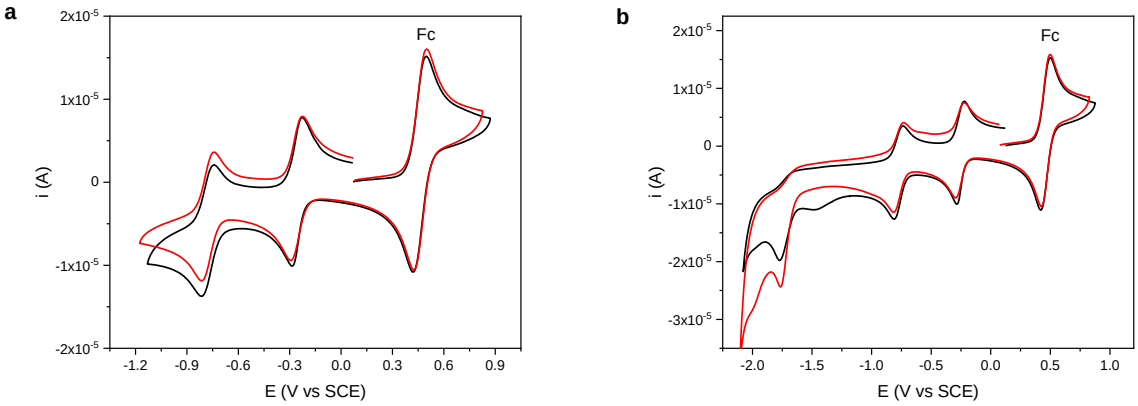

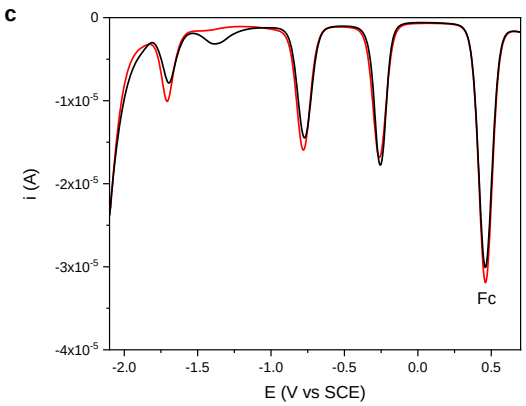

Figure S46 - CV (**a**-**b**, scan rate: 200 mV s^{-1}) and DPV (**c**, scan rate: 20 mV s^{-1}) of a 5.0× 10^{-4} M solution of **5**H^{4+} (black line) and upon addition of P1 base (1 equivalent, red line). Experimental conditions: argon-purged CH_2Cl_2, room temperature, 100 equivalents of $TBAPF_6$.

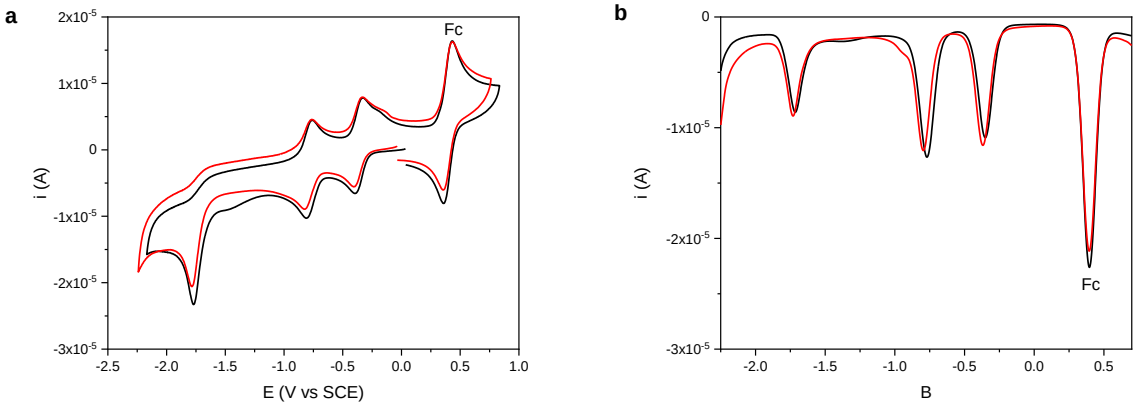

Figure S47 - CV (**a**, scan rate: 200 mV s^{-1}) and DPV (**b**, scan rate: 20 mV s^{-1}) of a 3.8 × 10^{-4} M solution of **5**H^{4+} (black line) and upon sequential addition of P1 base (1 equivalent, red line). Experimental conditions: argon-purged CH_3CN, room temperature, 100 equivalents of $TEAPF_6$.

Compound 6^{3+} in CH_2Cl_2 and CH_3CN

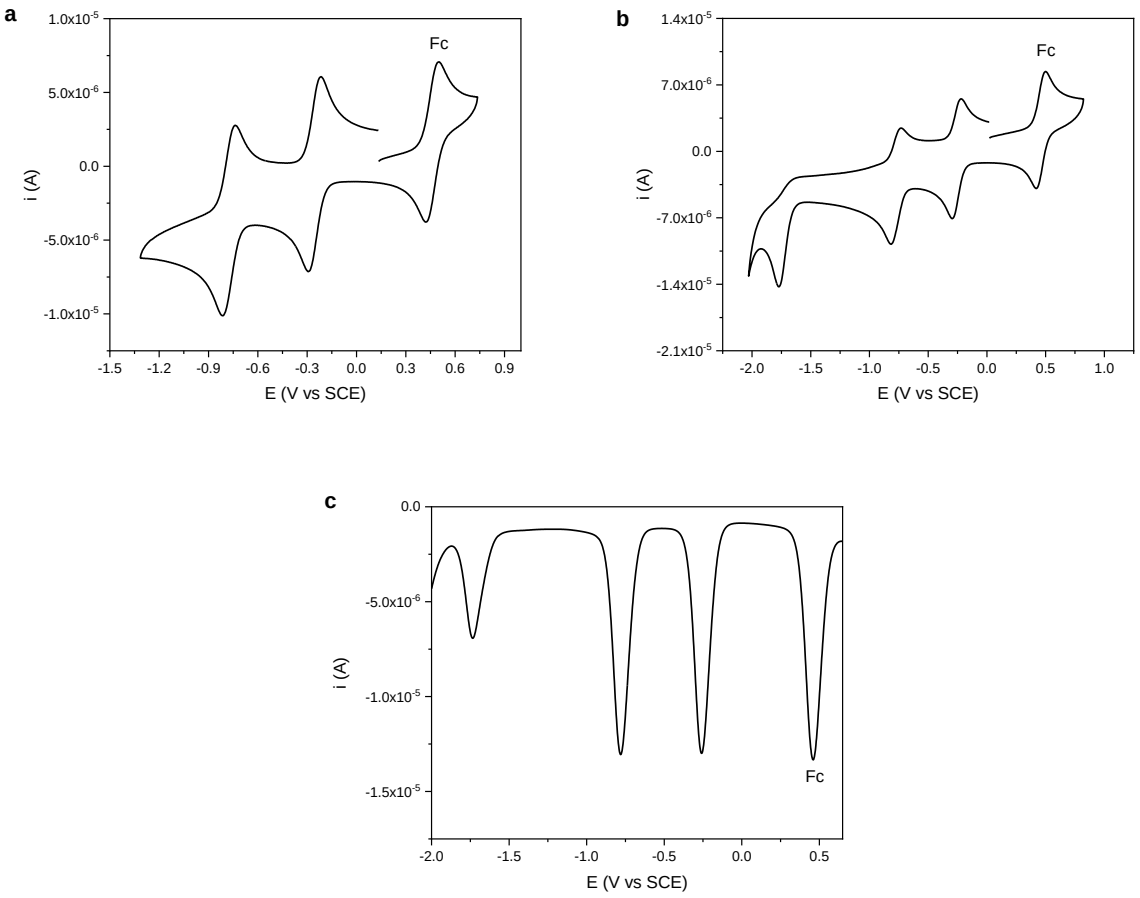

Figure S48 - CV (**a**-**b**, scan rate: 200 mV s^{-1}) and DPV (**c**, scan rate: 20 mV s^{-1}) of a 3.3 × 10^{-4} M solution of $\mathbf{6}^{3+}$. Experimental conditions: argon-purged CH_2Cl_2, room temperature, 100 equivalents of $TBAPF_6$.

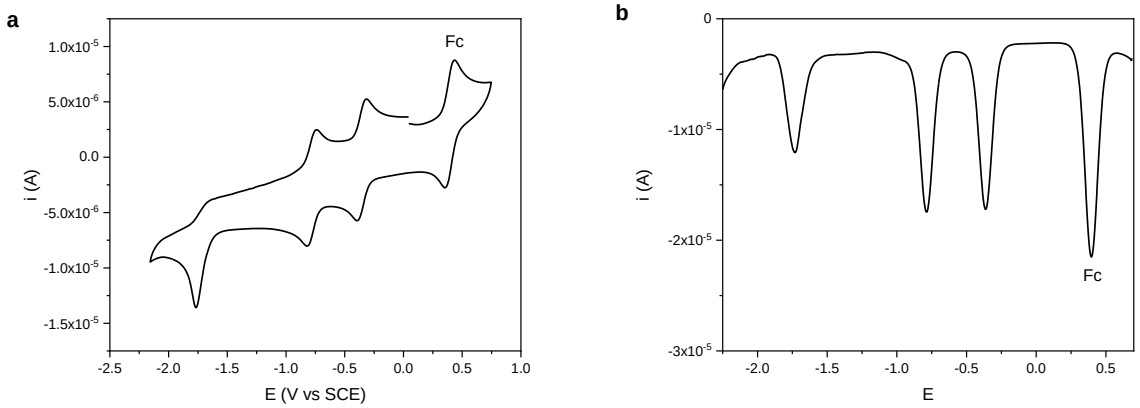

Figure S49 - CV (**a**, scan rate: 50 mV s^{-1}) and DPV (**b**, scan rate: 20 mV s^{-1}) of a 3.4 × 10^{-4} M solution of $\mathbf{6}^{3+}$. Experimental conditions: argon-purged CH_3CN, room temperature, 100 equivalents of $TEAPF_6$.

6.2 Cyclic voltammetries fitting

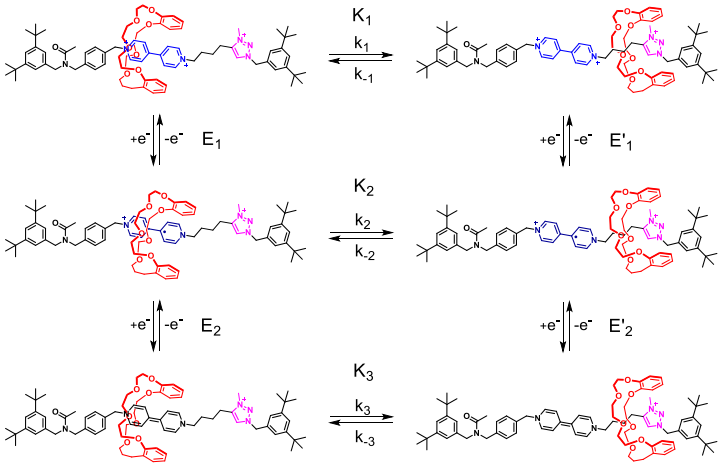

Scheme S5 - Scheme related to the co-conformational equilibria of **2**$^{3+}$ for the different redox states of the bipyridinium unit. The vertical processes represent the redox reactions of Bpy^{2+}, while the horizontal processes represent the shuttling of DB24C8 between Bpy (in its three oxidation states) and Trz^{+}. The counterions of the rotaxane are omitted for the sake of clarity.

The cyclic voltammetries of **2**$^{3+}$ were fitted to determine the values of K_1, K_2 and K_3 in CH_3CN and CH_2Cl_2 at 298 K, using the software DigiSim 3.05,[5] according to the square scheme mechanism reported in *Scheme S5*. CVs at different scan rates ranging from 50 mV/s to 300 mV/s were fitted and the equilibrium constant values, obtained from the fitting, were averaged. K_2 and K_3 are related to the values of K_1, E_1, E_1', E_2, E_2' through the equations:

$$K_2 = K_1\, e^{[-F(E_1 - E_1')/RT]} \quad and \quad K_3 = K_2\, e^{[-F(E_2 - E_2')/RT]}$$

The kinetics of the ring shuttling were considered to be much faster than the scan rate of the CV and the values k_1, k_2 and k_3 were fixed as 10^3 s^{-1}. The value of k_1 has no effect of the fitting outcome. As for k_2 and k_3, larger values do not affect the fitting, whereas smaller values affect the shape of the simulated voltammetries without reproducing the experimental curves. The reduction potentials E_1 and E_2 of the bipyridinium surrounded by the ring were taken from the model rotaxane **4**$^{2+}$ (-0.49 V and -1.01 V in CH_2Cl_2, -0.55V and -1.01 V in CH_3CN), where the bipyridinium is the only available station for the ring. In CH_3CN the first reduction process could not be properly fitted using such value (E_1=-0.55 V) and this parameter was also optimized during the fitting, obtaining a value of -0.51V. The reduction potentials E'_1 and E'_2 of the free bipyridinium were taken from the model axle **6**$^{3+}$ (-0.25 V and -0.78 V in CH_2Cl_2, -0.35 V and -0.79 V in CH_3CN). The heterogeneous electron transfer constants k_{ET} of all the processes were fixed as 1 cm s^{-1}, value representative of a reversible process under the experimental conditions. The charge-transfer coefficients α were taken as 0.5 in all cases.

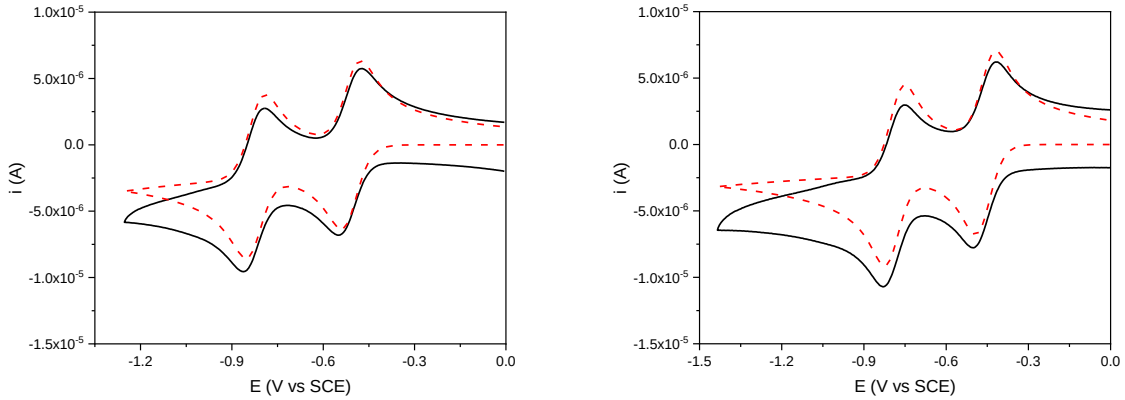

Figure S50 - Experimental (solid black line) and simulated (dashed red line) CV (scan rate: 100 mV s^{-1}) of $\mathbf{2}^{3+}$ in CH_3CN (left, 3.3 × 10^{-4} M) and CH_2Cl_2 (left, 3.5 × 10^{-4} M). Experimental conditions: argon-purged CH_3CN / CH_2Cl_2, room temperature, 100 equivalents of $TEAPF_6$ / $TBAPF_6$.

Table S2 - Thermodynamic constants of the co-conformational equilibria, related to the different oxidation states of the bipyridinium, in rotaxane $\mathbf{2}^{3+}$ (See *Scheme 5*), obtained by fitting of the cyclic voltammetries in CH_3CN and CH_2Cl_2.

Solvent	K_1	K_2	K_3
CH_3CN	4.6 × 10^{-4}	0.33	1738
CH_2Cl_2	2.8 × 10^{-4}	3.23	24930

7. Thermodynamic considerations

7.1 Relation between apparent acidity constant and co-conformation equilibrium constants of rotaxane $3H^{3+}$

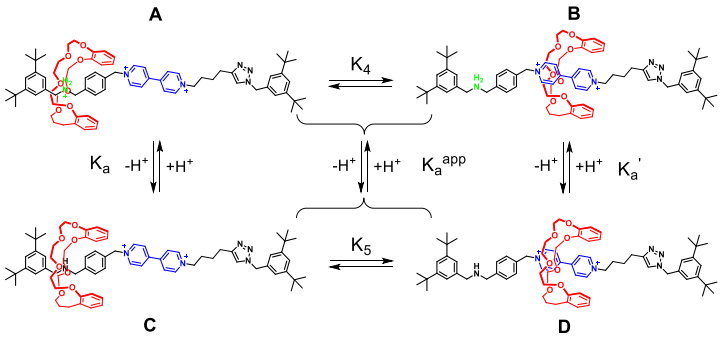

Scheme S6 - Scheme related to the co-conformational equilibria of $\mathbf{3}H^{3+}$ for the different states of the ammonium station. The vertical processes represent deprotonation of AmH+, while the horizontal processes represent the shuttling of DB24C8 from AmH^+ to Bpy^{2+}. The counterions of the rotaxane are omitted for sake of clarity. The four species are identified as **A**, **B**, **C** and **D**.

Considering Scheme 6, the apparent acidity constant K_a^{app} of rotaxane **3**H^{3+} is expressed as:

$$K_a^{app} = \frac{([C] + [D]) \times [H^+]}{[A] + [B]} \quad (1)$$

This form takes into account that, due to the shuttling of the ring, there are two acidic species (A and B) which can be deprotonated and the acidity constant measured experimentally K_a^{app} is influenced by the acidity constants of both species (K_a and K_a') and the co-conformational equilibrium constants, which determine the ratio between A and B (K_4) and C and D (K_5).

K_4 and K_5 are defined as:

$$K_4 = \frac{[B]}{[A]} \ (2) \quad K_5 = \frac{[D]}{[C]} \ (3)$$

The acidity constants K_a and K_a' are defined as:

$$K_a = \frac{[C] \times [H^+]}{[A]} \ (4) \quad K_a' = \frac{[D] \times [H^+]}{[B]} \ (5)$$

Combining Equations (1-5), Equation (1) can be rearranged as:

$$K_a^{app} = \frac{K_a + K_a' \times K_4}{1 + K_4} \quad (6)$$

And K_4 can be expressed as:

$$K_4 = \frac{K_a^{app} - K_a}{K_a' - K_a^{app}} (7)$$

While K_5 as:

$$K_5 = \frac{K_a' \times K_4}{K_a} \ (8)$$

These relations implies that the values of K_4 and K_5 can be obtained from the ones of K_a^{app}, K_a and K_a'.

7.2 pKa Determination *via* ^{1}H NMR Spectroscopy Experiments

The determination of K_a^{app} values of compound **3**H^{3+} and the K_a value of **11**H^{3+} *via* ^{1}H NMR titrations was performed by sequential additions of the base tributylamine (TBA, pKa = 18.09)[6] to ~5 mM solutions of the compounds in CD_3CN at 298K. The concentrations of the species were determined using tetrachloroethane (TCE, Merck) as internal standard. For each spectrum of the titration K_a^{app} (or K_a) were calculated considering the concentrations of every species. The final pK_a^{app} (or pK_a) value reported corresponds to the average of the pK_a^{app} (or pK_a) calculated excluding the initial 20% and final 20% points of the titration. The reported error was calculated as three times the standard deviation.

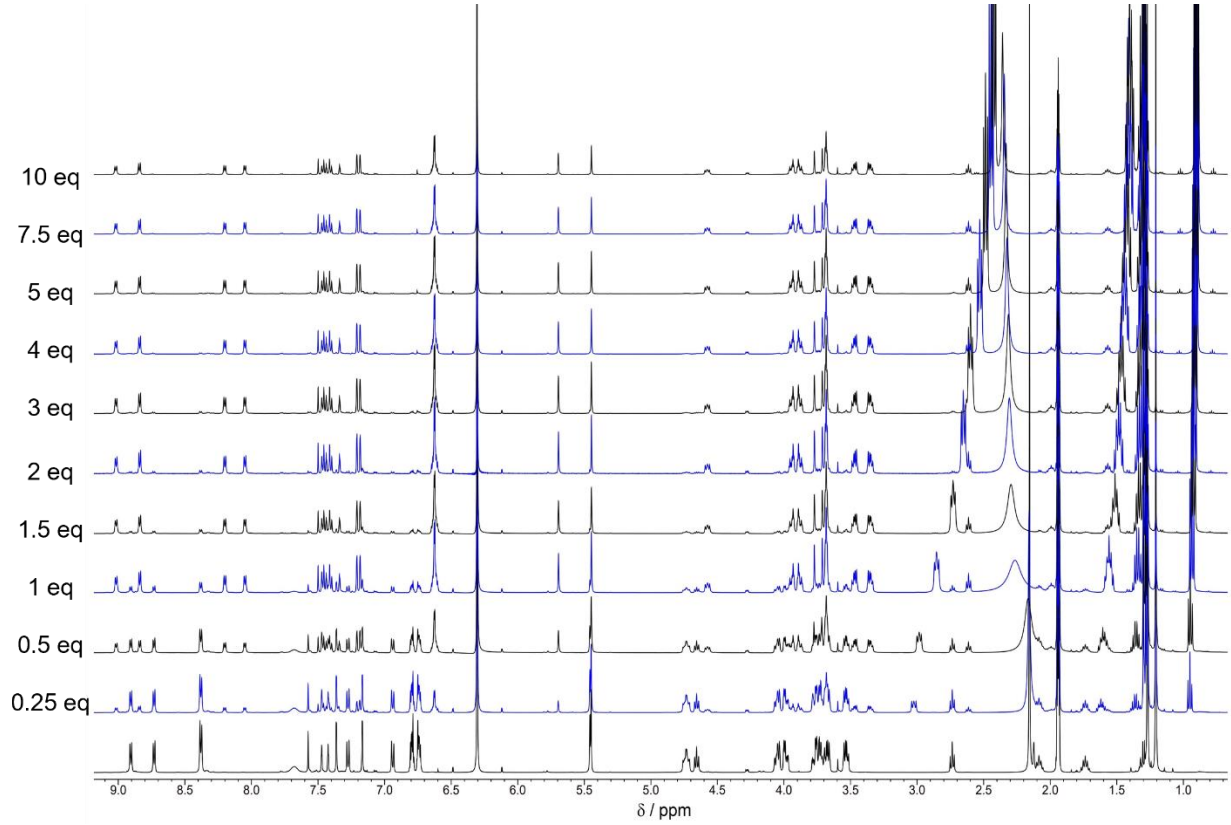

Figure S51 – ^{1}H NMR stacked spectra (500 MHz, CD_3CN, 298K) of the deprotonation of **3**H^{3+} ([**3**H^{3+}]$_i$ = 5.3 mM) after sequential additions of TBA.

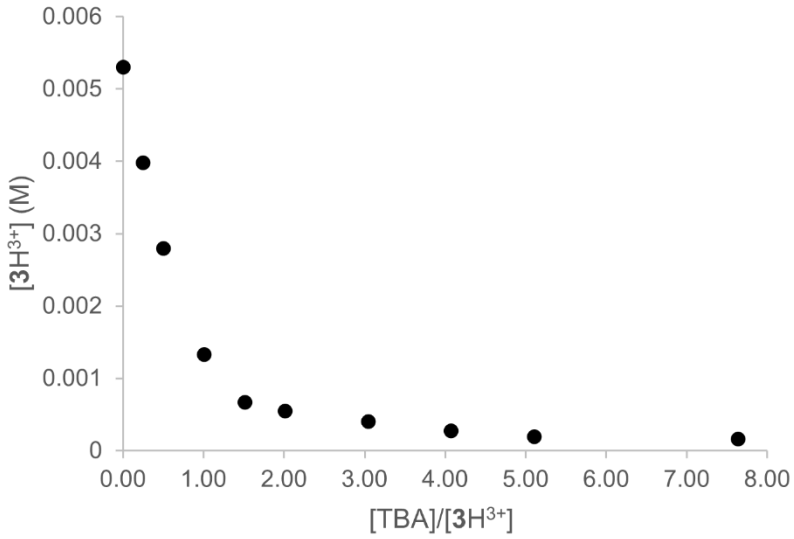

Figure S52 - Titration curve showing the variation of concentration of **3**H^{3+} ([**3**H^{3+}]$_i$ = 5.3 mM) after sequential additions of TBA base. Calculated pK_{app} = 17.2 ± 0.1.

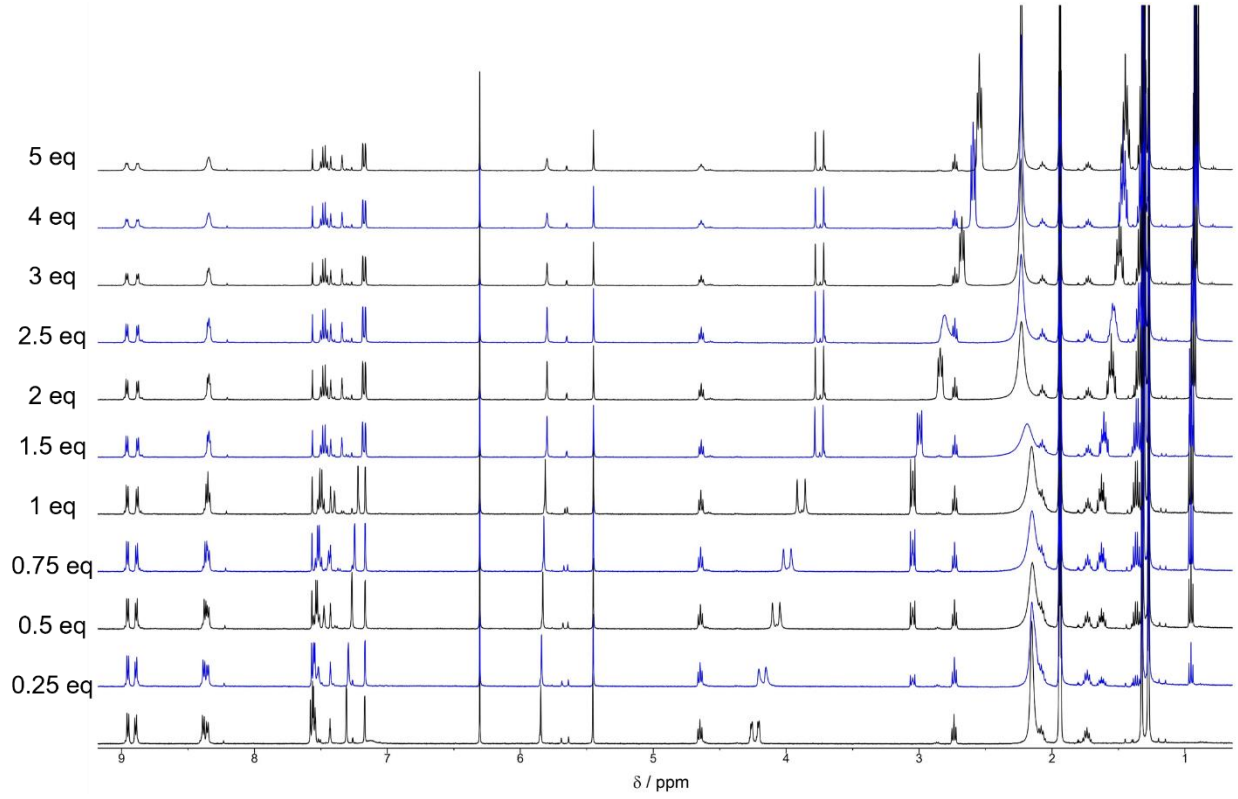

Figure S53 – ^{1}H NMR stacked spectra (500 MHz, CD_3CN, 298K) of the deprotonation of **11**H^{3+} ([**11**H^{3+}]$_i$ = 4.9 mM) after sequential additions of TBA.

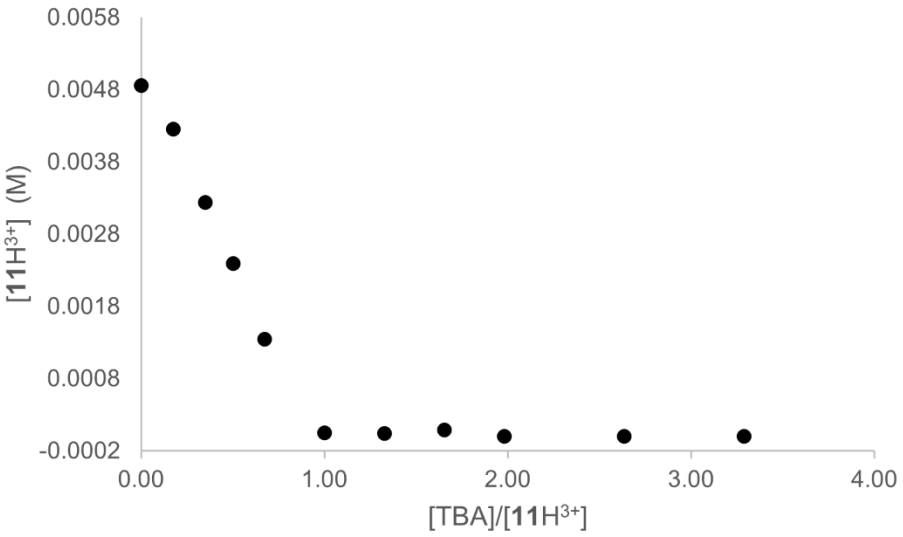

Figure S54 - Titration curve showing the variation of concentration of **11H^{3+}** ([**11H^{3+}**]$_i$ = 4.9 mM) after sequential additions of TBA base. Calculated pK_a = 15.2 ± 0.1.

Table S3 - Acidity constants and thermodynamic constants of the co-conformational equilibria in rotaxane **3**H^{3+} (See *Scheme 6*), in CH_3CN. [a]Value estimated from literature.[7]

pK_a [a]	pK_a'	pK_a^{app}	K_4	K_5
~26.3	15.2	17.2	1×10^{-2}	1×10^{9}

7.3 Energy levels of rotaxane 1H^{4+}

The fitting of the cyclic voltammetries of rotaxane **2**$^{3+}$ allowed to determine the equilibrium constants of the ring between the bipyridinium station (in its different oxidation states) and the triazolium station in CH_3CN and CH_2Cl_2 (K_1, K_2, K_3, see *Table S2*).

The determination of the apparent acidity constant K_a^{app} of rotaxane **3**$^{3+}$ allowed to calculate the equilibrium constants of the ring shuttling between the ammonium and the bipyridinium station in CH_3CN (K_4, K_5, see *Table S3*).

Combining these equilibrium constants and using rotaxanes **2**$^{3+}$ and **3**H^{3+} as models for **1**$^{4+}$, it is possible to evaluate the distribution of the ring on the different stations of the rotaxane in CH_3CN, assuming that the distribution of the ring between two stations is not affected by the presence of the third station. In other words, it is assumed that the presence of the ammonium station does not alter significantly the co-conformational equilibria investigated in rotaxane **2**$^{3+}$ and that the presence of the triazolium does not alter the ones investigated in rotaxane **3**H^{3+}. The equilibrium constant of the ring between two different stations can be used to determine the energy difference related to the ring on the two sites, and to build the energy level diagram reported in *Figure S55*,

arbitrarily setting the energy of the ring on the ammonium station as 0 kcal/mol. As an example, the energy difference between the ring on the ammonium and on the amine station can be evaluated considering the equilibria reported in Scheme S6. On the basis of the assumptions reported above, the energy of the ring on the Bpy^{2+} in B and D is identical, as it is not affected by the protonation state of the primary station. Therefore, the energy difference between the complexed AmH^+ and Am (levels α and α' in Figure S55) can be calculated from the co-conformational equilibrium constants K_4 and K_5:

$$\Delta\Delta G_{\alpha-\alpha'} = -R \times T \times ln\frac{K_4}{K_5} \quad (9)$$

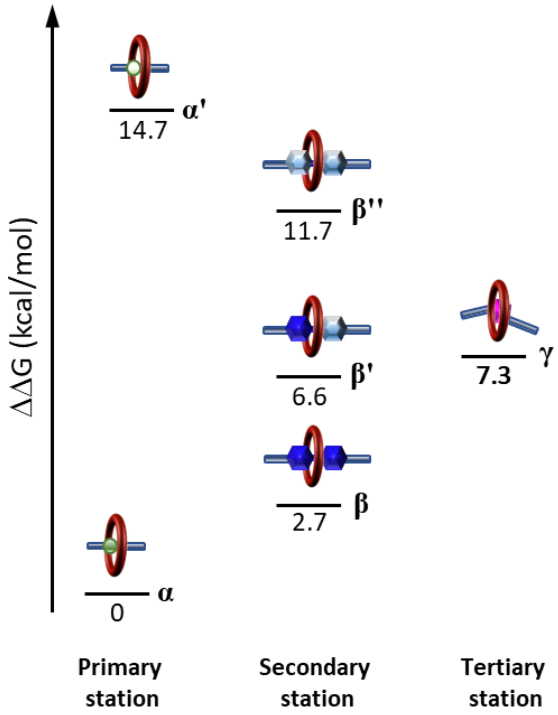

Figure S55 - Energy levels for the ring on the stations of rotaxane **1**H^{4+} in the different states (protonated/deprotonated for ammonium, oxidated/monoreduced/bireduced for bipyridinium) in CH_3CN at 298K.

Similar considerations can be applied to estimate the ΔΔG values corresponding to the ring on the bipyridinium station in its different oxidation states (Scheme S5 and Figure S55):

$$\Delta\Delta G_{\beta-\beta'} = -R \times T \times ln\frac{K_1}{K_2} \quad (10)$$

$$\Delta\Delta G_{\beta'-\beta''} = -R \times T \times ln\frac{K_2}{K_3} \quad (11)$$

The energy difference between the primary, secondary and tertiary stations are calculated from the equilibrium constants of the corresponding shuttling reactions:

$$\Delta\Delta G_{\alpha-\beta} = -R \times T \times lnK_4 \ (12)$$

$$\Delta\Delta G_{\beta-\gamma} = -R \times T \times lnK_1 \ (13)$$

The population of the energy levels for each state of rotaxane **1**H^{4+} can be evaluated using the Boltzmann distribution:

$$p_i = \frac{e^{-E_i/RT}}{\sum_{j=1}^{3} e^{-E_j/RT}}$$

Where p_i is the population of the i-th level, E_i is the energy of the level and the denominator is the sum of the population of the three levels.

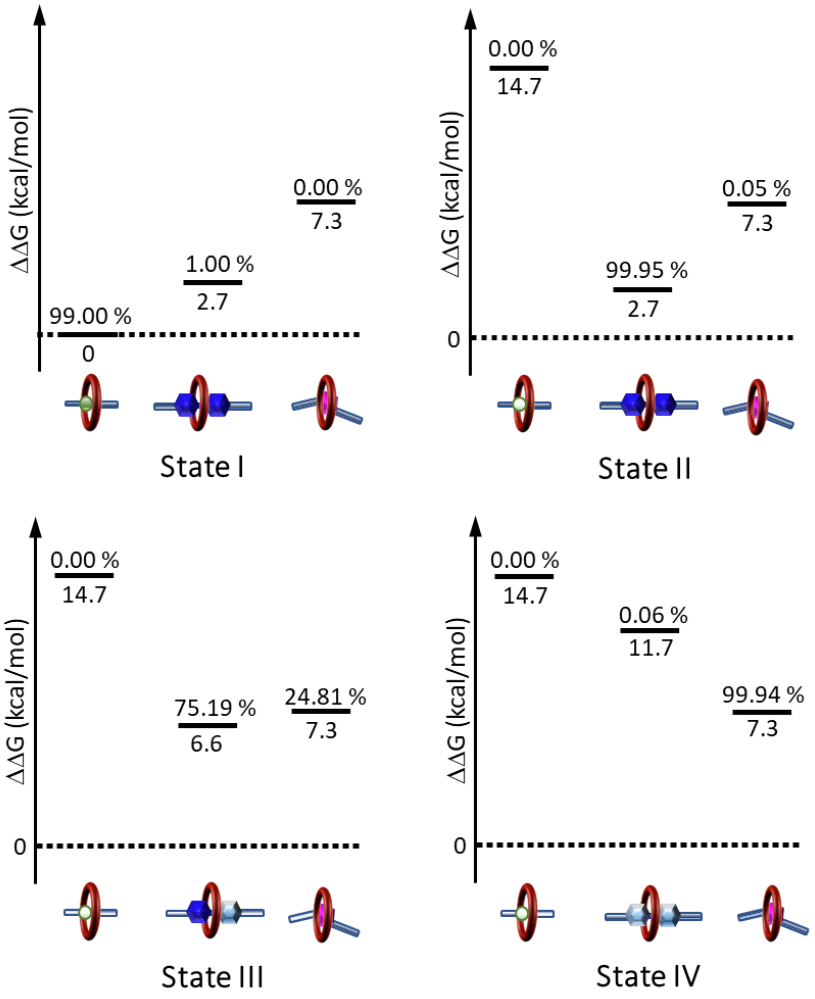

Figure S56 - Energy levels and relative population of the ring on the stations of rotaxane **1**H^{4+} in the different states (protonated/deprotonated for ammonium, oxidated/monoreduced/bireduced for bipyridinium) in CH_3CN at 298K.

8. High-Res Mass Spectra of compounds

8.1. Compound 1H^{4+}

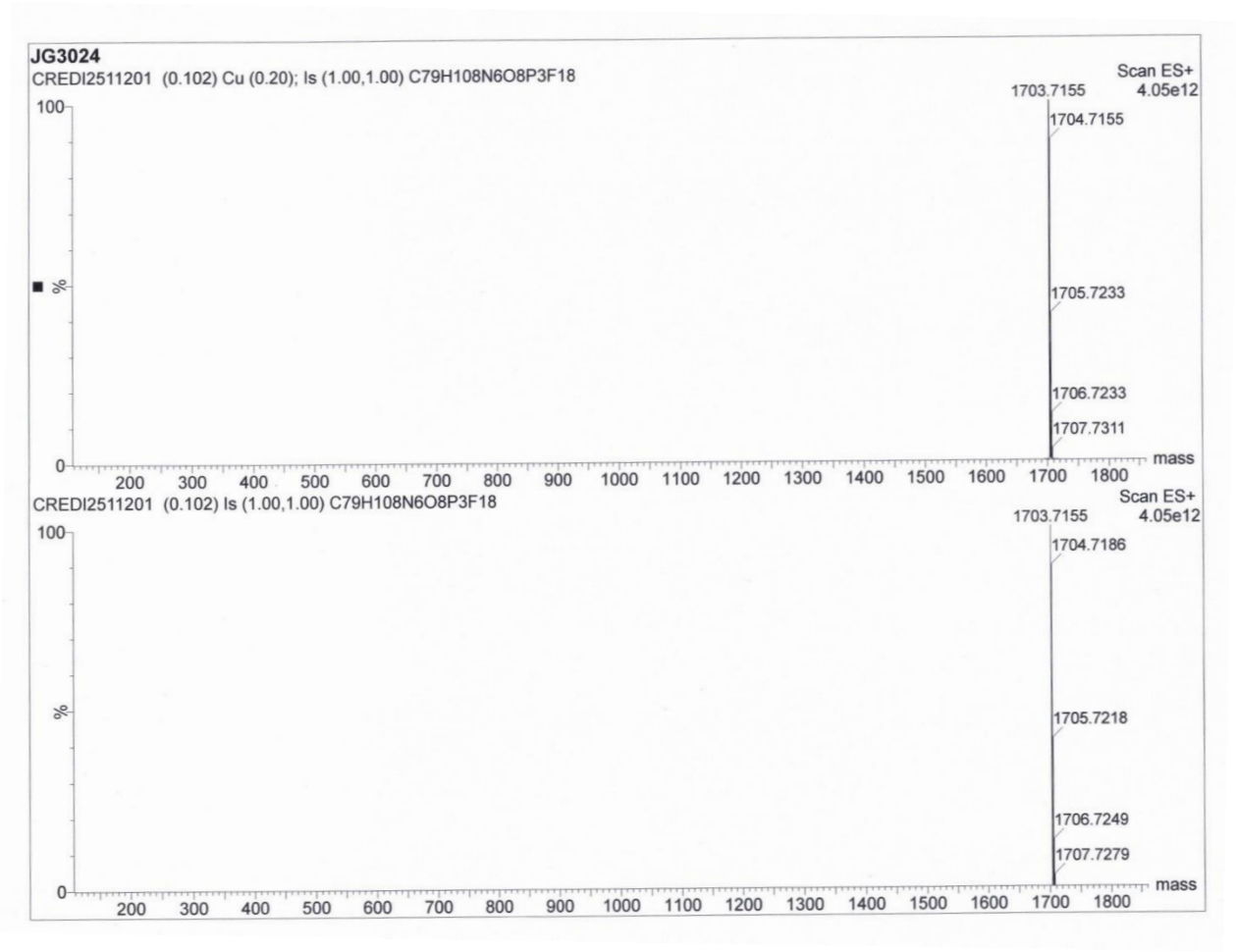

Figure S57 – Calculated (top) and measured (bottom) high-res mass spectra for compound **1H^{4+}**.

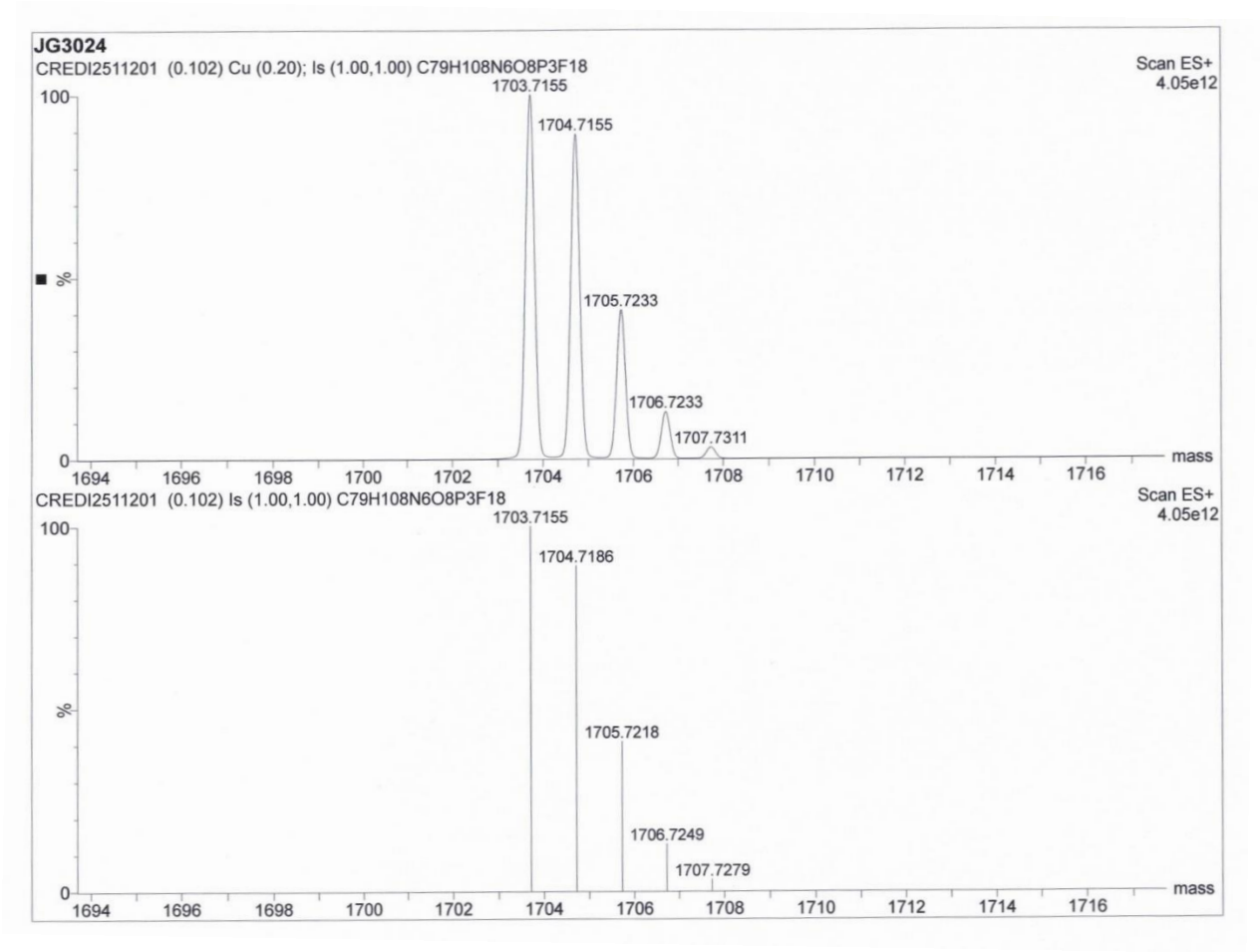

Figure S58 – Calculated (top) and measured (bottom) isotopic pattern of the peak at mass 1703.7155 for compound **1H**$^{4+}$.

8.2. Compound 2^{3+}

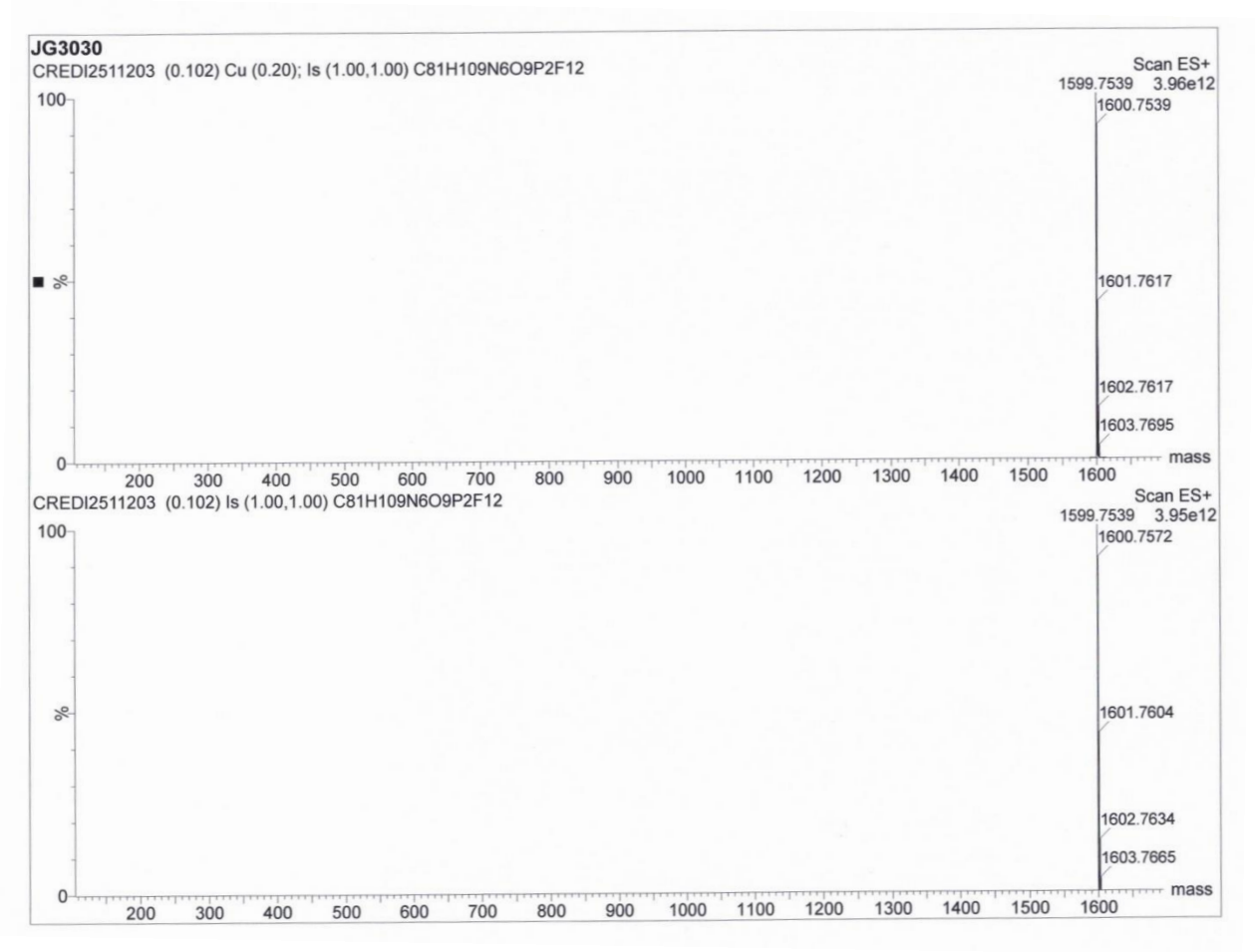

Figure S59 - Calculated (top) and measured (bottom) high-res mass spectra for compound **2^{3+}**.

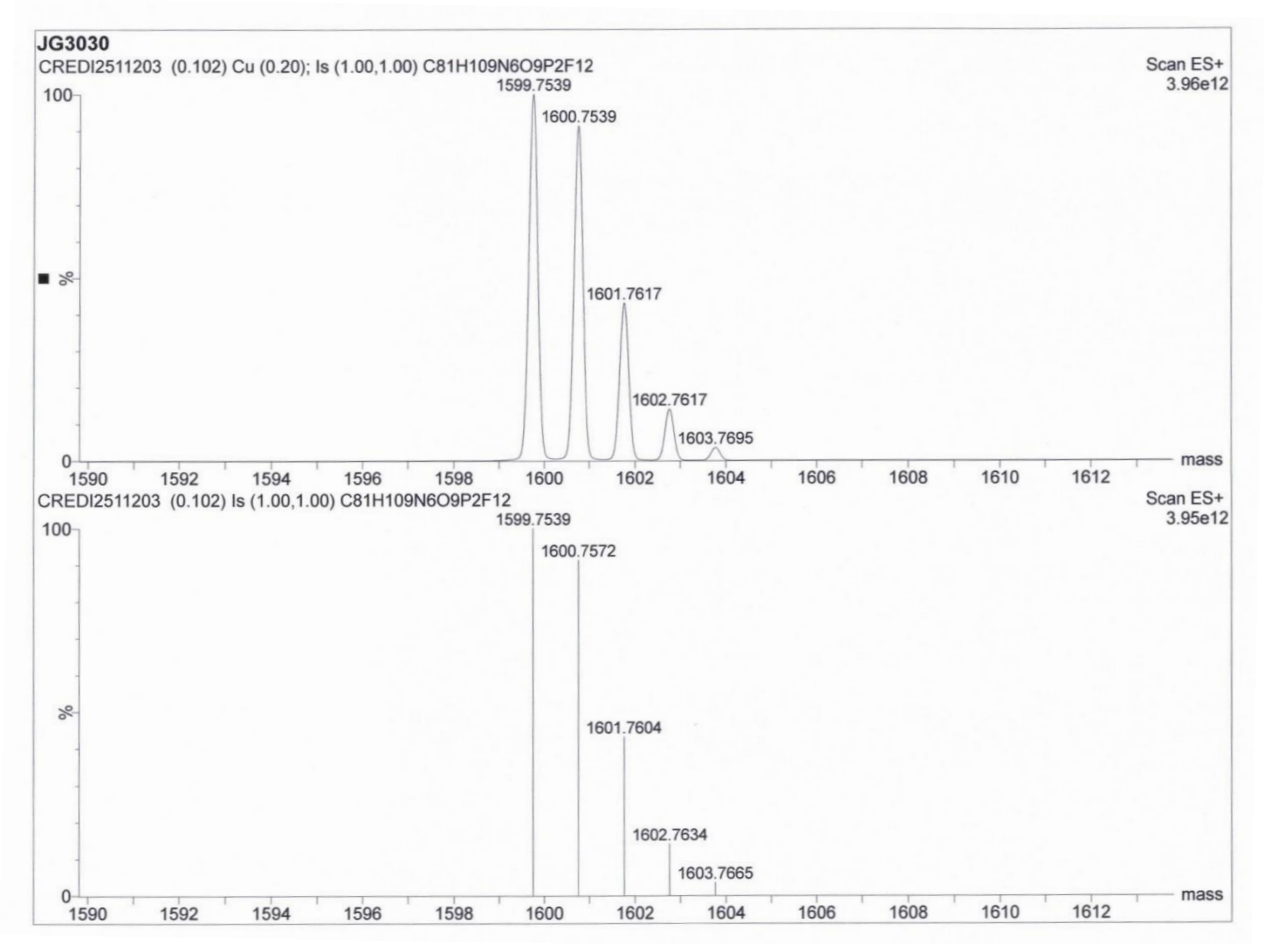

Figure S60 - Calculated (top) and measured (bottom) isotopic pattern of the peak at mass 1599.7539 for compound $\mathbf{2}^{3+}$.

8.3. Compound $3H^{3+}$

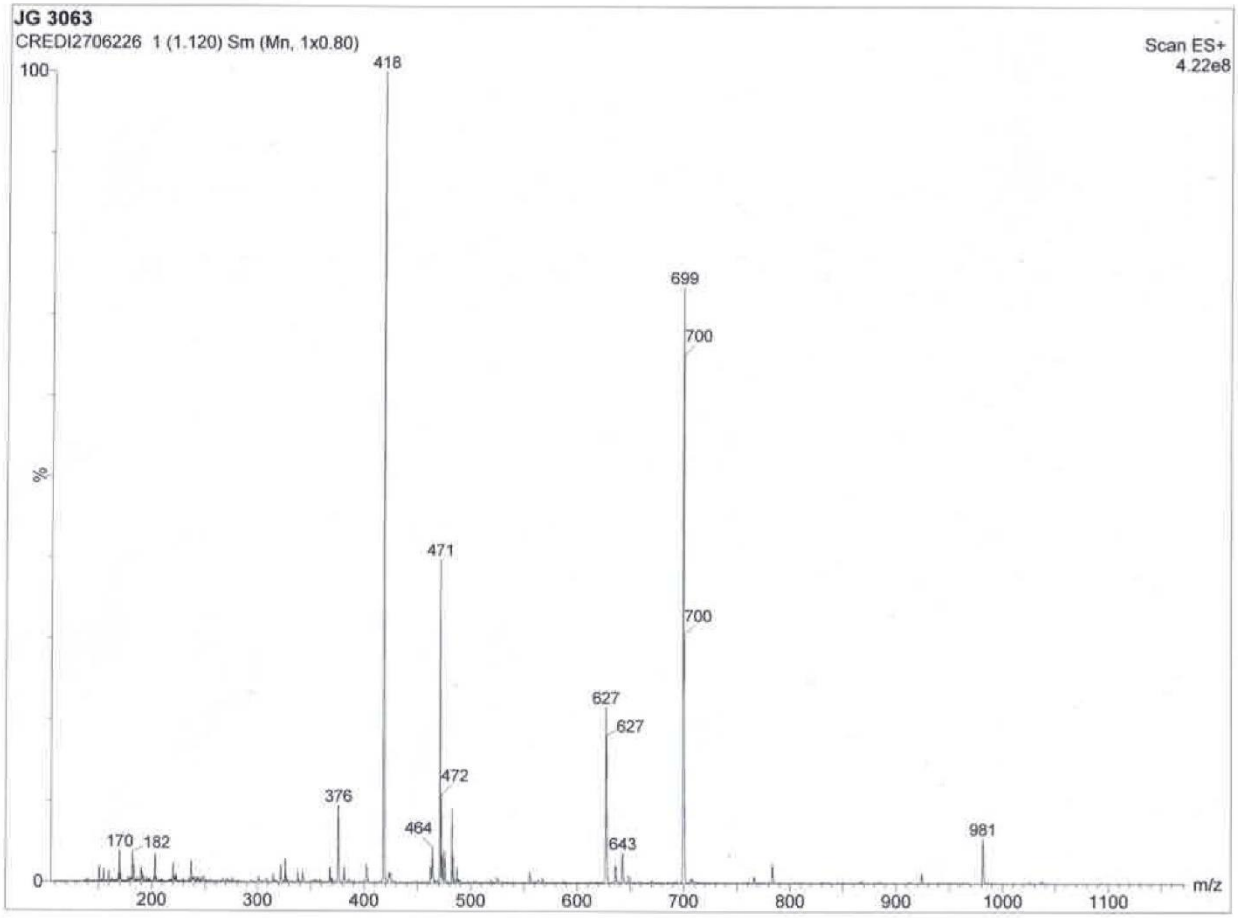

Figure S61 - Measured mass spectrum for compound **$3H^{3+}$**.

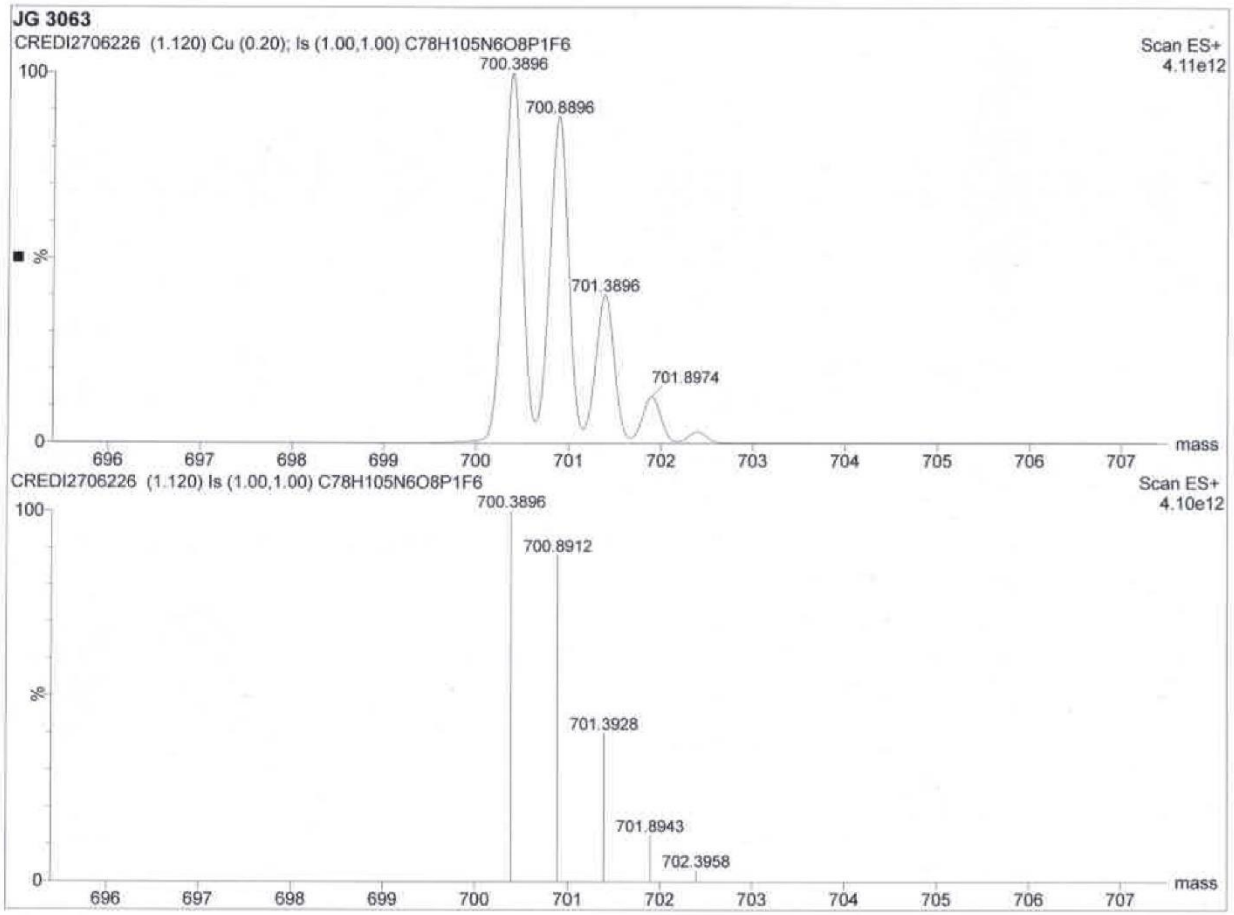

Figure S62 - Calculated (top) and measured (bottom) isotopic pattern of the peak at mass 700.3896 for compound **3H**$^{3+}$.

8.4. Compound $4H^{2+}$

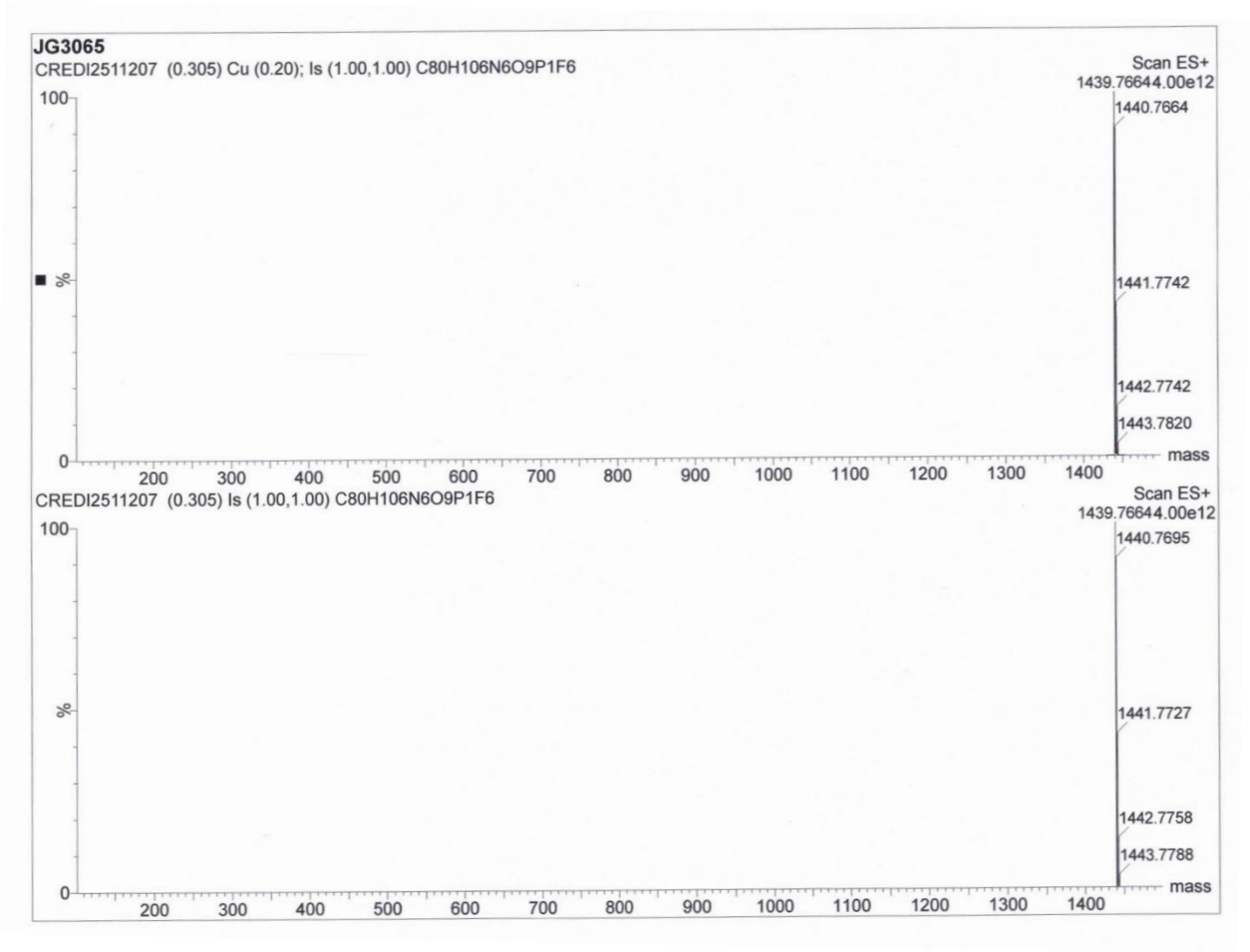

Figure S63 - Calculated (top) and measured (bottom) high-res mass spectra for compound **$4H^{2+}$**.

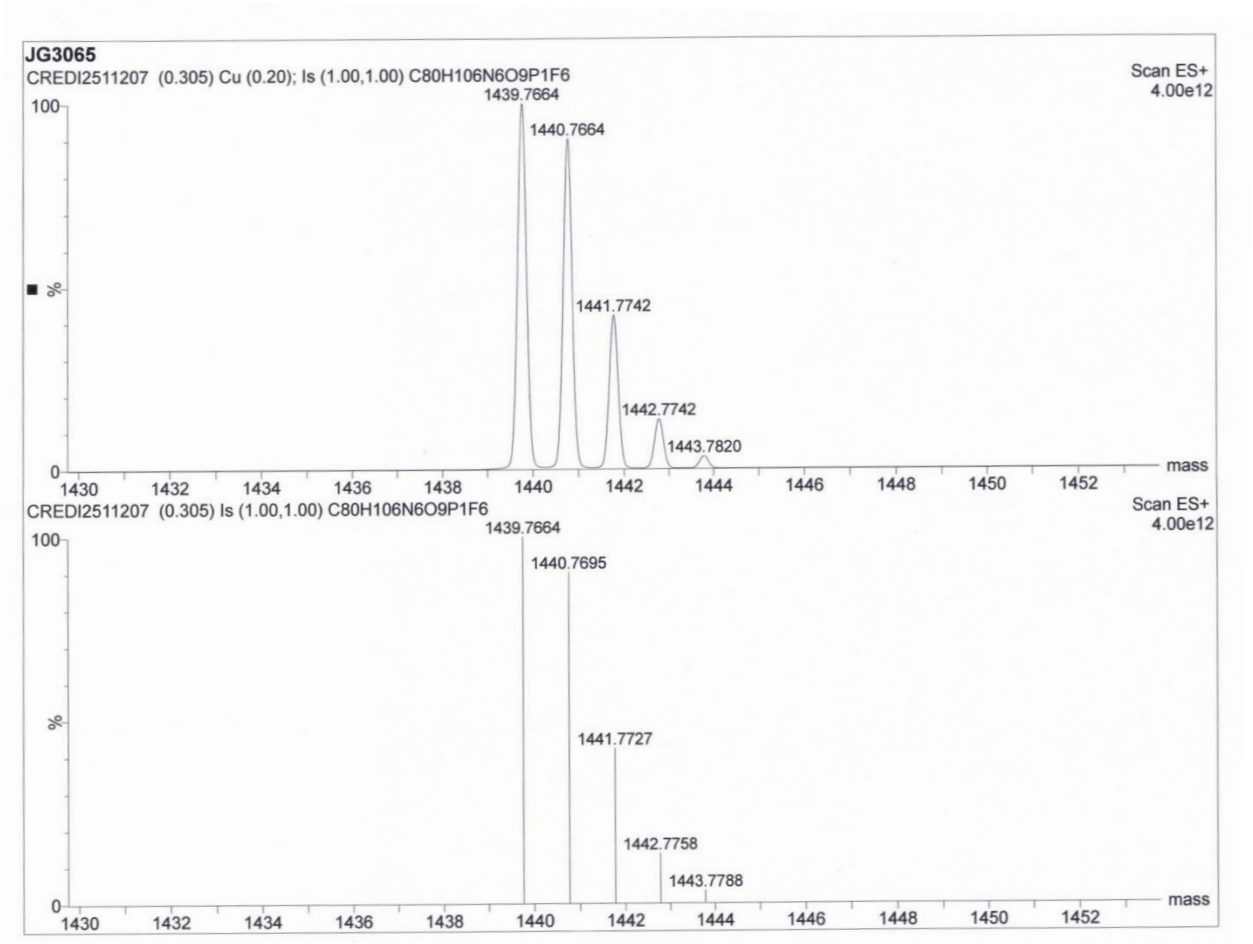

Figure S64 - Calculated (top) and measured (bottom) isotopic pattern of the peak at mass 1439.7664 for compound **4H^{2+}**.

8.5. Compound 5^{4+}

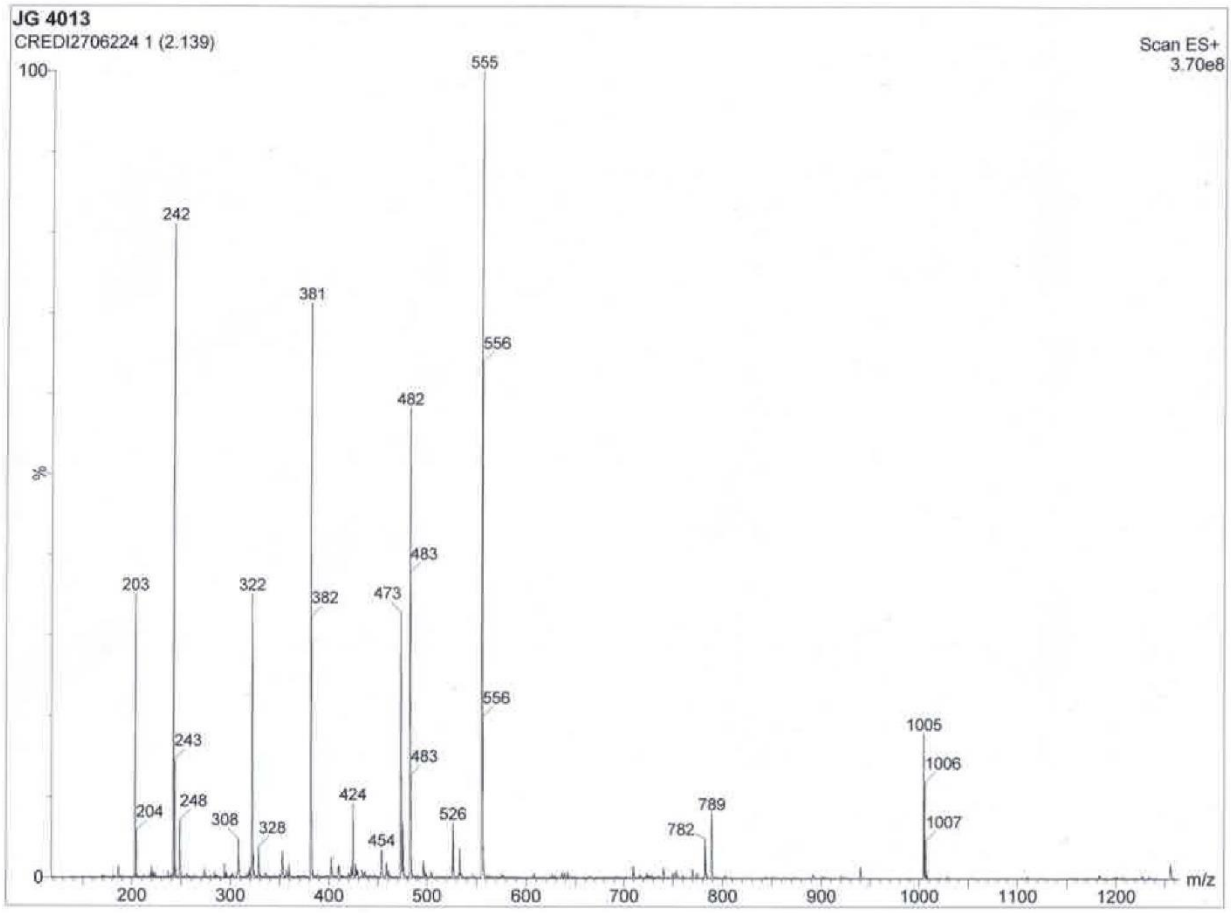

Figure S65 - Measured mass spectrum for compound **5^{4+}**.

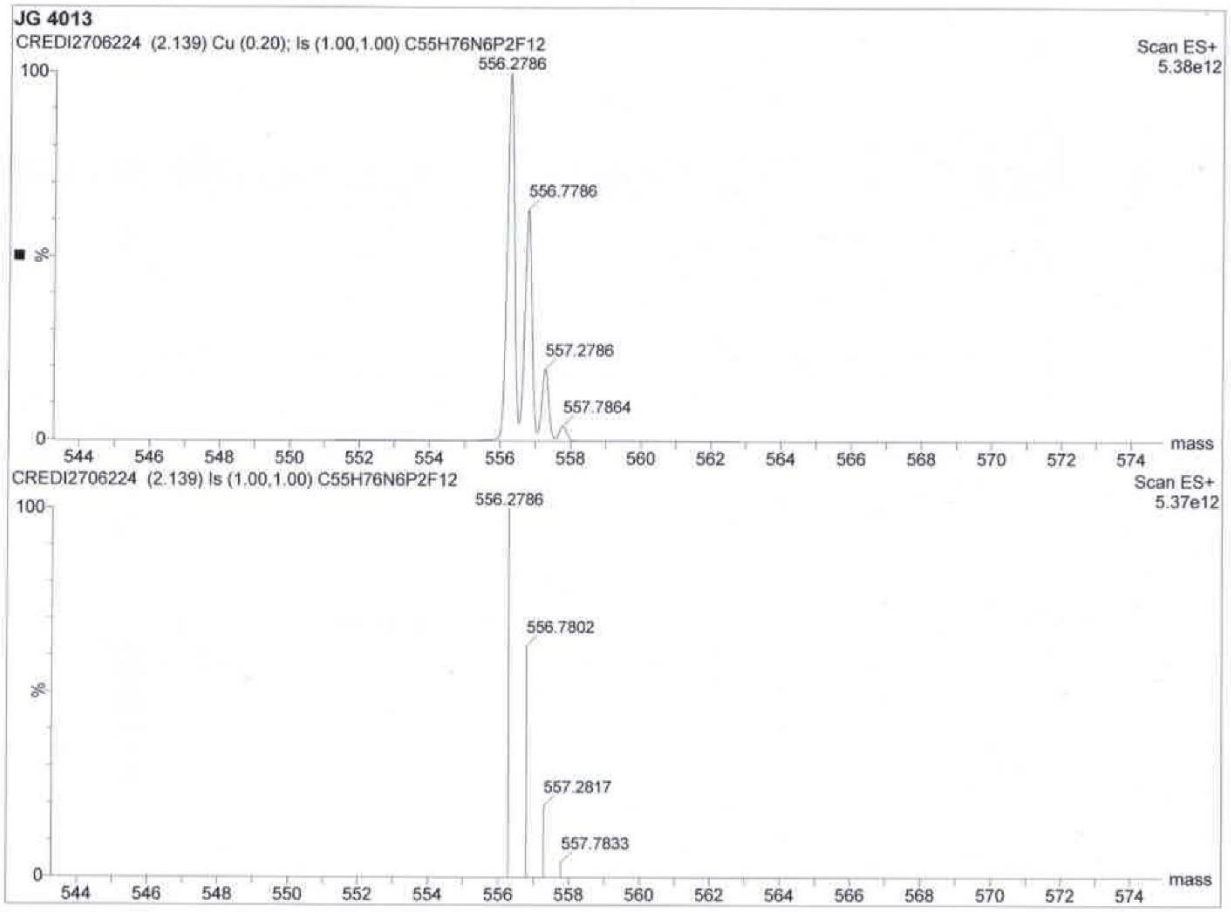

Figure S66 - Calculated (top) and measured (bottom) isotopic pattern of the peak at mass 556.2786 for compound $\mathbf{5}^{4+}$.

8.6. Compound 6^{3+}

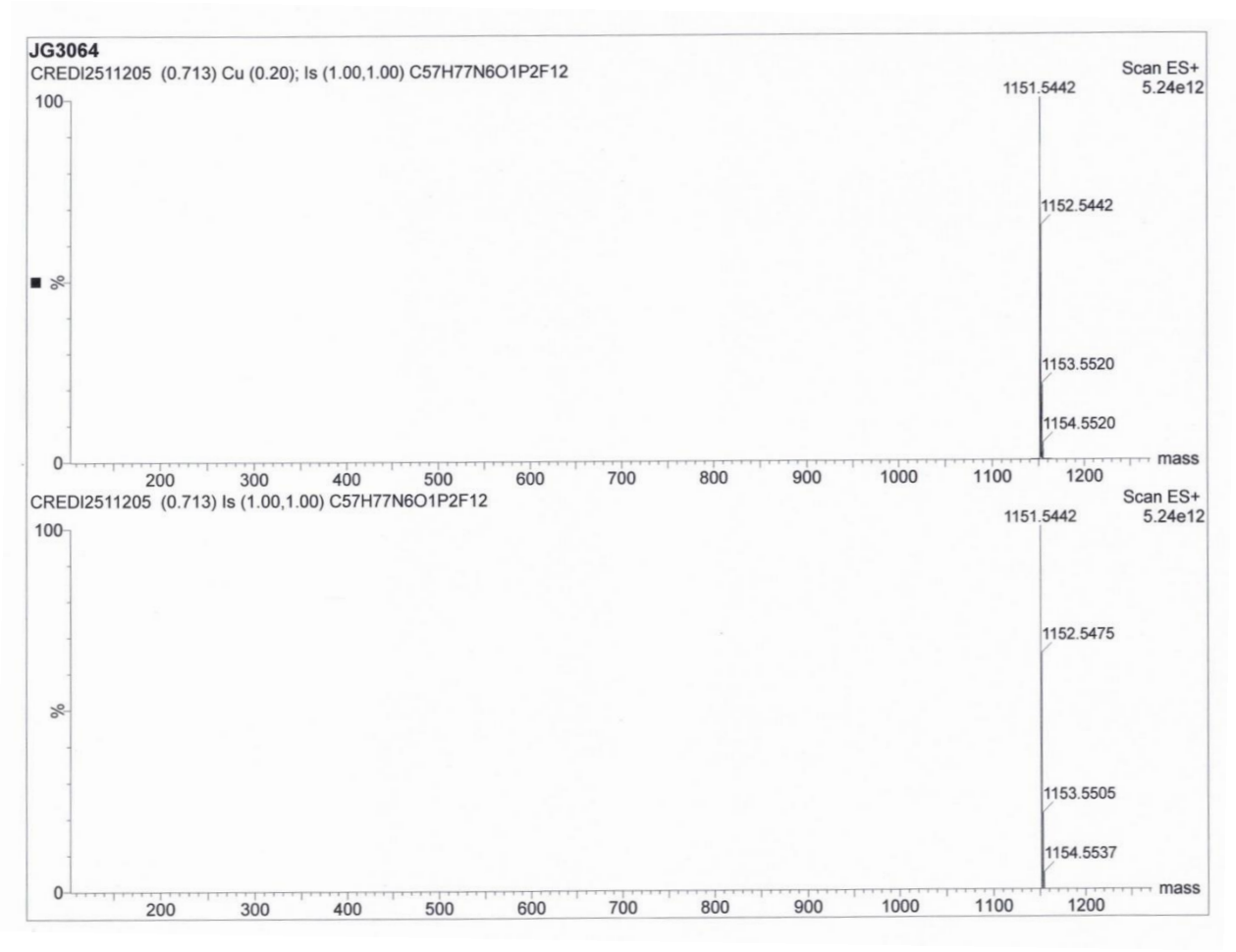

Figure S67 - Calculated (top) and measured (bottom) high-res mass spectra for compound **6^{3+}**.

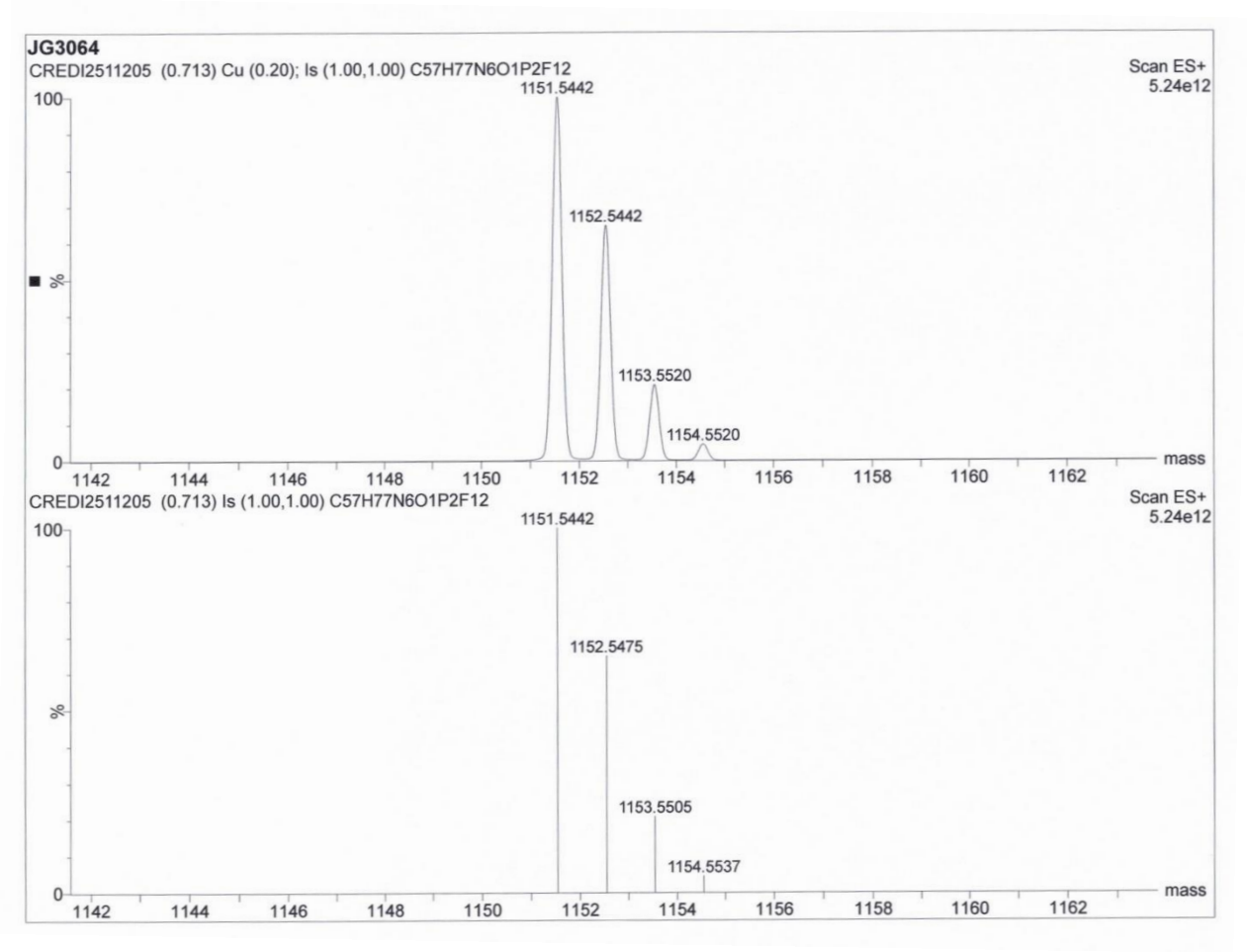

Figure S68 - Calculated (top) and measured (bottom) isotopic pattern of the peak at mass 1151.5442 for compound **6**$^{3+}$.

References

[1] P. R. Ashton, R. Ballardini, V. Balzani, I. Baxter, A. Credi, M. C. T. Fyfe, M. T. Gandolfi, M. Gómez-López, M.-V. Martínez-Díaz, A. Piersanti, N. Spencer, J. F. Stoddart, M. Venturi, A. J. P. White, D. J. Williams, *J. Am. Chem. Soc.* **1998**, *120* (46), 11932-11942.
[2] G. Ragazzon, A. Credi, B. Colasson, *Chem. Eur. J.* **2017**, *23*, 2149.
[3] W.E. Geiger, *J. Am. Chem. Soc.* **1974** *96* (8), 2632-2634.
[4] J. M. Bobbitt, N. A. Eddy, C. X. Cady, J. Jin, J. A.Gascon, S. Gelpí-Dominguez, J. Zakrzewski, M. D. Morton, *J.Org. Chem.* **2017**, *82*, 9279.
[5] https://www.basinc.com/products/ec/digisim
[6] J. F. Coetzee, G. R. Padmanabhan, *J. Am. Chem. Soc.* **1965** *87* (22), 5005-5010.
[7] M. J. Power, D. T. J. Morris, I. J. Vitorica-Yrezabal, D. A. Leigh, *J. Am. Chem. Soc.* **2023**, 145, 15, 8593–8599.